UNIVERSITA' DEGLI STUDI DI CATANIA

DEPARTMENT OF BIOLOGICAL, GEOLOGICAL AND ENVIRONMENTAL SCIENCES

PhD THESIS IN EARTH AND ENVIRONMENTAL SCIENCES

Antonio Stroscio

"Production of geopolymer materials through the use of Sicilian clay sediments"

Anno Accademico
2021-2022Ciclo
XXXIV

COORDINATOR

PROF. AGATA DI STEFANO

TUTOR

PROF. PAOLO MAZZOLENI

CO-TUTOR

PROF. GERMANA BARONE

Summary

List of Figures

probable transtensional component; 13. isobaths (in km) of the Moho; 14. hypothetical limit of ionic oceanic crust or passive margin-ionic ocean limit; 15. bathymetry.

Figure 6- Sampling sites of the three clay raw materials utilized in this work.

Figure 7- Geological map of the Licata fold belt, (south-central Sicily), scale 1:50.00. In red the sampling areas at Poggio Safanello and b, near C.da Martino.

Figure 8- Overview of the sampling areas; a) Poggio Safarello and b) C.da Martino.

Figure 9- Geological technical study to accompany the Provincial Territorial Plan of Enna (by Geol. Orazio Barbagallo et al.) with a detail on the studied area outcropping at Santa Margherita near Gagliano (EN).

Figure 10-Overview of the sampling area Santa Margherita near Gagliano (EN).

Figure 11- Detail of the Geological Map of the Termini Imerese Mountains and Western Madonie (Abate et al., 1988; scale 1: 50 000) with the outcropping of Caltavuturo Formation (Palermo).

Figure 12- Overview of the sampling area of Caltavuturo (PA).

Figure 13- Vicat needle usage diagram by Civil Engineering, Vicat apparatus.

Figure 14- Comparisons are shown between spectra obtained on the oriented samples and the same glycolates: a) Plio-pleistocenic clay; b) Numidican clay; c) Varicolored clay: Calt1; d) Varicolored clay: Calt2; e) Varicolored clay: Sclafani;

Figure 15- Mineralogical composition of samples PS RAW, PS550 °C and PS700 °C.

Figure 16- Mineralogical composition of samples NU RAW, NU550 °C and NU700 °C.

Figure 17- Mineralogical composition of samples VC RAW, VC550 °C and VC700 °C.

Figure 18- Ternary diagram on the composition of clay sediment, Plio-Pleisocenic clay (PS), Numidican Clay (NU) and Variegated clay (VC).

Figure 32- Mineralogical composition of the obtained AAMs by using Variegated clay.

Figure 33- FTIR-ATR spectra of calcinated clay raw material PS700 (red line), geopolimyer binder PS700-4M (black line) geopolymers binders (PS700-6M and PS700-8M, blue and green lines respectively) cured at 85 °C for 20h; b) FTIR-ATR spectra of calcinated clay raw m material PS700 (red line), geopolimyer binder PS700S-4M (black line) geopolymers binders (PS700S-6M and PS700S-8M, blue and green lines respectively) cured at 85 °C for 20h.

Figure 34- FTIR-ATR spectra of calcinated clay raw material PS700 (red line), geopolimyer binder PS700-4M (black line) geopolymers binders (PS700-6M and PS700-8M, blue and green lines respectively) cured at cured at room temperature for 28d; b) FTIR-ATR spectra of calcinated clay raw m material PS700 (red line), geopolimyer binder PS700S-4M (black line) geopolymers binders (PS700S-6M and PS700S-8M, blue and green lines respectively) cured at room temperature.

Figure 35- FTIR-ATR spectra of calcinated clay raw material (red line), geopolimyer binder NU700-4M (black line) geopolymers binders (NU700-6M and PS700-8M, blue and green lines respectively) cured at 85 °C for 20h; b) FTIR-ATR spectra of calcinated clay raw m material (red line), geopolimyer binder NU700S-4M (black line) geopolymers binders (NU700S-6M and NU700S-8M, blue and green lines respectively) cured at 85 °C for 20h.

Figure 36- FTIR-ATR spectra of calcinated clay raw material (red line), geopolimyer binder NU700-4M (black line) geopolymers binders (NU700-6M and NU700-8M, blue and green lines respectively) cured at room temperature for 28d; b) FTIR-ATR spectra of calcinated clay raw m material (red line), geopolimyer binder NU700S-4M (black line) geopolymers binders (NU700S-6M and NU700S-8M, blue and green lines respectively) cured at room temperature.

Figure 37- FTIR-ATR spectra of calcinated clay raw material (red line), geopolimyer binder VC700-4M (black line) geopolymers binders (VC700-6M and VC700-8M, dashed and dotted lines respectively) cured at 85 °C for 20h; b) FTIR-ATR spectra of calcinated clay raw m material (red line), geopolimyer binder VC700S-4M (black line) geopolymers binders (NU700S-6M and NU700S-8M, dashed and dotted lines respectively) cured at 85 °C for 20h.

Figure 38- FTIR-ATR spectra of calcinated clay raw material (red line), geopolimyer binder VC700-4M (black line) geopolymers binders (VC700-6M and VC700-8M, dashed and dotted lines respectively) cured at room temperature for 28d; b) FTIR-ATR spectra of calcinated clay raw m material (red line), geopolimyer binder VC700S-4M (black line) geopolymers binders (VC700S-6M and VC700S-8M, dashed and dotted lines respectively) cured at room temperature.

Figure 39- DRIFT spectra in the 5500-650 cm^{-1} range of the Plio-Pleistocene clay and respective geopolymers.

Figure 40- DRIFT spectra in the 5500-650 cm^{-1} range of the Numidic clay and respective geopolymers.

Figure 41- DRIFT spectra in the 5500-650 cm^{-1} range of the Variegated clay and respective geopolymers.

Figure 42- DRIFT spectra in the 1320-750 cm^{-1} range of the Plio-Pleistocene (PS), Numidic (NU), and Variegated (VC) clays and respective geopolymers.

Figure 43- Score plot (PC1 and PC3) of the 29 chosen DRIFT spectra for PCA treatment. Blue: PS, black: NU, red: VC; square: 85°C 20h, circle: room temperature 28 days; empty symbols: only NaOH activator, full symbols: NaOH+Na_2SiO_3 activators' mixture; NaOH molarity (4M, 6M, 8M) is marked in the symbols.

Figure 56- Scanning electron microscopy and EDS analyses of NU700S-8M sample cured at room temperature for 28d.

Figure 57- Scanning Electron Microscopy of NU700S-8M sample cured at room temperature for 28d: a) geopolymer gel appears to be coating the unreacted particle; b) detail of the matrix characterized by the presence of diverse cracks and voids.

Figure 58- Al_2O_3/SiO_2 vs. Na_2/SiO_2 ratios for gels precipitating in hybrid cements (based on EDS findings) on the samples NU700-4,6,8M and NU700S-4,6,8M.

Figure 59- Ternary diagram Al_2O_3-SiO_2-CaO for gels precipitating in hybrid cements (based on EDS findings)) on the samples NU700-4,6,8M and NU700S-4,6,8M.

Figure 60 a-d- Scanning Electron Microscopy at diverse magnification of VC700-8M sample cured at 85 °C for 20h.

Figure 61- Scanning electron microscopy and EDS analyses of VC700-8M sample cured at 85 °C for 20h.

Figure 62- Scanning electron microscopy on samples cured at 85 °C for 20h: a) sample VC700-8M; b) VC700S-4M; c) VC700-6M; d) VC700S-8M.

Figure 63- Al_2O_3/SiO_2 vs. Na_2/SiO_2 ratios for gels precipitating in hybrid cements (based on EDS findings) on the samples VC700-4,6,8M and VC700S-4,6,8M.

Figure 64- Ternary diagram Al_2O_3-SiO_2-CaO for gels precipitating in hybrid cements (based on EDS findings)) on the samples VC700-4,6,8M and VC700S-4,6,8M.

Figure 65- Total Pore Volume expressed in g/cm3 of the samples NU700-4,6,8M; b) Total Pore Volume expressed in g/cm3 of the samples PS700-4,6,8M;

Figure 66- Example of capillary water absorption tests carried out according to UNI EN 10859:2000 on all obtained samples.

Figure 67- Vicat Needle test on the samples.

Figure 68 - Needle penetration depth on PS700S-8M sample.

Figure 69 - Needle penetration depth on NU700S-8M and VC700S-8M samples

Liste of Tables

Tab.12- Compression strength values of samples obtained by using only sodium hydroxide and cured at 22+3°C for 28d.

Table 13- Mineralogical composition after Rietveld refinement of both geopolymer obtained by using Plio-pleistocenic clay and cured at 85° for 20h- Qtz=Quartz, Ab= Albite, Clc=Calcite, Ms=Muscovite, Sme=Smectiti, To= Tobermorite, So= Sodalite, Hm= Hematite;

Table 14- Mineralogical composition after Rietveld refinement of both geopolymer obtained by using Numidican clay and cured at 85° for 20h – Qtz=Quartz, Ab= Albite, Or=Orthoclase, Ms=Muscovite, Sme=Smectiti, Do= Dolomite, K=Kaolinite, Fj= Faujasite;

Table 15- Mineralogical composition after Rietveld refinement of both geopolymer obtained by using Variegated clay and cured at 85° for 20h - Qtz=Quartz, Hm= Hematite, Ab= Albite, Or= Ortoclase, Sme= Smectiti;

Table 16- Hg intrusion Porosimeter sample (NU and PS) cured at 85°C for 20h.

Table 17- Amount of water absorbed per unit area as a function of time (t) of the obtained geopolymer binders.

PREFACE

In recent years, considering the growing interest in the scientific community regarding the themes of sustainability and CO_2 footprint reduction, a new class of materials mainly known as Alkali Activated Materials (AAMs) have been studied. These innovative materials, including those classified as geopolymers, were introduced as new construction materials as alternative to traditional cements, Ordinary Portland Cements (OPC). The raw materials normally used in the production of these kind of materials are amorphous aluminosilicates (such as clay, slags, fly ash, volcanic ash) which are dissolved and react in alkaline environment. Many research studies have been carried out to investigate the possibility to reuse waste materials as precursors in the production of geopolymers with the aim to minimize the impact on the environment.

It has been assessed that, depending on the raw materials utilized and the processing conditions, AAMs can exhibit a wide variety of properties, (e.g. high level of resistance to different acids and salt solutions, fire resistance, low shrinkage and low thermal conductivity, high mechanical strength). Furthermore, considering the versatility of AAMs and their compatibility with natural stones, their application in the restoration of stone materials is being evaluated.

This PhD project is focused on the potentiality and suitability of the use of clay sediments cropping out in Sicily as precursors for the production of new alkaline-activated binders able to provide properties similar to those of Portland cement. The main advantages of the use of clay sediments are the simplicity in finding materials of this type anywhere in the world, thus obtaining a reduction of transport distances and favoring local economies. Furthermore, the use of these alternative materials allows to obtain a reduction in CO_2 emissions compared to traditional cement, as firing at high temperatures is no longer necessary.

The thesis can be divided as follows:

1. The **first part** looks at the State of the art with the introduction of AAMs. Their characteristics, the geopolymerization process and their applicability are discussed in detail.
2. The **second part** concerns the Geological Setting of Sicily and the raw materials utilized in this thesis as precursors. The multi-analytical characterization of the raw materials utilized for AAMs synthesis carried is discussed in detail.

3. Finally, the **third part** describes the geopolymers synthesis, and the characterization of all the specimens obtained through different techniques such as (Integrity test, X-Ray Diffraction (XRD), Scanning Electron Microscopy (SEM), Fourier-transform infrared spectroscopy (FTIR), Diffuse Reflectance Infrared Fourier Transform Spectroscopy (DRIFT), Raman spetroscopy, Mercury Intrusion Porosimetry (MIP), Capillary water absorption test, Vicat Nedlee Test).

PREFAZIONE

Negli ultimi anni, considerando il crescente interesse della comunità scientifica sui temi della sostenibilità e della riduzione nell'emissioni di CO_2, una nuova classe di materiali, conosciuti principalmente come Alkali Activated Materials (AAMs), è stata studiata. Questi materiali innovativi, compresi quelli classificati come geopolimeri, sono stati introdotti come materiali da costruzione in alternativa ai cementi tradizionali, gli Ordinary Portland Cements (OPC). Le materie prime normalmente utilizzate nella produzione di questo tipo di materiali sono gli alluminosilicati amorfi (come argilla, scorie, ceneri volanti, ceneri vulcaniche) che si dissolvono e reagiscono in ambiente alcalino. Al fine di valutare la possibilità di riutilizzare i materiali di scarto come precursori nella produzione di geopolimeri con lo scopo di minimizzare l'impatto ambientale, sono stati condotti diversi studi di ricerca. A seconda delle materie prime utilizzate e delle condizioni di lavorazione, i materiali attivati alcalinamente presentano un'ampia varietà di proprietà come ad esempio: un alto livello di resistenza a diversi acidi e soluzioni saline, resistenza al fuoco, basso ritiro e bassa conducibilità termica, alta resistenza meccanica. Inoltre, considerando la versatilità di questi materiali innovativi e la loro compatibilità con le pietre naturali, si sta valutando la loro applicazione nel restauro di materiali lapidei.

Considerato quanto detto, questo progetto di dottorato è stato incentrato sulle potenzialità e l'idoneità dell'uso dei sedimenti argillosi che affiorano in Sicilia come precursori per la produzione di nuovi leganti alcalini in grado di fornire proprietà simili a quelle del cemento Portland. I principali vantaggi dell'utilizzo dei sedimenti argillosi sono la semplicità nel reperire materiali di questo tipo in qualsiasi parte del mondo, ottenendo così una riduzione delle distanze di trasporto e favorendo le economie locali. Inoltre, l'utilizzo di questi materiali alternativi permette di ottenere una riduzione delle emissioni di CO_2 rispetto al cemento tradizionale, in quanto non è più necessaria la cottura ad alte temperature.

La tesi è stata suddivisa nel seguente modo:

1. La prima parte esamina lo stato dell'arte dei materiali di nuova generazione. In particolare vengono descritte le loro caratteristiche, il processo di geopolimerizzazione e la loro applicabilità.

2. La seconda parte riguarda il contesto geologico della Sicilia e le materie prime utilizzate in questa tesi come precursori. Nel dettaglio viene approfondita la caratterizzazione multi-analitica delle materie prime utilizzate per la sintesi delle AAMs.

3. La terza ed ultima parte descrive la sintesi dei geopolimeri e la caratterizzazione di tutti i campioni ottenuti attraverso diverse tecniche analitiche quali: test di integrità, diffrazione dei raggi X (XRD), microscopia elettronica a scansione (SEM), spettroscopia infrarossa a trasformata di Fourier (FTIR), spettroscopia infrarossa a riflessione diffusa a trasformata di Fourier (DRIFT), spettroscopia Raman, porosimetria ad intrusione di mercurio (MIP), test di assorbimento d'acqua capillare, Vicat Nedlee Test;

1. State of the art

1.1 Alkali Activation process

In the last decades, scientific literature reported that the preparation of alkali activated materials (AAMs) with the use of different local raw materials promises valuable ecological benefits and lower costs, in addition to the reduction in CO_2 emissions compared to traditional materials such as cement or bricks (Caijun Shi, n.d.); Liu et al. 2019; Thomas Poinot et al. 2018; Polettini, R. Pomi, G. Carcani 2005). Nowadays, AAMs is the most popular term used to describe these inorganic polymers, also called geopolymers, created by mixing aluminosilicate precursors with concentrated alkali hydroxide or alkali silicate mediums (Djobo et al. 2017; Bernal and Provis 2014; John L. Provis and van Deventer 2014; Yadollahi, Benli, and Demirbog 2015; Leonelli C., et al 2013). In detail, in Provis and Van Deventer, 2014a, geopolymers are shown as a subset of AAMs characterized by the highest Al and lowest Ca concentrations as shown in Fig.1, to enable the formation of a network structure rather than the chains characteristic of calcium silicate hydrates. The most prevalent precursors used in geopolymer synthesis are: low-calcium fly ashes and calcined clays (Provis and van Deventer 2014; Barbosa, V.F., MacKenzie 2003; Rees, C. A., et al. 2007). However, the technology of alkali activation was attributed to a first patent awarded to Kühl in 1908, (Kühl 1908), to the researchers conducted by Purdon in the 1930s-1950s, (Purdon 1940), and to the work of Glukhovsky from the 1950s onwards (Glukhovsky 1959). The term geopolymer was coined by Davidovits in the 1970s through developing and patenting materials obtained after alkali activation of metakaolin. Currently, the term geopolymer highlights the similarities between these synthetic materials and the structures of feldspathoids and zeolites (Davidovits 1988; 1991). In addition to these definitions, there are other terms used to describe such alkali activated materials, as mineral polymers (Wastiels, J., et al. 1994), inorganic polymers (Barbosa, V.F.F., MacKenzie, K.J.D., Thaumaturgo 2000), soil-cements (Krivenko 1997; Krivenko, et al. 2007), hydro ceramic (Siemer 2002), low temperature aluminosilicate glass (Rahier, et al. 1997), Zeo-cements (Krivenko, P., et al. 2007), zeo-ceramics (Fernández-Jiménez, A., et al. 2008), inorganic polymers glass, alkali bounded-ceramics and alkali ash materials.

The chemical composition and the structure of the precursor play an important role in the geopolymeric process. A silica and alumina content of approximately 70% in the precursor are required in order to improve the reactivity to the alkaline solution, which

then influences the final proprieties of geopolymeric product (Davidovits, 1991)(Deventer 2007; Provis, J.L., Bernal 2014). However, the optimum mechanical proprieties, durability and thermal stability can also be achieved but these depend on many factors: mineralogical and chemical composition of the aluminosilicate sources, particle size distribution of the raw material, curing temperature, composition of the alkaline solution and liquid to solid (L/S) ratio (Djobo et al. 2017; Provis and Van Deventer 2009.

Nowadays, the growing interest on the production of AAMs, starting from waste industrial products (e.g. fly ashes and blast furnace slag) are mainly related to two factors: the similarity with the traditional cements (OPC) and the good mechanical performance after 28 days comparable to these latter. Actually, the production of OPC is the principal responsible of the emission of carbon dioxide from industrial activities (for about 80%). This CO_2 emission is mainly generated by two processes: the combustion of fossil fuels and the decomposition of $CaCO_3$ into CaO and CO_2 as main reaction chemistry. For the production of these innovative materials, also thermal treatment are required in a low temperature range to reach densification and so complete alkali consolidation process. Indeed, thermal treatments represent an important synthesis parameter for low reactivity materials, such as volcanic ones (Kamseu, E., et al. 2009; Kani, E.N., Allahverdi 2009). Considering the low CO_2 emission and low energy consumption during the synthesis, the production of these innovative materials (AAMs) can be considered environmentally sustainable.

Many studies have been carried out with the goal of reducing the CO_2 footprint (Duxson, P., et al. 2007; FLATT, R.J., et al. 2012), demonstrating that the potential reduction of CO_2 depends on the particular formulation mix and source of feedstock (Habert, et al. 2011).

Furthermore, the AAMs have shown a good mechanical performance after 28 days of curing at room temperature or, in some cases, after 1 day of curing at temperatures 40 °C-100 °C and good resistances to different chemical attacks or degradation agents (C. Ruiz-Santaquiteria A. et al. 2013)

Studies have shown also that these materials present very minute structural damages at high temperatures (e.g. 700-800°C), (Barbosa, V.F., MacKenzie 2003; Fernández-Jiménez, A., et al. 2010). Generally, AAMs have several fields of application as for example building materials and hazardous waste encapsulation, guaranteeing low shrinkage, low carbon emission, high strength performance and so on (Shi, C., Fernandez-Jimenez 2006; Duxson, P., et al. 2007).

1.2 Raw materials as a precursor

Two main classes of materials are used in the alkaline activation process, either solid natural or industrial aluminosilicate precursors and alkaline activators. The chemical composition of the starting raw materials plays an important role in the geopolymerization process. Considering this, raw materials rich in Al (e.g. calcinated clays, metakaolin and others) and Si (e.g. fly ash, blast furnace waste) can be used. The reactivity of these different starting materials in the alkaline environmental changes according to the following order: metakaolin > zeolites> blast furnace waste > fly ash > pozzolan > kaolin. Among the natural raw materials, the most used are clay minerals such as kaolinite, illite and smectite (Khalifa et al. 2020; Buchwald, A., et al. 2009). These natural materials need to be thermally activated to improve their reactivity under alkaline conditions. Generally, clay is activated in a temperature range between 500 °C and 800 °C during which a loss of structural hydroxyl ions of the clay mineral occurs (Hanzlíček et al. 2009; Elimbi, A., Tchakoute, H., Njopwouo 2011; Gasparini, et al. 2013). Among the calcined clays, metakaolin represents the most studied precursor, due to its high reactivity and the good properties in terms of resistance and durability of the final products (Duxson, P., Lukey, G.C., van Deventer 2007; Rashad 2013).

In regards to industrial products, many studies can be found on the different types of industrial products used and their characteristics (Duxson, P., Provis 2008; Fernández-Jiménez, A., Palomo 2005; Puertas, F., et al. 2000). The main products largely used are blast furnace slags (BFS) from iron-making process and fly ashes from coal combustion power plants. The fly ashes, that are most used in the geopolymer synthesis, are classified in low Calcium (Class F) and higher Calcium (Class C) (John L. Provis and Van Deventer 2009; Occhipinti R., et al. 2021).

Alkaline activators are liquid or solid compounds, able to generate a basic environment in order to hydrolyze the starting materials. The alkaline activators commonly used in the geoplymerization process are sodium or potassium hydroxides (NaOH, KOH) and sodium silicates. The use of sodium hydroxides is very widespread due to its low cost and wide availability and low viscosity. In this thesis, a pure solid sodium hydroxide provided by Carlo Erba company (code: 373908) and a liquid sodium silicate provided by Ingessil s.r.l. are used, both with a molar ratio $SiO_2/Na_2O = 3$.

1.3 Geopolymerization process

The alkaline activation process can be described as the mixing of an alkaline solution with a reactive, finely milled, aluminosilicate powder such as natural raw materials or industrial products (e.g. metakaolin, fly ash, calcinated clay and others) (Palomo, A., Glasser 1992; Duxson, P., et al. 2007; Davidovits 2008; Fernández-Jiménez and Palomo 2003). Through this process, a disordered alkali aluminosilicate gel phase is formed. This is known as the geopolymeric gel binder phase. The proprieties of these innovative materials depend on many factors such as chemical composition, grain size distribution, chemical and mineralogical composition of the starting materials, composition of the alkaline solution, liquid to solid ratio and curing temperature

In detail, the obtained alkali activation slurries are mixed for 5 minutes by using a mechanical mixer in order to obtain good workability, molded and compacted by mechanical vibrations for 60s to remove air bubbles. The maturation phase, commonly called curing, can be carried out at low temperature (25-100°C) for different lengths of time, or at room temperature (22±3°C) in controlled relative humidity (RH) conditions (99%) for 28 days (Duxson, P., et al. 2007; Fernández-Jiménez, A., Palomo 2005; Zuhua et al. 2009).

Various other studies (M.L. Granizo 1998; Alonso and Palomo 2001) suggest that the geopolymerization process is an exothermic reaction that can be conceptually described using the model proposed for the formation of some zeolites that involves a three steps process:

i) dissolution of the precursor in the alkaline solution;
ii) reorganization and diffusion of dissolved ions, with formation of small coagulated structures;
iii) growth and polycondensation of the aluminosilicate gel phase to form the hydrate products.

The process that leads to the formation of zeolites can be proposed as the simpler method to better explain the alkaline activation procedure. In this regard, the main difference between zeolites and product obtained from the alkali activation is related to the structure order. In fact, the first one shows a structure perfectly crystalline, while the inorganic polymer presents an amorphous structure.

Glukhovsky (1967) proposed a general model to describe the process involved during alkaline synthesis of aluminosilicate materials. This model involves three main

steps that can be summarized as follows: in the starting materials, the process of raw material disaggregation by breaking of the M-O (M indicates the alkali cation), Si-O-Si, Al-O-Al, and Si-O-Al bonds due to the presence of a strongly basic environment. The dissolution rate increases linearly with the pH of the solution, and at high pHs, the fast dissolution rate leads to the formation of a supersaturated aluminosilicate solution, which, through condensation, leads first to the formation of oligomers and then to large gel network. During geopolymerization, Si-O-Si and Si-O-Al covalent bonds break down into colloid phase upon contact with alkaline solution. The final geopolymer gel formed is different from the initial gel due to the unbound water expelled during the curing process. As reported in Glukhovsky (1967) and displayed in Fig.2, the resulting product is an alkaline aluminosilicate hydrate ($Na_2O{\cdot}Al_2O_3{\cdot}2SiO_2{\cdot}nH_2O$ type gel (N-A-S-H gel)), with a three-dimensional structure that resembles zeolitic structures (J. L. Provis et al. 2005; Shi, C., et al. 2011). The chemical process involved in the hydration of traditional cement differs from that of alkaline activation in which the main reaction product is a calcium silicate gel ($CaO{\cdot}SiO_2{\cdot}nH_2O$ gel type (C-S-H)) (Shi, C., et al. 2011).

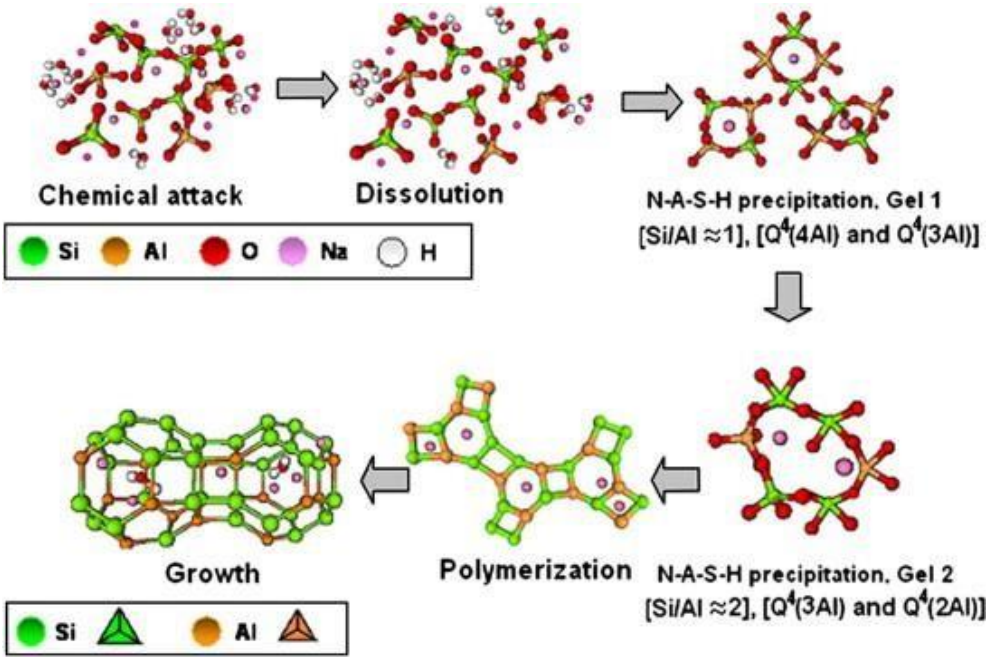

Fig. 1- Descriptive model for alkali activation of aluminosilicates (Shi et al., 2011).

The dissolved phases interact forming coagulated structures. Indeed, the intermediate product named Gel 1 in Fig.2, that has high amounts of Al, transforms during the curing into Gel 2 which has a higher Si content than the first one. After geopolymerization, the gel structure continues its evolution modifying the structure, increasing oligomers connectivity

and developing a three-dimensional aluminosilicate network as shown in Fig.3, (Duxson et al.2007a). To this purpose, different research work such as (Duxson et al.2007a; Shi, C., et al. 2011) proposed schematic models of N-A-S-H and C-A-S-H gel reaction process.

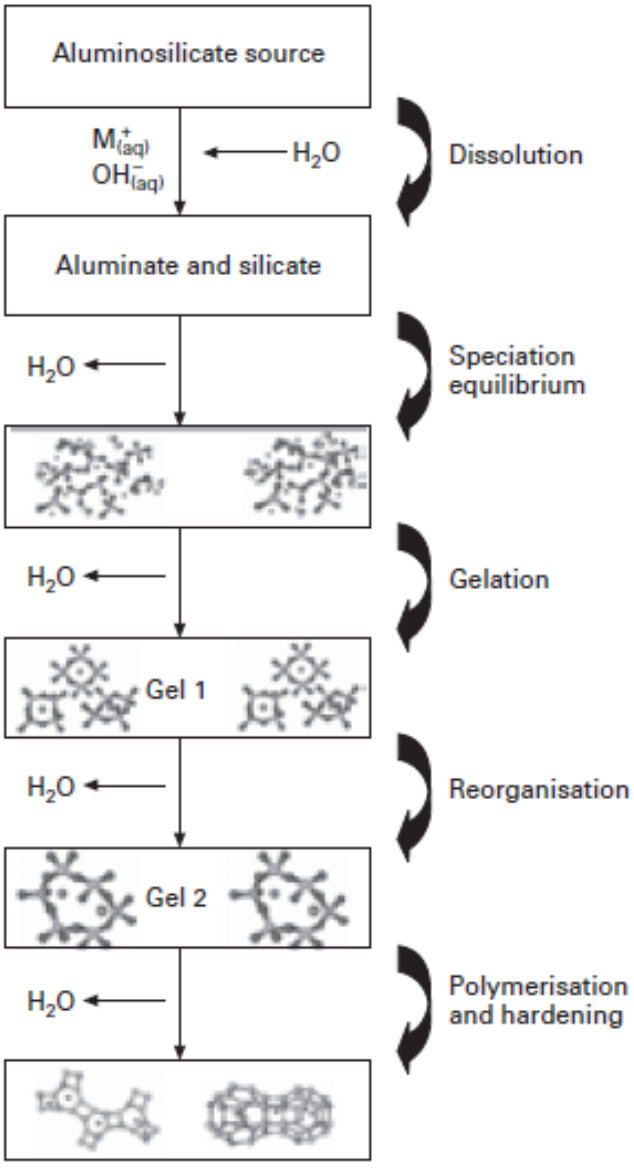

Fig. 2- Model of geopolymerization proposed by Duxon et al. (2007a)

1.4 Chemistry and structure of alkali activated materials

The chemistry and the structure of the AAMs is based primarily on the basis of the nature of starting precursors, in which the aluminosilicate sources and alkali activators are responsible for the good mechanical, physical and chemical properties of these latter. In the AAMs, calcium appears the main determinant element in terms of silicates structure, and they can be divided in two groups accordingly: low-calcium and high-calcium AAMs. In fig.3 is displayed a scheme through which Provis and Bernal, (Provis, J.L., Bernal 2014), proposing the primary reaction products: an alkali aluminosilicate N-A-S-H type gel or a calcium aluminosilicate hydrate C-A-S-H type gel. In the first type of gel (N-A-S-H), sodium can also be replaced by potassium or calcium, these changes can be described by the following formula: N,K-(C)-A-S-H.

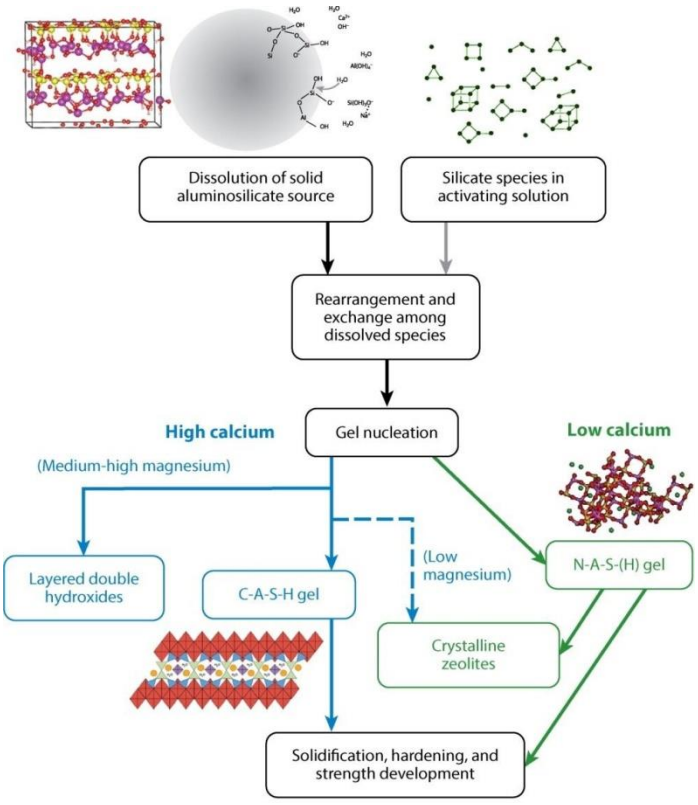

Figure 3- Process and reaction products of alkaline activation of a solid aluminosilicate precursor. High-calcium systems react according to the left-hand (blue) pathway; low-calcium systems react according to the right-hand (green) pathway (Provis and Bernal, 2014).

In Davidovits, 1991 and Provis et al., 2005, the N-A-S-H type gel is also considered as a precursor of zeolites, considering zeolite formation as a secondary reaction product in particular after 28 days of curing.

For what concerns C-A-S-H gels, these latter are formed by calcium-rich clays in which tetrahedrally coordinated silicate chains form a dreierketten structure (i.e. triple

chain structures typical of traditional cements). The interlayer region contains Ca^{2+} cations that balance the negative charge generated when Al^{3+} replaces Si^{4+} in the tetrahedral chain sites (Fernández-Jiménez and Palomo 2003).

1.6 Alkali-activated materials as a new class of building materials and their applications.

In the last decades, interest in new construction materials which are environmentally friendly and cost-efficient increased exponentially thanks to their versatility and potentiality compared to the traditional materials used like cement mortars and organic resins, that exhibit low efficiency due to their lack of compatibility and insufficient durability (Mendes et al.,2015.; Geraldes, C.F.M., et al. 2016). In this scenario, alkali activated materials, including geopolymers, have shown high potentiality and suitability as new class of construction materials in the field of conservation and restoration of historical buildings (Ricciotti et al. 2017; Clausi et al. 2016).

Various case studies have been explored regarding the applications of geopolymers in Cultural Heritage buildings (Hanzlíček T, et al. 2009; Elert, K., et al. 2015). Studies regarding the consolidation of terracotta structures are also published (Hanzlíček T, et al. 2009) thanks to the versatility of geopolymers in terms of workability and similar color to the original ceramic material.

In this context, in recent studies, pumice stone from the Eolian islands or volcanic ash from Mt. Etna were identified as potentially suitable materials to be used as geopolymeric precursors thanks to a good compatibility with the original substrate and colour compared to the traditional materials (Barone et al. 2021; Occhipinti et al. 2020).

In addition, metakaolin was also considered another important precursor for the synthesis of AAMs applied in the restoration of historical buildings due to its properties such as high resistance to acids or salt solutions, low thermal conductivity, low shrinkage. All factors that are important in the restoration field (Duxson, P., Lukey, G.C., van Deventer 2007; Lee, W.K.W., van Deventer 2007; Clausi et al. 2016).

On the basis of these considerations, the aim of this PhD Thesis is the synthesis of alkali activated materials, utilizing clay as a starting material, that can provide good chemico-physical and mechanical characteristics compared to traditional materials utilized in building construction.

2. Starting materials

2.1 Geological setting and sampling sites

Sicily is located in the center of the Mediterranean Sea and from a geological point of view it is characterized by three structural domains, divided as follows: the Foreland Domain, the Orogenic Domain, and the Inner Domain.

While the Foreland Domain represents the areas that today are characterized by orogenic deformation, the Orogenic Domain extends from the southern Apennines through the Calabrian-Peloritanian Arc to North Africa, including most of Sicily, with particular reference to central- western Sicily. In this area, two of the three overlapping thrust structures, that are attributed to this domain, i.e., the Outer Thrust System (STE) and the Apennine-Maghrebid Chain (CAM) outcrop, while the Kabyle Calabrian Chain (CCP) outcrops in northeastern Sicily.

Finally, the Inner Domain is represented by the Sardinian-Corsican Block and the Tyrrhenian Basin. The first one is what remains of the European crust and of the Tyrrhenian basin, while the second one was formed at the beginning of the Serravallian period, as displayed in Fig.4. Both domains manifest kinematic behavior that in general can be defined as homogeneous (Lentini et al. 1990).

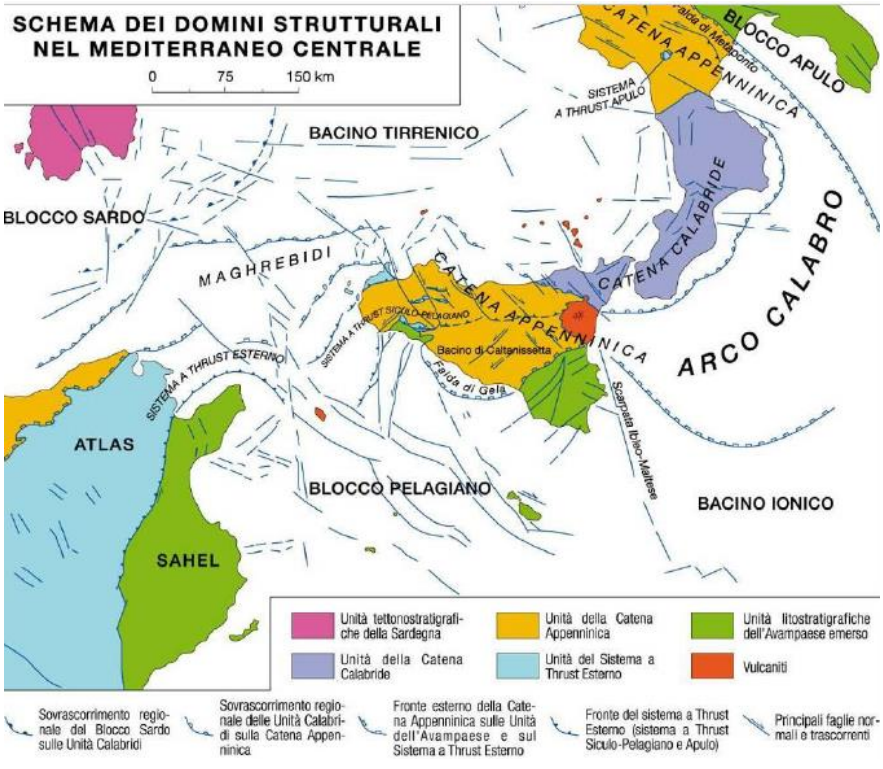

Figure 4- Structural domains in the Meditterranean center, from Lentini et al., 1994, modified), from Volume "Memorie descrittive Carta geologica d'Italia", Sicilia centro occidentale.

2.1.1 Apennine-Maghrebid Chain in the South-eastern area of Central Sicily

In the South-eastern area of central Sicily, west of the Hyblei, outcropping sediments of Plio-Quaternary prevail. In detail, this area has been characterized by a paleogeographic evolution since the Miocen period, during which two mountain chains emerged: Madonie-Nebrodi-Peloritani and the central part of Hyblei mountains. From a stratigraphic point of view, this area is characterized by the following litostratigraphic units as reported below:

- Predominantly clayey complex, with indistinct marly and clayey patches from various Miocene ages and stone blocks of various types - (Tortonian)

-Terravecchia Formation: clays, sandy clays, and sands - (Upper Tortonian)

-Tripoli: white foliated marls with Diatoms rich in fish remains - (Messinian)

-Calcare di Base: compact limestones, vacuolar with more or less evident stratification, literally passing through Cattolica Eraclea Gypsums: macrocrystalline gypsums of large aspect and with intercalated calcareous lenses; marly intercalations are almost completely absent - (Messinian)

-Medium- to fine-grained gypsarenite underlying the previous formation, sometimes laterally passing to a whitish calcarenite and sometimes to a mixed formation consisting mainly of tripoli blocks; saline masses; rock salt and potassium salts - (Messinian)

-Arenazzolo: silty-micaceous clays. Pasquasia chalks: stratified, large-crystal and saccharoid chalks, with marly clay intercalation - (Messinian)

-Trubi: globigerine marls and calcareous marls; clay breccias overlying and intercalated with trubi incorporating "exotics" of various nature and age - (Lower Pliocene)

-Mount Narbone Formation: more or less silty blue-grey clayey marls - (Middle-Upper Pliocene)

-Agrigento Formation: more or less coarse cross-stratified calcarenites with sandy intercalations; grey-blue clayey marls intercalated and in lateral heteropia with calcarenites - (Lower Pleistocene)

-Clayey rocks overlying and sometimes intercalated with the underlying calcarenites encompassing "exotics" of various nature and age.

-Montallegro Formation: yellow Aeolian sands and lagoon sandy clays with gypsum lenses - (Lower Pleistocene)

-Continental deposits (mainly eluvial) attributed to a morphological cycle corresponding to marine terraces between 0-15 m.

-Marine terraces.

-Current coastal sands and dunes.

-Current and recent valley floor floods, sometimes terraced in multiple orders.

- Detritus. Sulfide ore rubble dumps.

2.1.2 Apennine-Maghrebid Chain in the Eastern area of Sicily

The study area(Fig.4) is characterized by a complex structural framework that represents part of the Eastern Sicily. This area shows the Calabride crystalline basement in the north which belongs to the European paleo-margin and, in the south, the Meso-Cenozoic successions of the subducted Ionian Tethys basin. In this framework, the Numidian formation represents a new sedimentary supply formed at the beginning of the collision between the European and African plates and defined the earliest terrigenous Oligocene-Miocene foredeep deposit (Carbone, S., et al.1987). The Numidian Formation is made up of three tectonic units: Serra del Bosco, Nicosia e Monte Salici. In all these units the stratigraphic succession consists of alternations of mudrock levels and quartz-arenites in which the upper part of the Serra del Bosco Unit is characterized by the presence of glauconitic arenaceous horizons very similar to the Upper Oligocene-Serravallian levels of the Monte Judica Unit.

2.1.3 Apennine-Maghrebid Chain in the central-western area of Sicily

Ionide outcrops are identifiable in the Sicani Mountains (Sicani Units), in the Mountains of Palermo, Trabia and Termini Imerese and in the Madonie Mountains (Imerese Units). In central-eastern Sicily, the Ionide outcrops only in the vicinity of Mount Judica, while in the rest of central Sicily they are intercepted only by soundings, as demonstrated by the Gagliano101" survey (Gagliano Unit), which allows us to define the lateral passage between the latter and the Sicanian Units, Fig.5 (Catalano, R., et al.1998). In this context, it is possible to observe the outcrop of the Panormid carbonate platforms

that tectonically overlap the Imerese Unit after becoming detached from the continental crust. The Oligo-Miocene terrigenous covers of the Ionides, instead, are divided into two groups: the first one of "epicontinental" environment, characteristic of the Sicani and Mount Judica Units which is made up of clayey-sandy and bio-calcarenitic sediments characterized by a more or less abundant glauconitic fraction, while the other one is present at the roof of the Gagliano Unit, of the Imerese Unit, within the Lercara Unit and common also to the Panormide Units consisting of clayey-arenaceous deposits, with a prevalence of quartz detritus.

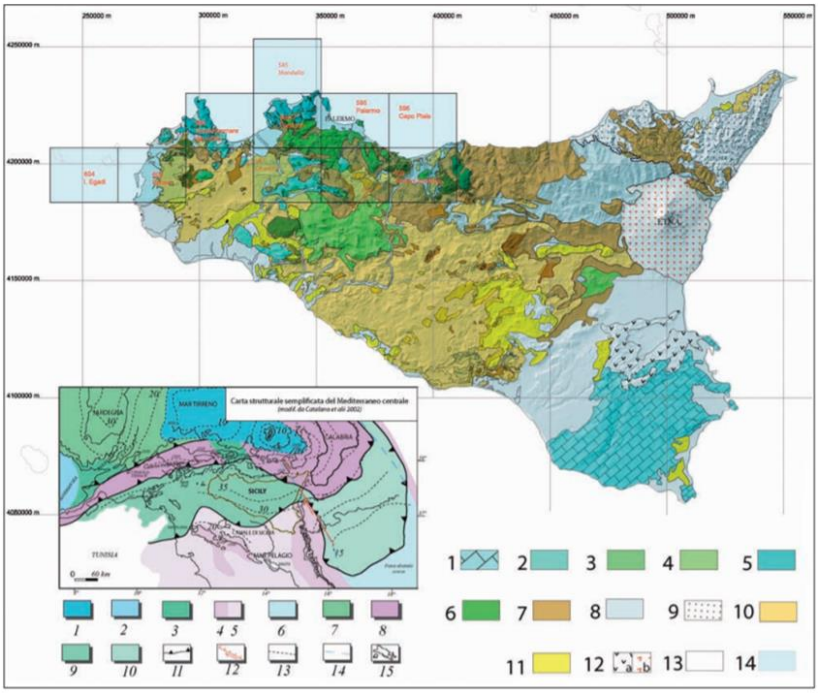

Figure 5- Structural map of Sicily (Di Maggio et al., 2009): 1. Hyblaean Avampaese Unit; 2. Carbonate-Pelagic platform unit (Trapanese-Saccense); 3. Monte Genuardo unit (platform-basin transition); 4. Deep-sea unit (Sicano); 5. Carbonate platform unit (Panormide) 6. Escarpment-basin unit (Imerese-Prepanormide); 7. Miocene flysch unit (Numidian and inner flysch); 8. Sicilid units; 9. Calabro-Peloritan crystalline units; 10. Mio-Pliocene synorogenic deposits; 11. Plio-Pleistocene syntectonic deposits;12. Plio-Quaternary volcanites; 13. Pleistocene deposits; 14. framework of union of CARG geological sheets in scale 1:50.000. The map shown in (b) illustrates the different crustal sectors of the central Mediterranean region (modified from Catalano et al, 2002): 1. oceanic crust of the Tyrrhenian Sea; 2. oceanic crust of the Algerian Basin; 3. thinned Kabyle-Sardinian continental crust; 4. continental (5. thinned) African crust; 6. oceanic crust of the Ionian Sea; 7. Sardinian tectonic units; 8. Kabyle-Calabrian units; 9. Sicilian-Maghrebid units; 10. ionic accretionary prism; 11. overthrust fronts; 12. fault with probable transtensional component; 13. isobaths (in km) of the Moho; 14. hypothetical limit of ionic oceanic crust or passive margin-ionic ocean limit; 15. bathymetry.

2.2 Sampling sites

In the present work, three different clay raw materials have been used as precursor in the alkali activation process:

- Plio-pleistocenic clay
- Numidican clay
- Variegated clay

All materials have been sampled in different parts of Sicily, Fig.6, and show different characteristic according to the geological area in which it outcrops, as reported below:

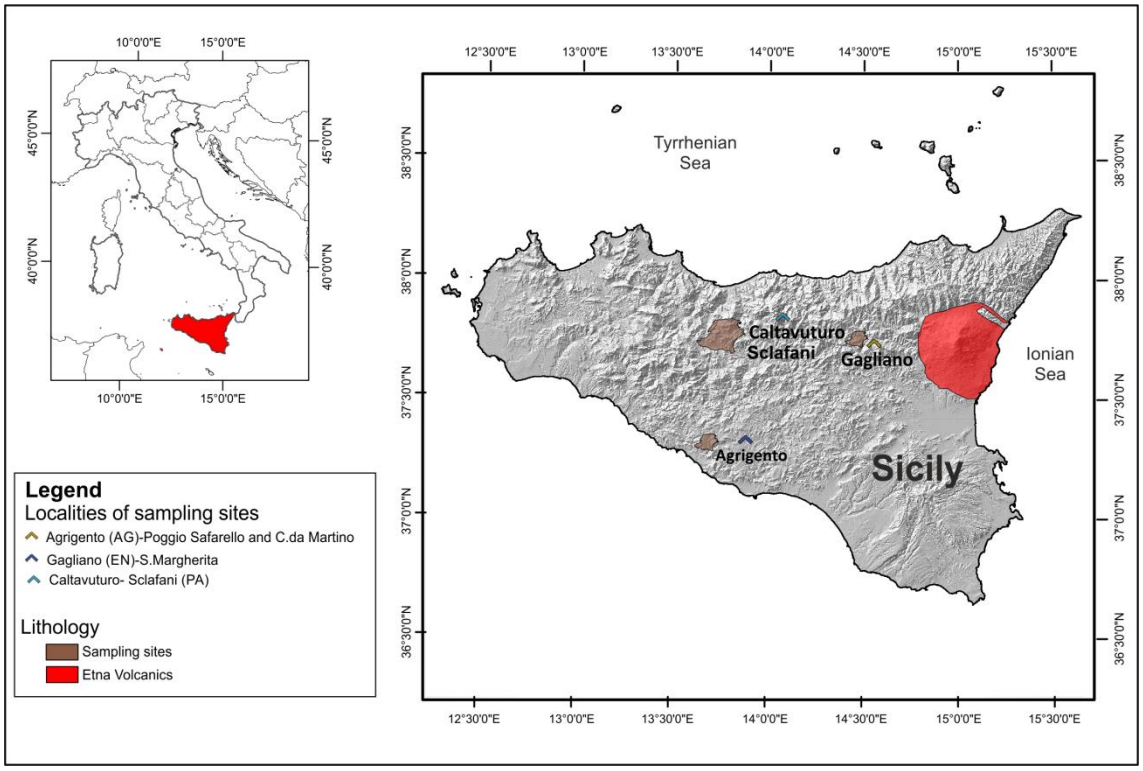

Figure 6- Sampling sites of the three clay raw materials utilized in this work

2.2.1 Plio-pleistocenic clay

The sampling area is represented on the Geological Map of Licata Folded Structure (Central-Southern Sicily) scale 1:50.000 as shown in Fig.7.

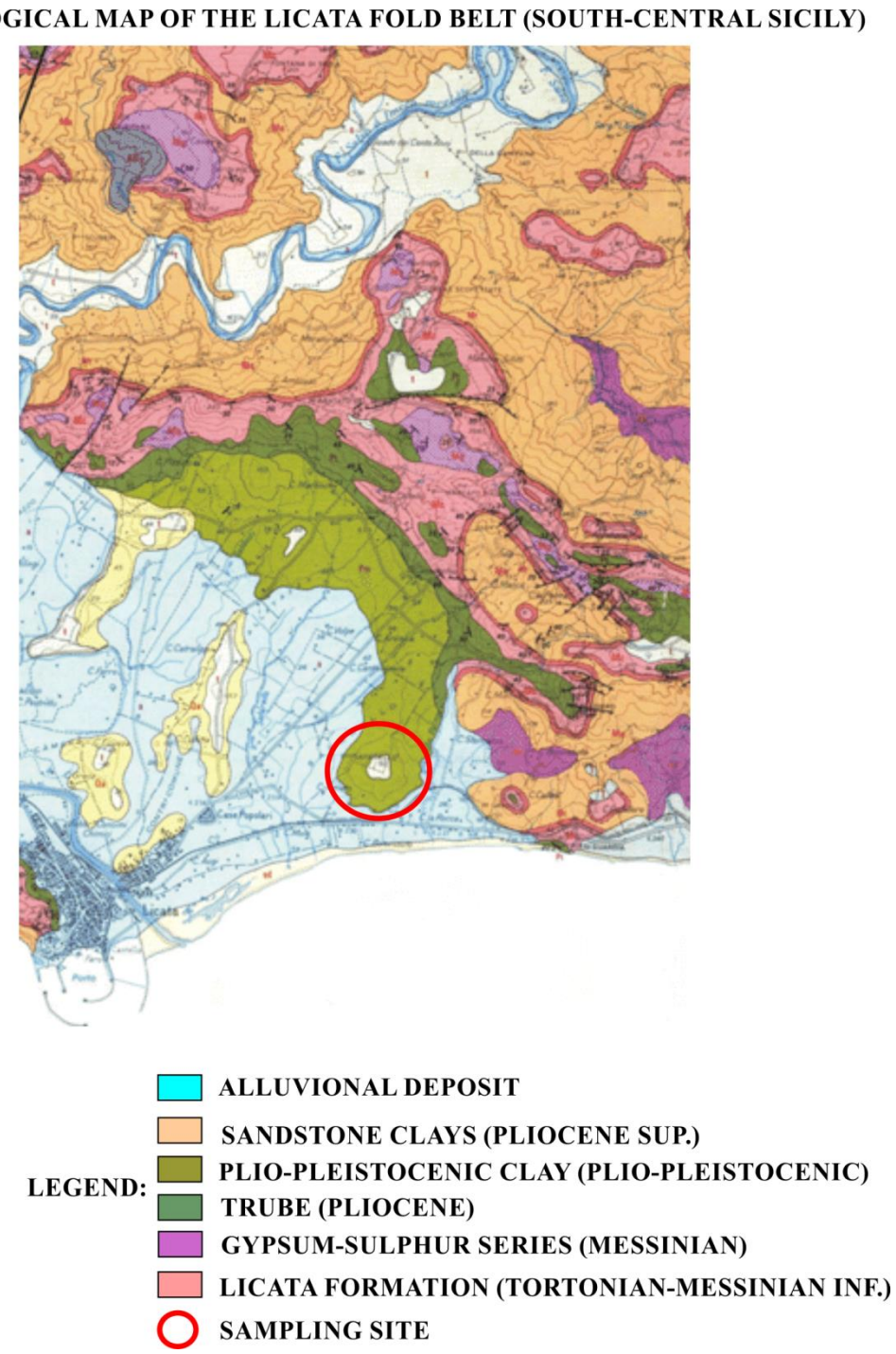

Figure 7- Geological map of the Licata fold belt, (south-central Sicily), scale 1:50.00. In red the sampling areas at Poggio Safanello and near Martino district.

In detail, clay samples outcropping at Poggio Safanello and near Martino district have been used. These formations present limited thickness with shallow slopes, as shown in Fig.8, and a grayish color with an homogeneous granulometry.

Figure 8- Overview of the sampling areas; a) Poggio Safarello and b) Martino district.

2.2.2 Numidican clay

This type of clay has been sampled at Santa Margherita near Gagliano (EN) as reported in the geological map in Fig.9. Macroscopically the sandstones mainly consist of massive-hard quartzose rocks whilst the mudrocks are grey to brown and frequently characterized by a scaly fabric Fig.10.

GEOLOGICAL MAP OF ENNA(CENTRAL-EASTERN SICILY)

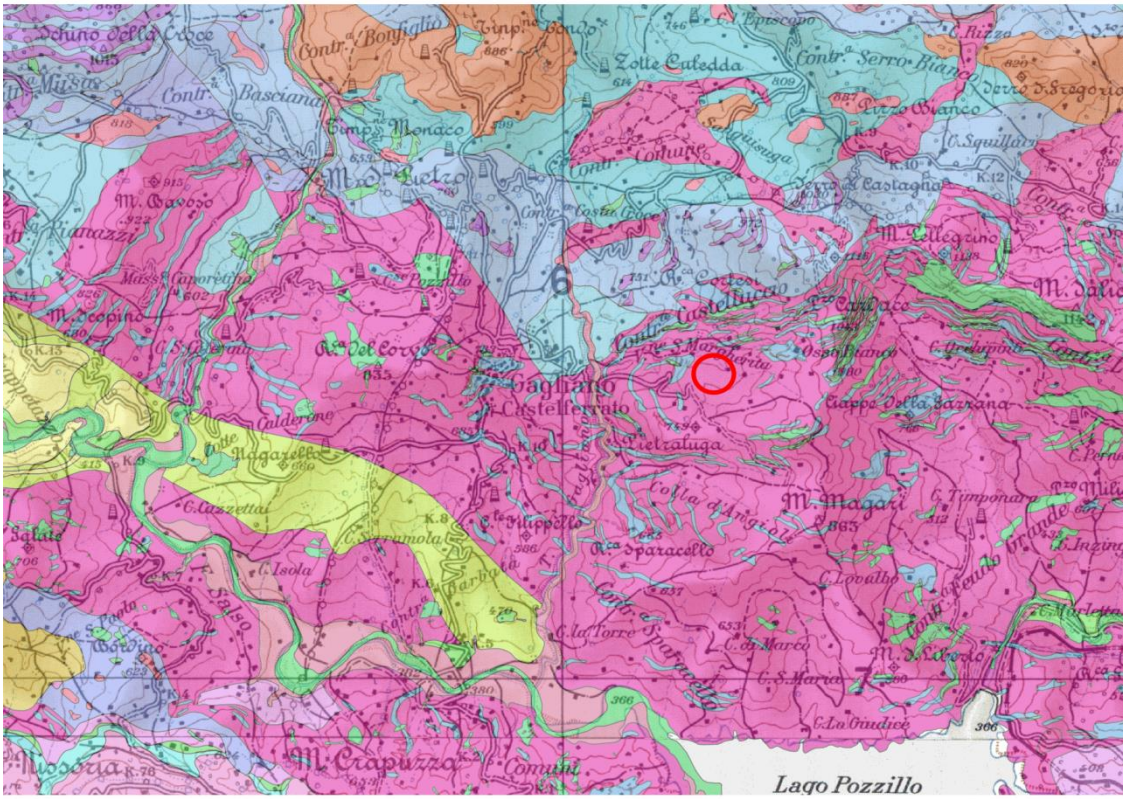

LEGEND:

- ALLUVIONAL DEPOSITS
- NUMIDICAN FLYSCH (NICOSIA UNITS)
- MARLS (TORTONIAN)
- NUMIDICAN FLYSCH (MT. SALICI UNITS)
- SAMPLING SITE

Figure 9- Geological technical study to accompany the Provincial Territorial Plan of Enna (by Geol. Orazio Barbagallo et al.) with a detail on the studied area outcropping at Santa Margherita near Gagliano (EN)

Figure 10- Overview of the sampling area Santa Margherita near Gagliano (EN).

2.2.3 Variegated Clay

The sampling area covers central-western Sicily, near Caltavuturo, where different clay sediments classified as clastic sedimentary rocks have been sampled. As reported in Friedemberg et al.1960, these clay sediments belong to Caltavuturo Formation or to variegated clays and marls, as indicated in the geological map of Mt. Termini Imerese (Cretaceous sup-Oligocene), dating from between 25 and 100 million years (Fig.11). In addition, the clay sampled are referred to the Imerese Unit and to the Caltavuturo Formation of the middle Eocene-lower Oligocene, which is generally characterized by limestones, marly limestones and red, whitish, or grey marls, in layers of 5-30 cm, sometimes associated with grey calcarenites (Lentini F., et al. 1996).

The sedimentary rocks sampled are variegated flaky clays, with reddish-colored portions (CALTAV.1) and greenish-gray portions (CALTAV.2), with a flaky structure formed by elements between about 2-20 cm in size, alternating with calcilutites and calcareous argillites as displayed in Fig.12.

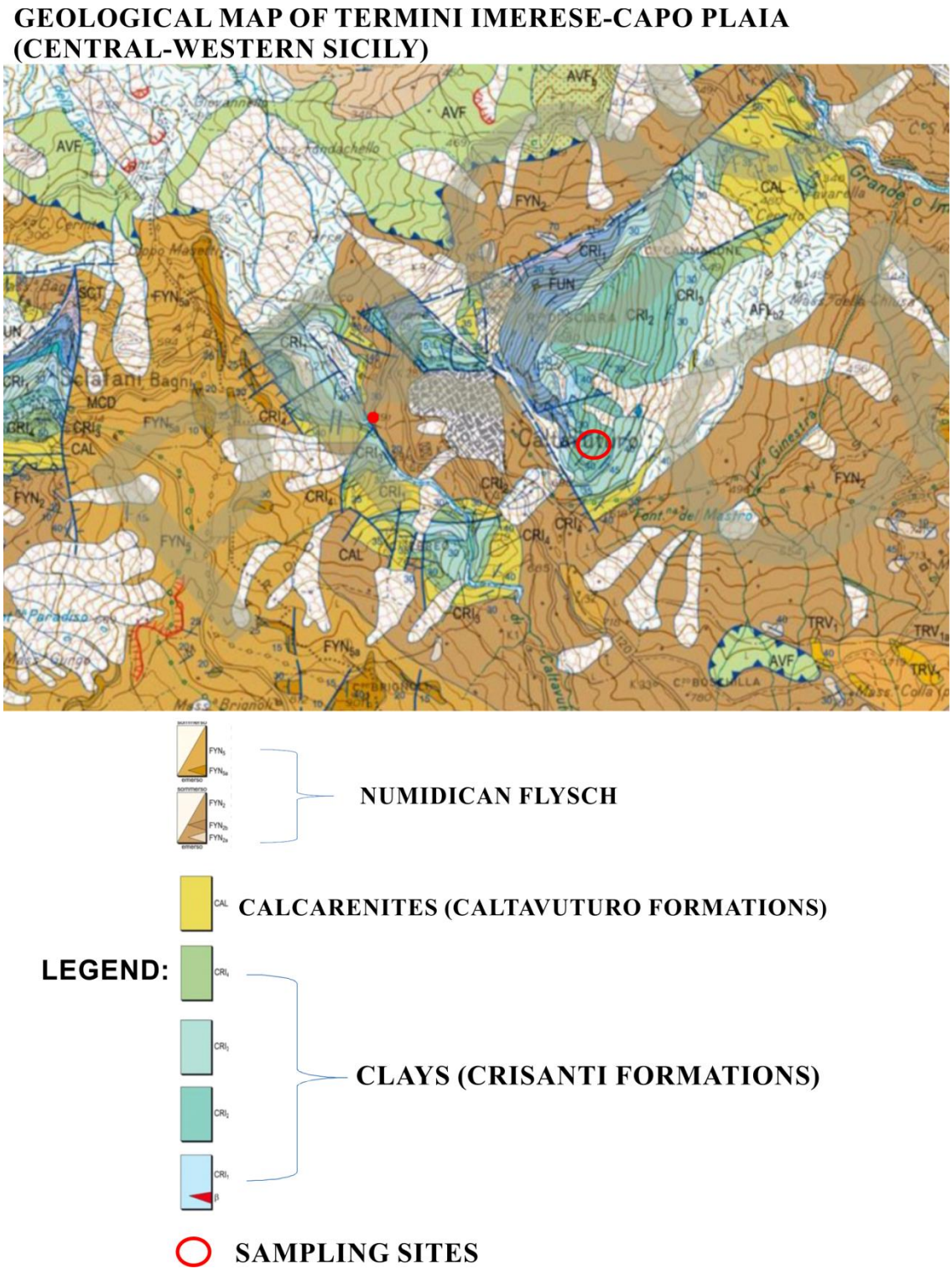

Figure 11-Detail of the Geological Map of the Termini Imerese Mountains and Western Madonie (Abate et al., 1988; scale 1: 50 000) with the outcropping of Caltavuturo Formation (Palermo).

Figure 12- Overview of the sampling area at Caltavuturo (Pa).

3. Characterization methods and results

3.1 Analytical techniques

The selected raw materials and the obtained AAMs have been characterized by different analytical techniques.

- **X-Ray Diffraction (XRPD) -Mineralogical analysis**

Mineralogical investigations were carried out using a Siemens D5000 diffractometer. The instrumental conditions were: Cu-Kα radiation; Ni filter; 2θ angle 3-70°, angular step of 0.02° 2θ; step time 5s; divergence and anti-scatter slits of 1° and receiving slit of 0.2 mm. Profex software was used for mineral identification and semi-quantitative evaluation (Toby and Von Dreele 2013).

In addition to the fraction in toto in which the amorphous abundance was calculated by means of internal corundum standard addition, (Gualtieri et al. 1998), qualitative and semi-quantitative analysis by XRD of clay minerals having particle size <2μm were carried out, adopting a series of procedures concerning sample preparation, acquisition of the diffractograms and their processing. The preparation of the clay fraction <2μm is done by preparing an aqueous suspension in bi-distilled water; then the suspension is centrifuged in order to separate the desired fraction in suspension. The oriented preparations are obtained using a filtration device provided by Millipore™; the filter must be inverted on a slide so that the clay film adheres perfectly to the surface of the glass support, without leaving any air bubbles. The slide is allowed to air dry, and subsequently analyzed. Low-charge expandable clay minerals have the property of interacting with certain organic molecules, such as ethylene glycol, which intercalate within the mineral packages, changing the basal distance. The preparation is carried out by exposing the sample slide placed on a ceramic support to the reagent vapors for at least 8 hours at 60°C in a desiccator placed inside a thermostated oven. Then the glycated sample is analyzed and the two diffractograms (that of the air-dried sample and the glycated one) are compared to verify the presence of expandable minerals.

- **X-ray fluorescence (XRF)- Chemical analysis**

The chemical composition of the three selected raw materials were determined by using a Bruker Tracer IV-SD system equipped with an X-ray tube with Rh target (and Pd slits) source and a mm^2 Silicon Drif Detector (SDD). The pXRF was used directly in situ for a speditive approach. Results were expressed in % by weight as oxides. The instrumental setups used for this study are: i) 15 kV, 35 mA, no filter and vacuum condition for elements from Na to Ca; ii) 40 kV, 17 mA, Ti-Al filter for the heavier elements. Each measurement was carried out as accumulations of 60 s each. The portable spectrometer was mounted on a tripod with an extending arm allowing us to place the measuring head very close to the material to be analyzed. The identification of the elements peaks was acquired directly on the laptop connected to the instrumentation by means of the software S1PXRF. Quantitative data were obtained using PyMCA software based on fundamental parameter calculations. The configuration files were designed considering the Tracer IV-SD specifications, the measurement setup and the rock matrix. Also these results were expressed in % by weight as oxides.

- **Thermogravimetric Analysis - Differential Thermal Analysis (TGA-DTA)**

Regarding Numidican clay, simultaneous TGA-DTA analyses were performed in the laboratory of the Instituto de Ciencias de la Construcción Eduardo Torroja by using a SDT Q600 V20.9 Build 20, while Plio-pleistocenic clay and variegated clay were analyzed on the laboratory of the Environmental Sciences of Firenze by using a TGA Q5000 V3.17 Build 265. For all selected clays, about 40 mg of finely ground clay precursor was dried in an oven at 100 °C in order to remove the humidity, and was then heated at 10 °C/min heating rate in the temperature range 20-1000 °C in an Al_2O_3 crucible.

- **Fourier Transform Infrared spetroscopy (FTIR-ATR)**

FTIR-ATR spectra were obtained on the powdered samples by means of an *Agilent technologies Cary 630 FTIR* infrared spectrometer. Data were recorder at room temperature and the spectra were calculated by Fourier transformation of 64 interferometer scans in a range of wavenumbers between 650 and 4000 cm^{-1} with 4 cm^{-1} resolution. In detail, Infrared (IR) spectroscopy studies the interaction between matter and infrared radiation, (0.7 and 1000 μm).

- **Diffuse Reflectance Infrared Transform Spectroscopy (DRIFT)**

DRIFT analysis were carried out as innovative method applied at these AAMs and results obtained on all the geopolymer pastes cured at 85°C for 20h or at room temperature for 28 days are reported in comparison with the respective raw materials. DRIFT spectra were collected on the powdered samples by means of an *Agilent technologies Cary 630 FTIR* infrared spectrometer. Data were recorder at room temperature and the spectra were calculated in reflectance with 512 interferometer scans in a range of wavenumbers between 5500 and 450 cm^{-1} with 4 cm^{-1} resolution. The software Agilent MicroLab PC controls the system. The spectra are here presented with absorbance (A'= log(1/R)) intensity unity.

- **Raman spectroscopy**

Preliminary tentative investigations were carried out with a portable instrumentation with a handheld measuring head (i-Raman® Plus spectrometer by B&W Tek), equipped with a 785 nm diode laser. Nevertheless, the analyses were mainly conducted with a fixed micro-Raman instrumentation, a Jasco NRS3100 spectrometer equipped with a Notch filter and a Peltier-cooled (-49°C) 1024x128 CCD. In this work, the 532 nm excitation wavelength was employed, reaching, with the 1800gr/mm grating, a spectral resolution of ~3 cm^{-1}. The calibration of the system was verified using the 520.7 cm^{-1} Raman band of silicon before each experimental session.

In order to account for sample in homogeneity, ten spectra per each powdered sample were acquired on different spots employing an Olympus (Japan) 20× objective (N.A.=0.45), with a spatial resolution of about 4 μm. The laser power value was controlled through optical density filters and kept around 1 mW to avoid heating effects. Time and number of accumulations were regulated according to the sample response. In all cases, both the low wavenumber region (130-1200 cm^{-1}) and the high one (3100-3700 cm^{-1}) were investigated.

- **Scanning Electron Microscopy and Energy Dispersive X-ray Analysis (SEM-EDX)**

Morphological analyses were performed utilizing Field Emission Scanning Electron Microscope (SEM) (Zeiss FEG-SEM Supra 25 Microscope) equipped with InLens detector coupled with an energy dispersive X-ray spectroscopy (EDX) system from EDAX to investigate both the samples texture and their chemical mapping from micrometric to nanometric scale. Data were collected by focusing the e-beam on the sample at an energy of 25kV and current of 0.2 nA. The measurements were performed on fragments of

samples fixed on a metal support by using carbon tape and then sputtered with gold. Chemical compositions were expressed in wt% oxide on H_2O- and CO_2-free basis.

- **Vicat Needle Test**

Vicat needle test is the most common procedure for testing cement pastes as indicate in the *ASTM C191* and reported in Fig.13.

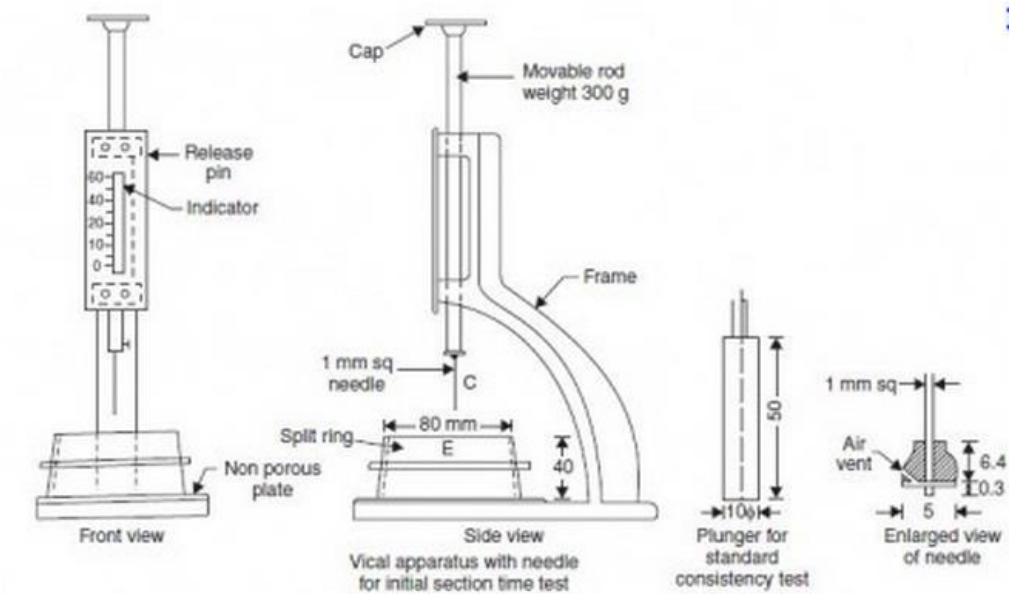

Figure 13- Vicat needle usage diagram by Civil Engineering, Vicat apparatus

This test was carried out in order to better define the setting time of the concrete, mortar or paste as an indicator of workability (Ferraris 1999). The Vicat needle apparatus consist of a 300 g moveable rod with a 1 mm diameter needle at one end. The rod slides through a frame, where an indicator on the rod moves over a scale mounted to the frame. A specimen of fresh cement paste is placed in a conical ring below the frame. Thirty minutes after adding the alkaline solution to the precursor, the mixture is put under the needle, which is released and allowed to settle under its own weight. After this first measure, the test is repeated every 15 minutes until a penetration depth of less than 25 mm is obtained.

- **Mechanical tests**

The specimens were tested for flexural and compressive strength (three specimens for flexural and six for compressive strength) by means of a 70-T1182 Uniframe (Controls) mechanical press in according to the NORMAL UNI EN 1926:20073. Compressive strength were carried out on samples with 324 mm^2 of area, and a speed of 2400 N/s. Flexural strength was determined via three-point bending failure tests with the supports spaced at 6 cm by using samples with 88.88 mm^2 of area and a speed of 20 N/s.

- **Hg intrusion porosimetry (MIP)**

Selected samples were characterized by means Hg-intrusion porosimetry (MIP) to investigate the porosity at sub-micrometric scale once removed humidity in the oven at 100 °C. Porosimetric analysis was carried out with a Thermoquest Pascal 240 macropore unit in order to explore the porosity range ~0.0074 mm < r < ~15 mm (with r indicating the radius of the pores), and by a Thermoquest Pascal 140 porosimeter instrument in order to investigate the porosity range ~3.8 mm < r < ~116 mm.

- **Capillary water absorption test**

The test consists in the determination of capillary water absorption, according to *UNI EN 10859:2000*. In detail, after drying to a constant mass in a oven at 70 °C for 24h, so that the specimens are free of moisture, these are cooled in a dryer. Then, the three edges (x,y,z) are measured with a caliper and the dry weight measured with a precision balance. Finally, three samples for each formulation are placed in a container with 3 mm thick filter paper soaked in distilled water at the base, and weighed at intervals defined as follows: 1 min, 3 min, 5 min, 10 min, 20 min, 30 min, 40 min, 60 min, 4h and 8h.

- **Basic attack in NaOH (8M)**

Basic attack in NaOH (8M) was carried out in order to determine the soluble phases of clay sediment. In detail, this basic attack was conducted by mixing 1.0 g of clay sediment with 100 ml of NaOH solution for 5 hours under stirring at 80±5°C. After the chemical attack, the solutions and the solid residues were separated by filtering, using Albert ash-less filter paper 40,125 mm Ø. The residues were washed with distilled water in order to obtain a neutral pH. Once the residues were completely dry, filters were calcined at 1000°C for 1 hour in a platinum crucible, and the percentage of the reactive phases was

obtained by subtracting the final mass of the residue from the initial mass as reported below:

% Reactive phase = [(Mi*-Mr*)/Mi] x 100

Mi= Initial aluminosilicate mass*

Mr= Residue Mass*

4. Characterization of raw materials and discussion

- **X-Ray Diffraction- Mineralogical analysis**

Clay sediments are mainly composed of clay minerals (smectite, kaolinite, illite, chlorite, interstratified) and, subordinately by quartz, feldspars, carbonates, oxides, etc. For the identification and quantification of all minerals in clay-rich rocks, X-ray powder diffraction was applied by studying interplanar distances (between lattice planes) and studying the distribution of atoms in those planes (Moore, D. M. & Reynolds, R. C. 1997). The XRD analysis of the clayey samples require appropriate treatments and different methods of preparation. For this purpose, two different methods were applied, one related to the clay fraction (<2μm) and the other to the total fraction:

- *Clay fraction <2μm*

The analysis of oriented samples of < 2μm grain size fraction, appropriately treated allows the identification of various clay minerals or groups of them, through the enhancement of basal reflections and the quantification of their abundance ratios.

Comparing the diffractograms of the examined samples (PS, NU and VC), both the air-dried sample and the glycolated sample (Fig.14a-e), the following mineralogical phases can be identified: Illite, Smectite, interstratified illite/smectite, Kaolinite and Chlorite. Semi-quantitative analysis of the clay fraction, reported in Tab.1, was calculated by evaluating the best-fit between the experimental and calculated profiles and was performed on a few representative samples from each sampled area.

Table 3- Semi-quantitative clay minerals: PS (Plio-pleistocenic clay), NU (Numidican clay) and VC (Variegated clay) in %.

ID SAMPLES	SMECTITE	ILLITE	I/S	KAOLINITE	CHLORITE
PS	>1	8	65	20	6
NU	1	10	37	52	n.d.
VC(Calt1)	0.2	5.9	44.6	40.4	8.9
VC(Sclafani)	-	-	80.3	15.4	4.3

In addition, the interstratified order of the samples was determined on the basis of three levels: R=0 disordered, R=1 partially ordered, R=2 ordered. Sample PS (Fig.13a) shows a partial order of the interstratified illite/smectite (R1) representing about 59% and with 24% of kaolinite. In the diffraction traces of Numidican sample (Fig.13b), kaolinite minerals are characterized by sharp peaks at 12.3 2θ and 24.6 2θ. Mixed-layered minerals exhibit several weak reflections in the 16.29-17.05 2θ region which confirms the presence of several types of mixed-layered illite/smectite with different amounts of expandable phases ranging from 20% to 50% with I/S 50 R0 and I/S 80 R1 prevailing (Barbera, G., et al. 2014). Regarding VC series, only two samples have been detected. The first one, labelled Calt1 (Fig.13c-d) shows a partial order of the interstratified illite/smectite (I/S70 R1) accounting for about 44.6% and with 40.4% of kaolinite, while the second, labelled Sclafani (Fig.13e) shows ordered interstratified illite/smectite (I/S90 R3) accounting for about 80.3% and only 15.4 % of kaolinite, as reported in Tab.2.

Table 4- Semi-quantitative analysis of clay minerals

ID Sample	DiSm	I/SR0	I/SR1	Kao	I	DiChl
Plio-pleistocenic clay	n.d.	n.d.	59	24	13	3
Numidican clay	1	19	11	60	10	n.d.
Variegated clay: Calt1			44	40	6	9
Variegated clay: Sclafani	**DiSm** n.d.	**I/SR0** n.d.	**I/SR3** 10	**Kao** 2	**I** n.d.	**DiChl** n.d.

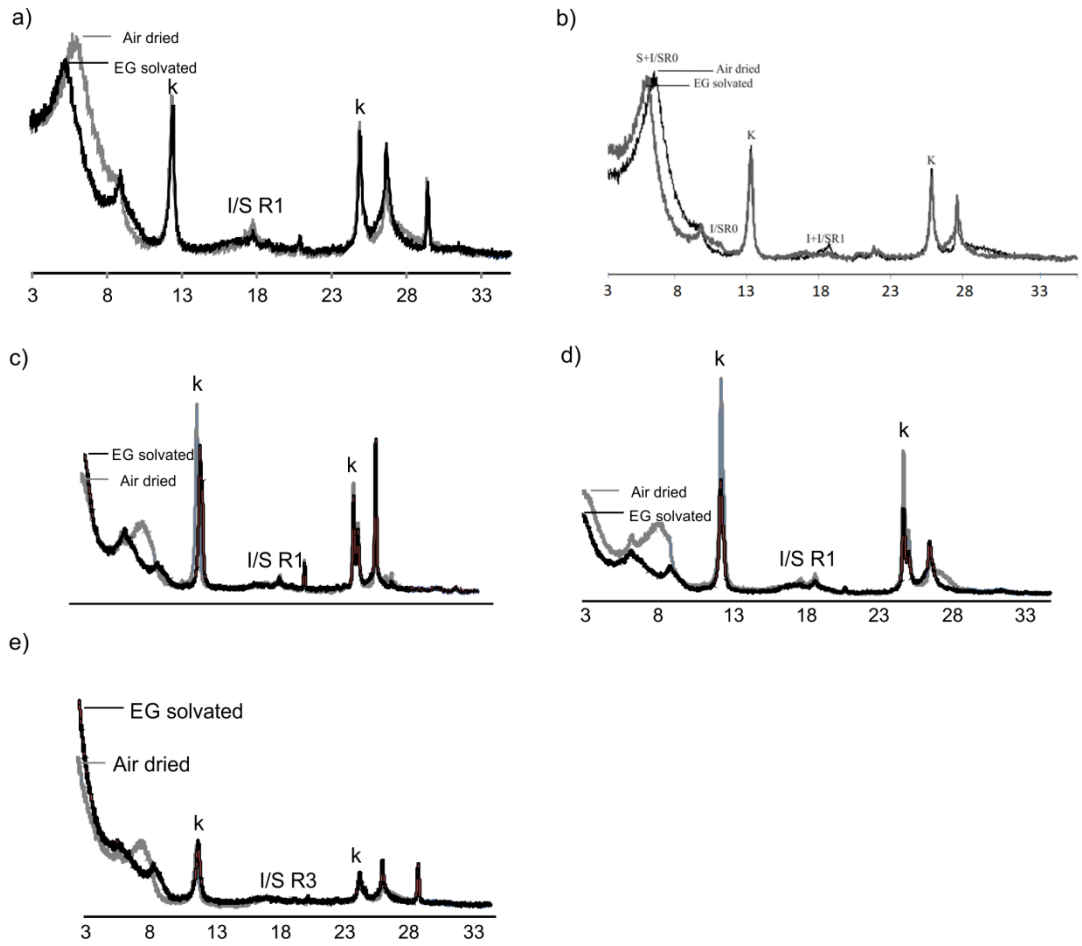

Figure 14-Comparisons are shown between spectra obtained on the oriented samples and the same glycolates: a) Plio-pleistocenic clay; b) Numidican clay; c) Varicolored clay: Calt1; d) Varicolored clay: Calt2; e) Varicolored clay: Sclafani; k: kaolinite; I/S: interstratified Illite/smectite; R=1 interstratified I/S partially ordered; R=3 1 interstratified I/S ordered.

- *Bulk samples*

As displayed in Fig.15, the XRD pattern shows the principal mineralogical phases for clay sediments and the modified mineralogical compositions due to the thermal treatments at two different temperature (550 °C and 700 °C for 3 h).

-Plio-pleistocenic clay: Fig.15 shows the XRPD pattern of Plio-pleistocenic clay raw material (PS), the same (PS500) after thermal treatment at 550°C for 3h and finally that calcinated at 700° for 3h.

Mineralogical composition of PS raw material shows the presence of quartz and calcite. Other phases as k-feldspar, albite and clay minerals are detected.

Clay thermally treated at 550 °C for 3h shows the same phases to the previously identified phases.

PS700 mineralogical composition is similar to the previous ones. As shown from the XRDP pattern, the most intense reflections are related to quartz and k-feldspars, while the others are related to calcite and illite. Peaks at 31°,36° and 52° 2θ show presence of lime while peaks related to kaolinite and montmorillonite disappear as a consequence of the thermal evolution of the crystalline structure in the calcinated clays.

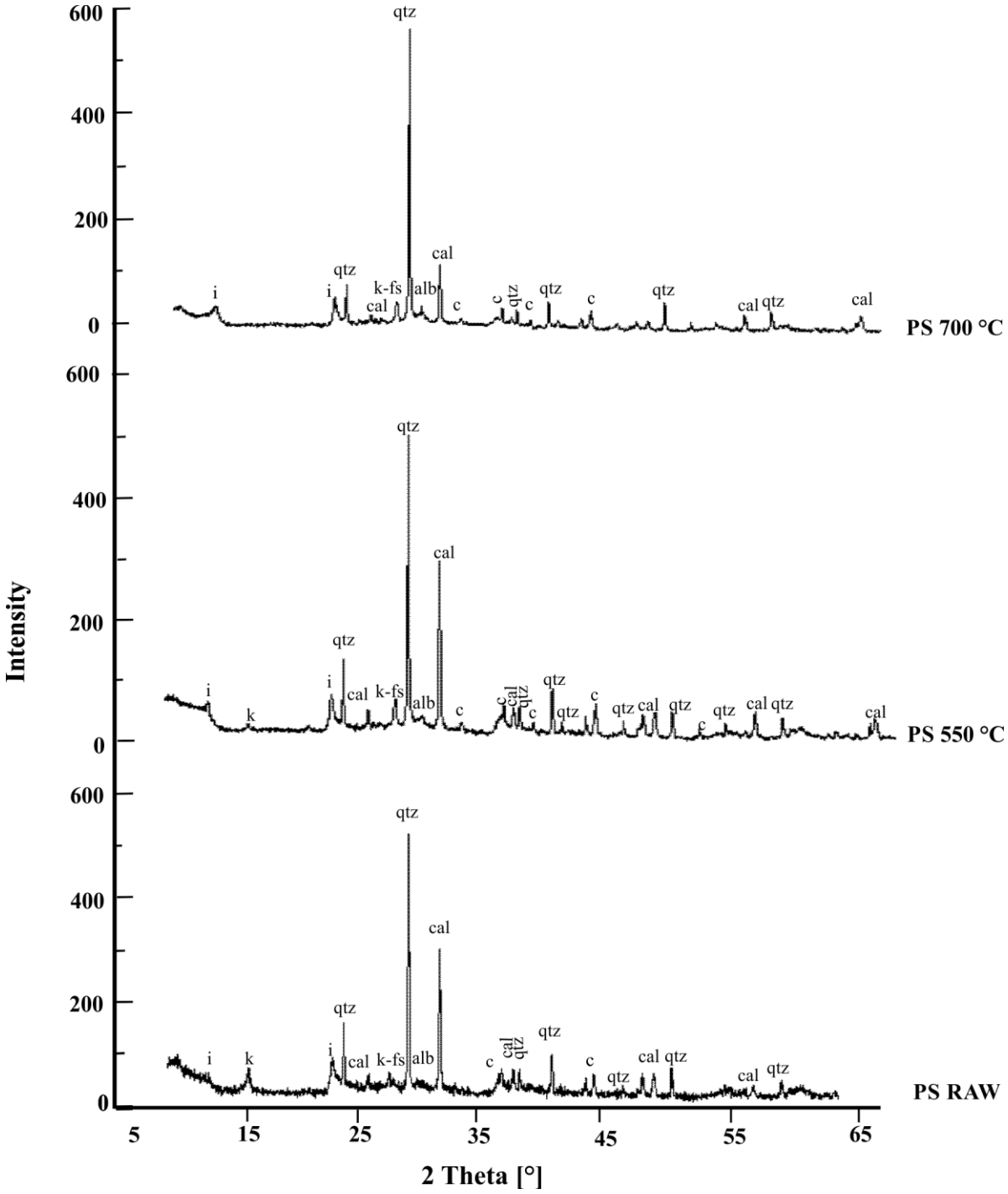

Figure 15- Mineralogical composition of samples PS RAW, PS550 °C and PS700 °C; i=illite; k=kaolinite; qtz= quartz; k-fs=k-feldspars; cal=calcite;

-Numidican clay: The mineralogical composition of the Numidican raw material, as reported in Fig.16, shows different mineralogical phases. The most intense reflections are related to quartz, k-feldspar, albite and clay minerals (montmorillonite, kaolinite, illite and chlorites). Calcite is not present.

Numidican clay calcinated at 550 °C and 700 °C for 3h, present the same mineralogical composition as the unfired material (Barbera, G., et al. 2014). In detail, the two calcinated samples labelled NU550 and NU700 show a structure evolution during which clay minerals as kaolinite, chlorites and montmorillonite, disappeared above 550°C, as confirmed in (Ferone et al. 2015). As shown from the XRPD pattern, the most intense reflections are related to quartz and k-feldspars. Defined peaks at 8°,19° and 34° 2θ reveal the presence of muscovite.

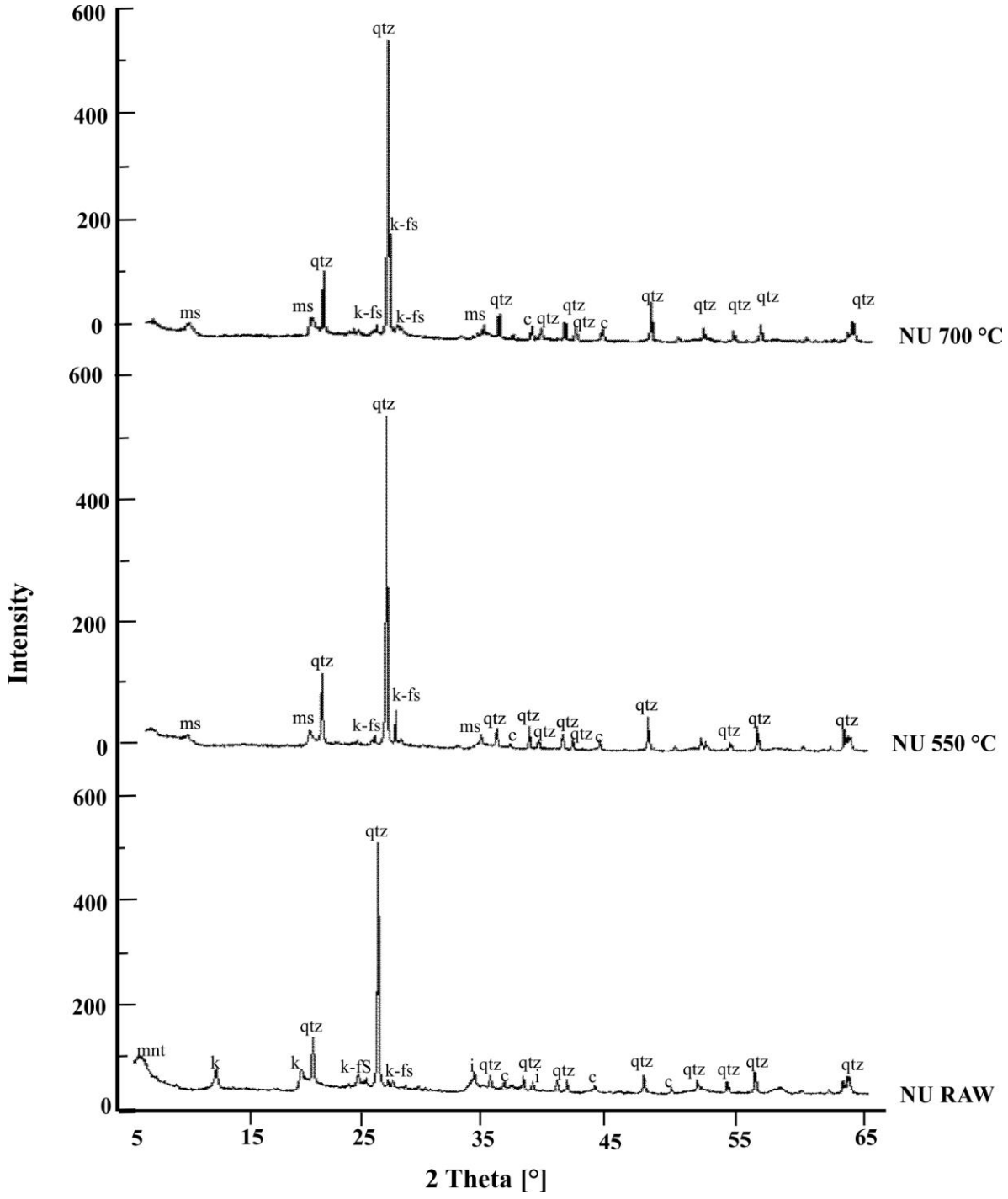

Figure 16- Mineralogical composition of samples NU RAW, NU550 °C and NU700 °C; mnt= montmorillonite; k=kaolinite; ms= muscovite; qtz= quartz; k-fs=k-feldspars; cal=calcite;

-Variegated clay:

In Fig.17, the same crystalline structure modification of the variegated calcinated clays in respect to the unfired clay can be observed. As shown from the XRPD pattern, the unfired clay shows the same mineralogical composition of the previous ones as quartz, k-feldspars and clay minerals as illite, montmorillonite, chlorites and kaolinite. In addition, peaks at 19°,24°,25°,62° and 64° 2θ reveal the presence of hematite.

Regarding the clay calcinated at 550 °C and 700 °C for 3h, with respect to the unfired material (Barbera, G., et al. 2014), they present the same mineralogical composition. In detail, the two calcinated samples labelled VC550 and VC700 show a mineralogical evolution in which the most intense reflections are related to quartz and k-feldspars while peaks related to kaolinite and chlorites disappear after thermal treatment at 550 °C.

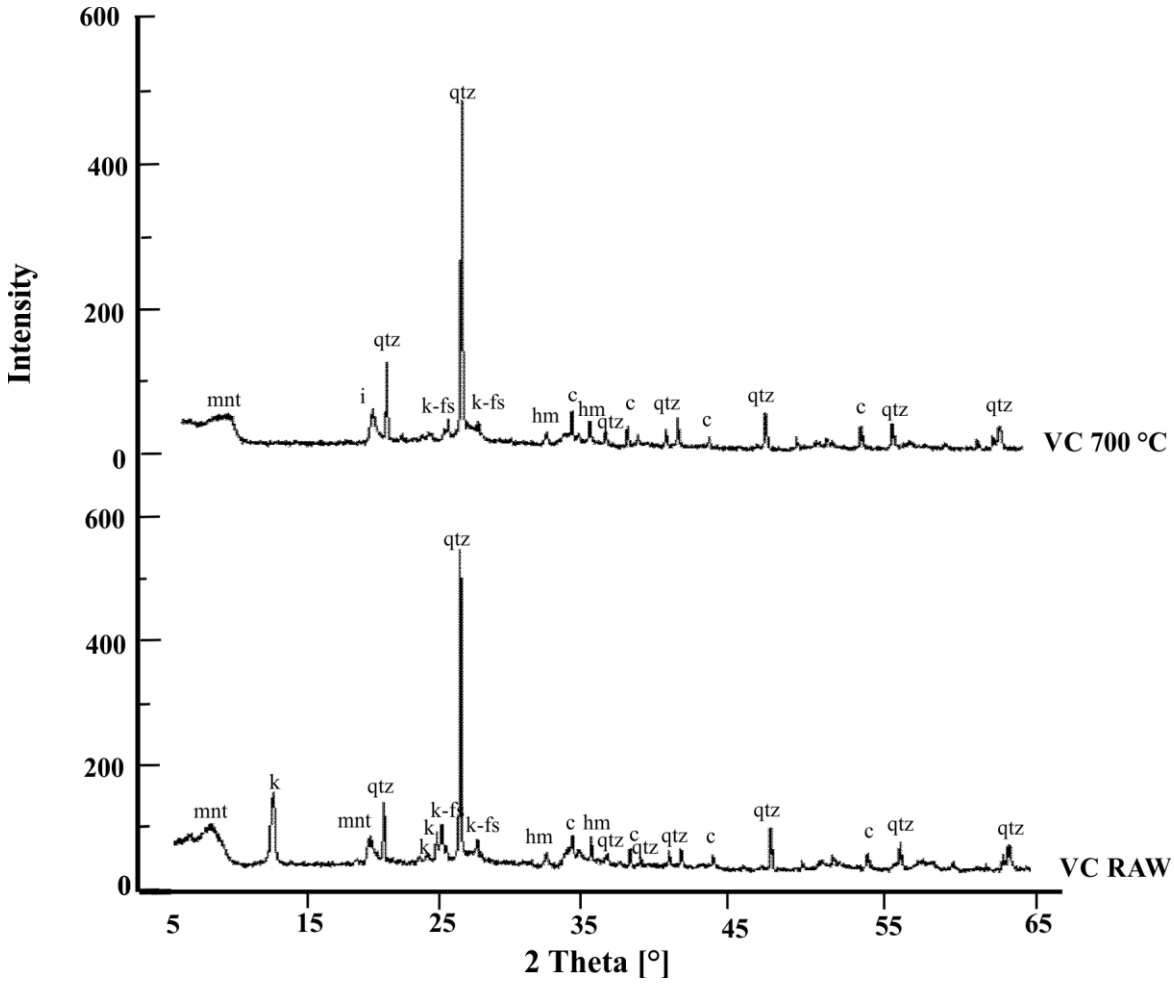

Figure 17- Mineralogical composition of samples VC RAW and VC700 °C; i=illite; k=kaolinite; mnt= montmorillonite; qtz= quartz; k-fs=k-feldspars; cal=calcite; hm= hematite.

Generally, comparing XRPD pattern of all clays it is possible to highlight the thermal evolution of the crystalline structure with particular reference to calcite which is still present in the unfired material. After increase the temperature up from 550 °C to 700 °C, the calcite content decreases while kaolinite that appears in the clay structure treated at 550 °C disappears at 700 °C. The presence of illite is noted in all patterns due to its high thermal stability.

- **X-ray fluorescence (XRF) - Chemical analysis**

The chemical composition of the clay raw materials are reported as oxides in Tab.3 and displayed in Fig.18. As regards Plio-Pleistocenic clay, SiO_2, Al_2O_3 and CaO represent the main components while, Fe_2O_3, K_2O and Na_2O were present in lower concentrations. Compared to the abovementioned one, the Numidican and Variegated clays both have a lower content of CaO.

Table 5- Chemical composition of clay sediment, Plio-Pleisocenic clay (PS), Numidican Clay (NU) and Variegatedclay (VC).

Samples	ID	SiO_2	TiO_2	Al_2O_3	Fe_2O_3	MnO	MgO	CaO	Na_2O	K_2O	P_2O_5
Plio-pleistocenic clay	**PS**	57.73	0.75	14.54	5.01	0.06	2.71	15.61	1.25	2.17	0.17
Numidican Clay	**NU**	65.5	0.98	17.3	4.97	-	0.83	0.08	1.11	1.68	0.09
Variegated clay	**VC**	58.59	0.82	25.11	8.7	-	2.68	0.34	1.49	2.27	-

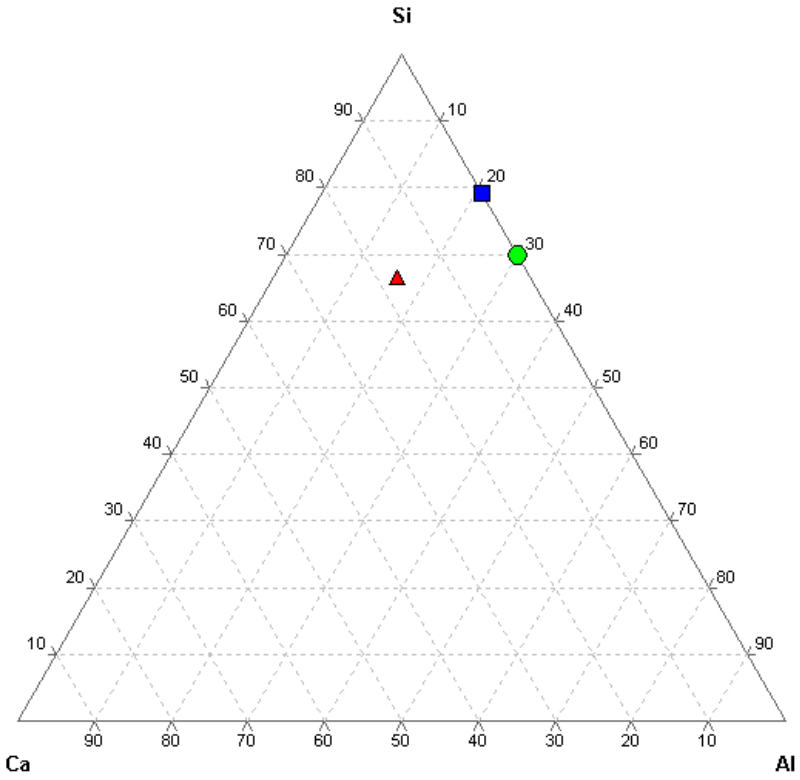

Figure 18- Ternary diagram on the composition of clay sediment, Plio-Pleisocenic clay (PS), Numidican Clay (NU) and Variegated clay (VC).

- **Thermogravimetric Analysis - Differential Thermal Analysis (TGA-DTA)**

The result of thermal analysis carried out on both clay raw materials and the weight loss are reported in Tab.4.

Table 6- Result of thermal analysis carried out on both clay raw materials and their weight loss: (PS3-Plio-pleistocenic clay; AS22- Variegated clay; NU- Numidican clay);

n° step	Temperature (°C) / weight loss (%w/w)		
	PS3	**AS 22**	**NU**
1	**57 °C**	**60 °C**	**65°C**
	(3.3%)	(2.8 %)	(0.65%)
2	**237 °C**	-	**235 °C**
	(0.4 %)	-	(2.40 %)
3	**502 °C**	**512 °C**	**515 °C**
	(4.1 %)	(4.9 %)	(5.53%)
4	**710 °C**	**-**	**715 °C**
	(7.4 %)	-	(7.80%)
Residue (900 °C)	**84.8 %**	**92.3%**	**83.6%**

Clays usually show three different steps of mass loss. The first, in a temperature range between 45° and 150°C, can be attributed to hygroscopic loss of surface water. The other two, around 500°C and 700°C respectively, are related to the loss of structural hydration water and to decarbonation phenomena. In some cases, (Numidican clays, Plio-pleistocenic clays), the presence of a small mass loss (about 1%) was observed around 250°C that could be due to the presence of organic matter.

Numidican clay thermal analysis is reported in Fig.19. In detail it is possible to observe a weight loss related to the adsorbed water in the range 20 °C - 100 °C, while in the range 400 °C - 700 °C it is possible to observe a weight loss related to the oxidation of different organic residues. This weight loss in the range 400 °C- 700 °C can be related to the structure collapse of the clay phases, indeed the greatest loss in weight begins at 515 °C for about 5.53% and ends at 715 °C for about 7.80% with a final residue of about 83.6%. This process finds support in the literature data in which clay sediments were thermally treated in a temperature range of about 500 °C – 800 °C to determine the reactivity of the clay materials (Ferone et al. 2015).

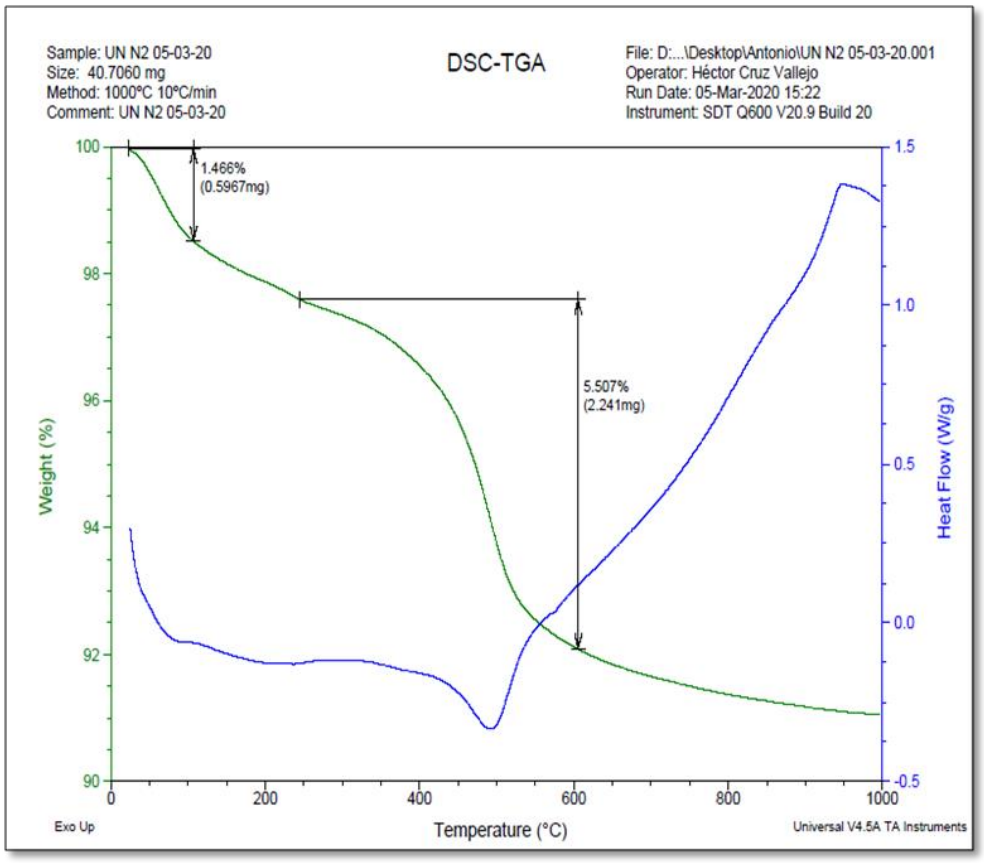

Figure 19- DSC-TGA on the Numidican clay raw material. The green line shows the loss in weight of the sample as the temperature increases, while the blue line indicate the heating ramp.

The TGA analyses carried out on the plio-pleistocenic and variegated clays are shown in Figg.20-21 and reported in (E. Pulidori et al. submitted), allows us to identify diverse weight loss in the range 25 °C- 900 °C. The first weight loss recorded is of 3.3% at 57 °C (temperature of maximum degradation rate) while the second at around 135 °C that can be attributed to the loss of surface hydration water; there is also a weight loss of 0.4% at 237 °C probably related due to the presence of organic matter or halloysite, and weight losses of 4.1% at 502 °C probably related to the loss of structural hydration water. At 701 °C a mass loss of about 7.4% is identified probably related to the decomposition of the calcite ($CaCO_3$) into CaO and CO_2.

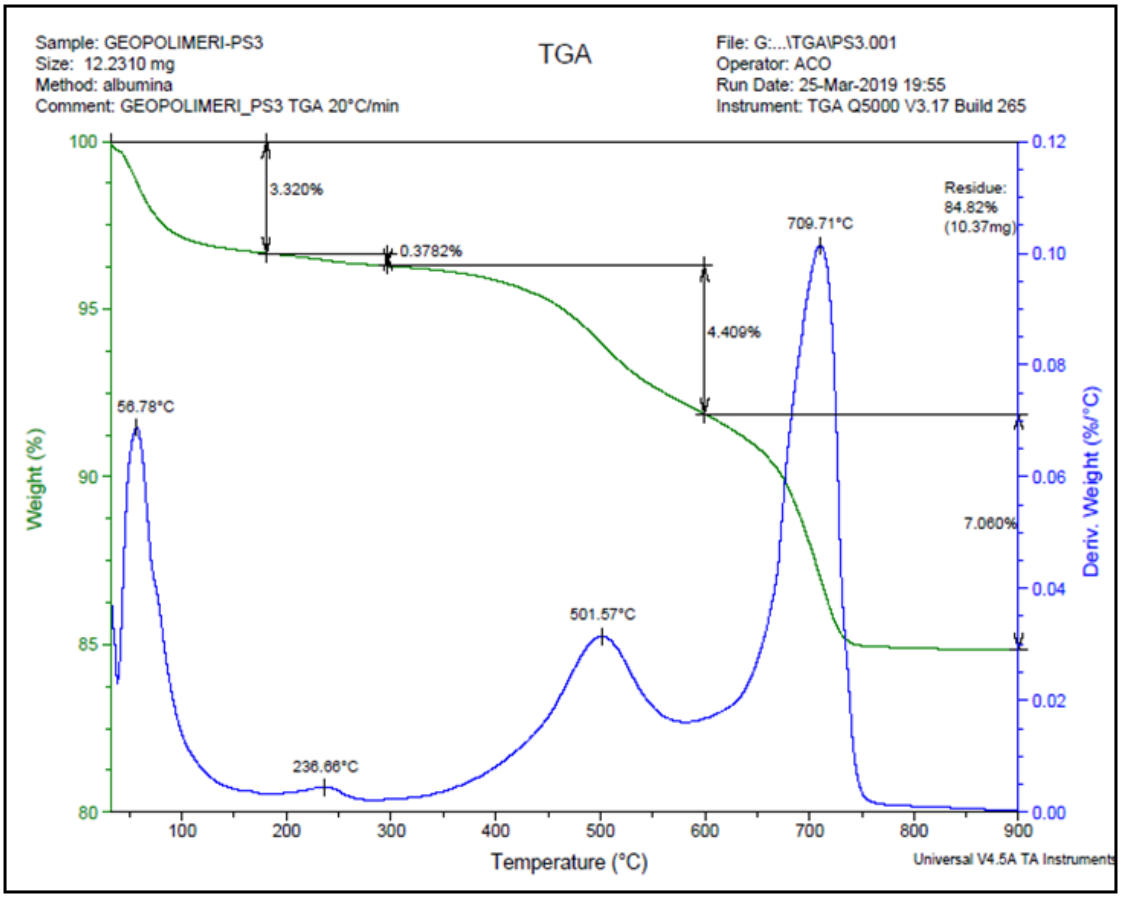

Figure 20- TGA on the Plio-pleistocenic clay. The green line shows the loss in weight of the sample as the temperature increases, while the blue line indicate the heating ramp.

For what concerns the variegated clay, three different points of weight loss were detected: the first one of 2.8% at 60 °C while the second at around 135 °C with an inflection that can be attributed to the loss of surface hydration water. Another weight loss was recorded at 512 °C of about 4.9% with a residue of 92.3% that remains stable up to the temperature of 1000 °C where the analysis was interrupted.

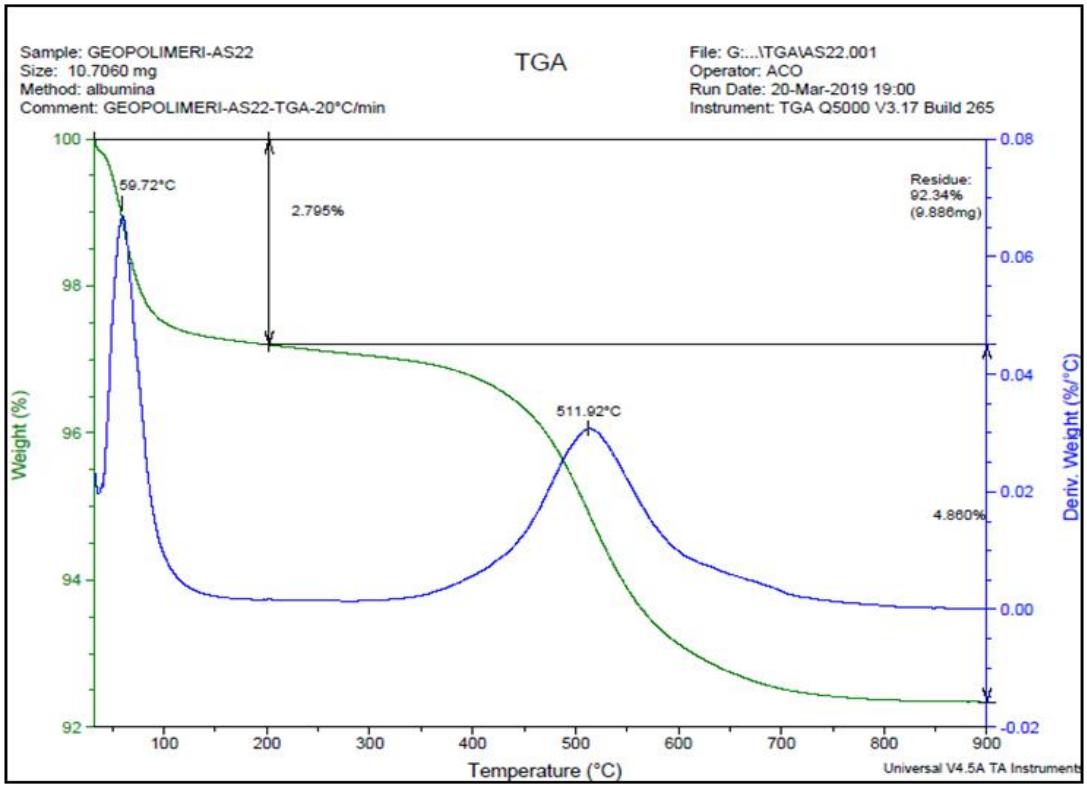

Figure 21- TGA on the Variegated clay. The green line shows the loss in weight of the sample as the temperature increases, while the blue line indicate the heating ramp.

It is interesting to note that, following the heating up to 1000°C, the coloration of both clays changed from a brown to a reddish colour, a sign that, even under nitrogen flow, partial oxidation processes of the iron oxides present in the clay occurred.

- Fourier Transform Infrared Spectroscopy in Attenuated Total Reflection (FTIR-ATR)

The FTIR spectra of the calcined clay materials, displayed in Fig.22 a,b,c, showed that the clay structure was collapsed after 3 hours at 700 °C. In detail, the spectra of clay raw materials show the presence of vibration bands, in the –OH stretching region, at 3704 and 3693 cm^{-1}, related to the octahedral $Al^{(VI)}$- OH layer. In the range 3400-1600 cm^{-1} bands related to tension deformation of H-O bonds of unstructured H_2O in this material were detected. Signal of the band generated in the range 1440-1400 cm^{-1} related to the C-O bonds of carbonates showed a low intensity are present only in the Plio-pleistocenic (PS) clay due to the presence of calcite, as confirmed by the XRD pattern. Finally, in the range 930-315 cm^{-1} bands representative of the clay minerals were observed (Hughes, T.L., et al. 1995). As regards FTIR spectra of the calcined clays, it is possible to observe how the band of the octahedral $Al^{(VI)}$ - OH layer disappeared as a consequence of the clay dehydroxylation. Around 1000 cm^{-1} an intense band related to the vibrations of the T-O and Si-O-T (T=Si/Al) bonds of the silico-alluminate phase of these materials appears. The signals at 793 cm^{-1}, 780 cm^{-1} and 685 cm^{-1} are characteristic of the vibration of Si-O bonds of the quartz (Farmer 1974; Gasparini, E., et al. 2015). The presence of quartz in the original raw materials, give rise to a series of bands at 793- 777 cm^{-1} (double band) and 693 cm^{-1}. Also feldspars show a broad band in the region between 1000 cm^{-1} and 1100 cm^{-1}, and at lower wavenumbers at 727 cm^{-1}. The same phases can also be observed at lower wavenumbers in the samples treated at 700°C for 3h.

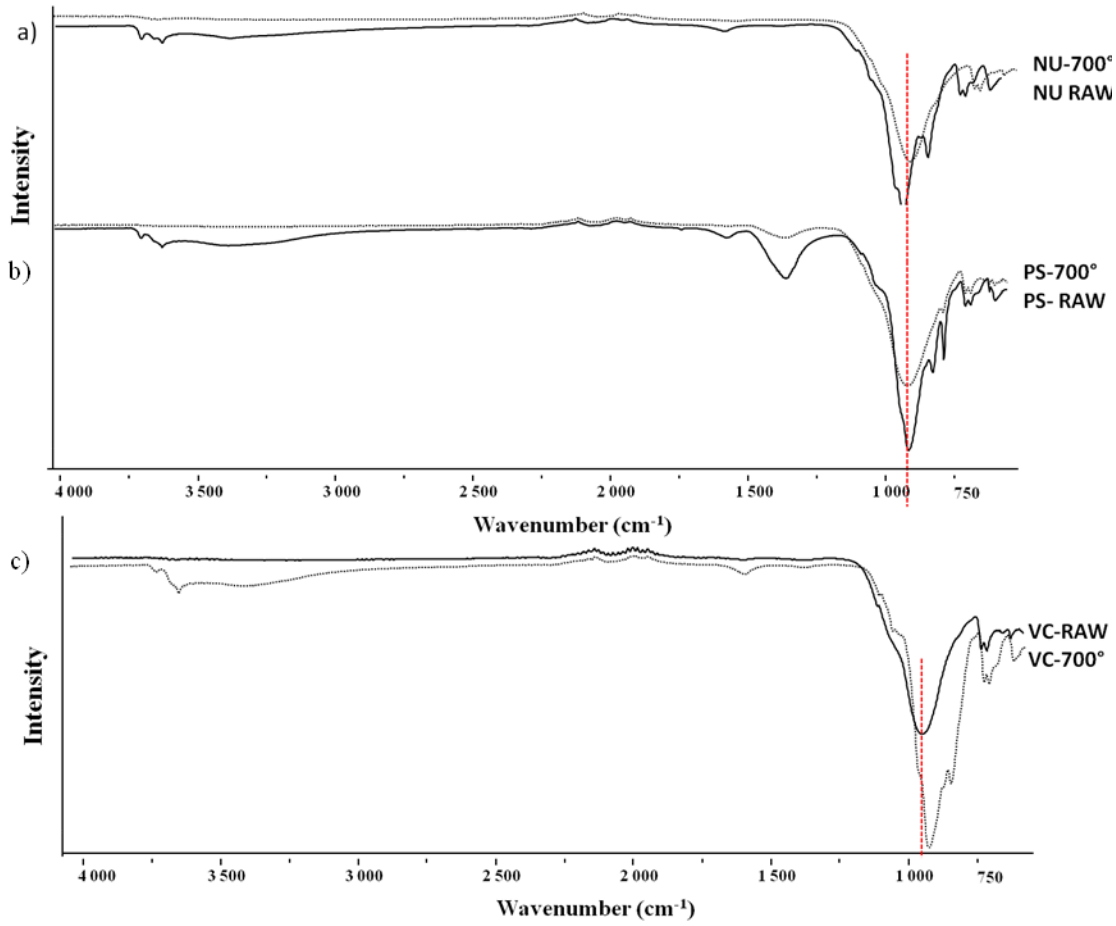

Figure 22- FTIR spectra of the three clay raw materials (linen black) and calcinated clay materials (line grey). In detail, a) Plio-pleistocenic clay, b) Numidican clay, c) Variegated clay. The black line represents the clay raw material while the grey one represents the calcinated clay at 700 °C. The red line indicates the center of the aluminosilicate band of the raw material to highlight the shift towards lower wavenumbers of the calcined clay band.

- **Raman spectroscopy**

Raman analysis were carried out only on the plio-pleistocenic clay calcinated at 700° for 3h. It is well known that Raman spectroscopy is not the ideal technique to be employed for clay minerals analysis, due to the low polarizable character of aluminosilicatic bonds in the clay lattice (V.Košařová, et al. 2013), giving weak Raman signals and overlapping fluorescence (Kloprogge 2017).

Nevertheless, in the calcined precursor, the signals of hematite can be recognized being iron oxides characterized by more covalent bonds (V.Košařová, et al. 2013) together with those of anatase (M.C. Caggiani, et al. 2021); The spectra acquired with the green laser are mainly dominated by hematite signature: this dissuades from the use of a red laser for the analyses, since it would further enhance its revelation to the detriment of the aluminosilicatic phases.

- **Basic attack in NaOH (8M)**

For all the calcinated clay sediments utilized in this study, the fraction of reactive phases in the starting material were determined by means a basic attack using NaOH (8M). The residues were washed with distilled water in order to obtain a neutral pH and were completely dry, filters were calcined at 1000°C for 1 hour in a platinum crucible, and after the percentage of the reactive phases were calculated by subtracting the final mass of the residue from the initial mass as reported below:

% Reactive phase = [(Mi*-Mr*)/Mi] x 100

Mi= Initial aluminosilicate mass*

Mr= Residue Mass*

Considering the obtained results, all clay raw materials have shown potentially soluble phase of 74 wt% for Plio-pleistocenic clay (PS), of 57 wt% for Numidican clay (NU) and of 42% for Variegated clay (VC) as reported in Tab.5. After basic attack with NaOH 8M, Plio-pleistocenic clay display a greater solubility towards alkaline activation process due to the presence of some mineralogical phases, as kaolinite, that tend to dissolve in alkaline environment in a range of pH ~12-13.

ID SAMPLES	SOLUBLE PHASE wt%
PS	74
NU	57
VC	42

Table 5- Potentially soluble phases for the starting aluminosilicate materials

5. AAMs binders

- Samples preparation

The three raw materials used for this study such as *Plio-Pleistocenic clay* (labelled PS), *Numidican clay* (labelled NU) and *Variegated clay* (labelled VC) have been thermally treated in order to improve their reactivity before being employed as precursors for AAMs. As reported in literature, thermal activation generally involves a dehydroxilation of clay minerals in a temperature range of about 500 °C to 800 °C (Heller-Kallai 2006). The thermal treatment can determine the increase of the geopolymeric reactivity and a consequent increase in terms of compression strength of the obtained final product (Xu and Van Deventer 2002). For this study, the three selected clays were grounded in a ring mill, after drying at 100 °C in an oven for 1 hour and finally were thermally treated at two different temperatures (550 °C and 700 °C for 3 h) in order to assess differences in reactivity in the geopolymeric process (Buchwald, A., et al. 2009).

The selected starting materials for the preparation of AAMs were activated with sodium hydroxide solutions (NaOH 4M, 6M and 8M), provided by Carlo Erba company (*code: 373908*), and sodium silicate solution provided by Ingessil s.r.l. with a molar ratio $SiO_2/Na_2O = 3$, Fig. 23-24.

The Liquid/Solid ratio is an important factor to consider, during the samples preparation, in order to obtain a highly viscous paste and for casting it in the moulds. For each formulation, it has been chosen a L/S ratio variable from 0.40 to 0.58. Moreover, different $NaOH/Na_2SiO_3$ % weight percentages were considered in order to investigate the best conditions to avoid efflorescence on samples' surface after air exposition.

The obtained alkali activated pastes, were mixed for 5 minutes by using a mechanical mixer in order to obtain a good workability and were then cast in moulds of 1×1×6 cm in size and compacted by mechanical vibrations for 60 s to remove air bubbles. All samples were cured at 85°C for 20h, in order to improve the alkaline reaction, and at room temperature (22±3°C) for 28 days keeping the humidity level always > 90%. At the end of the curing, specimens were demoulded, stored and analyzed.

In order to investigate the physical and mechanical properties of the obtained geopolymer binders, two set of formulations were produced:

- the first one was obtained by mixing all selected clay materials thermally treated at 550°C with sodium hydroxide solutions (NaOH 4M, 6M and 8M) and sodium silicate solution Na_2SiO_3;

- the second one was prepared by using mixtures of clay, only thermally treated at 700 °C, activated with sodium hydroxide solutions (NaOH 4M, 6M and 8M) and sodium silicate solution Na_2SiO_3;

Only samples activated with clay thermally treated at 700 °C have reach maturity after curing at 85 °C for 20h and 28d at room temperature, while pastes obtained by using clay thermally treated at 550 °C for 3h did not generate the best conditions for alkaline activation due to the poor reactivity of the raw material.

Figure 23- Geopolymer preparation scheme

Details of each paste (starting materials proportions and synthesis parameters), shown in Fig.25, are reported in Tab.6.

Figure 24- Geopolymerization process: a) clay raw material; b) and c) manual press and sieves < 75 and 20 µm; d) aluminosilicate clay precursor with grain size <20 µm; e) Sodium hydroxide 8 molar; f) geopolymer mixture; g) geopolymer sample;

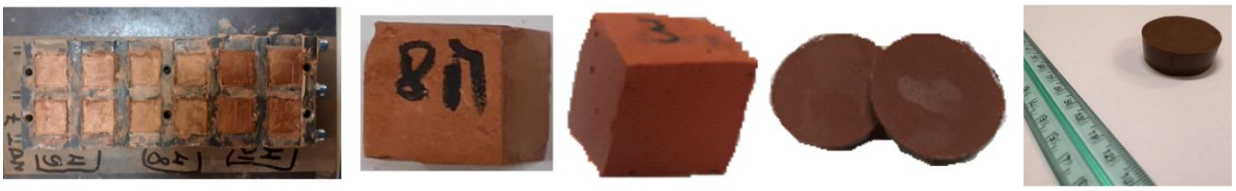

Figure 25- Same geopolymer samples obtained after Alkali-activation process

Table 6- Detail of each formulation

ID	*Powder (%)*	*NaOH (8M) (%)*	*Na_2SiO_3(%)*	*L/S ratio*	*curing conditions*
PS700-4M	*63.29*	*36.71*	*-*	*0.58*	*85°C*20h - 22±3°C for 28d*
PS700-6M	*63.29*	*36.71*	*-*	*0.58*	*85°C*20h - 22±3°C for 28d*
PS700-8M	*63.29*	*36.71*	*-*	*0.58*	*85°C*20h - 22±3°C for 28d*
PS700S-4M	*63.69*	*21.02*	*15.29*	*0.57*	*85°C*20h - 22±3°C for 28d*
PS700S-6M	*63.69*	*21.02*	*15.29*	*0.57*	*85°C*20h - 22±3°C for 28d*
PS700S-8M	*65.79*	*16.16*	*21.05*	*0.52*	*85°C*20h - 22±3°C for 28d*
NU700-4M	*71.43*	*28.57*	*-*	*0.40*	*85°C*20h - 22±3°C for 28d*
NU700-6M	*68.31*	*31.69*	*-*	*0.46*	*85°C*20h - 22±3°C for 28d*
NU700-8M	*68.49*	*31.51*	*-*	*0.46*	*85°C*20h - 22±3°C for 28d*
NU700S-4M	*71.43*	*8.57*	*20*	*0.40*	*85°C*20h - 22±3°C for 28d*
NU700S-6M	*68.31*	*15.30*	*16.39*	*0.46*	*85°C*20h - 22±3°C for 28d*
NU700S-8M	*71.43*	*8.57*	*20*	*0.40*	*85°C*20h - 22±3°C for 28d*
VC700-4M	*68.97*	*31.03*	*-*	*0.45*	*85°C*20h - 22±3°C for 28d*
VC700-6M	*66.14*	*33.86*	*-*	*0.51*	*85°C*20h - 22±3°C for 28d*
VC700-8M	*68.31*	*31.69*	*-*	*0.46*	*85°C*20h - 22±3°C for 28d*
VC700S-4M	*65.79*	*15.79*	*18.42*	*0.52*	*85°C*20h - 22±3°C for 28d*
VC700S-6M	*65.79*	*15.79*	*18.42*	*0.52*	*85°C*20h - 22±3°C for 28d*
VC700S-8M	*67.57*	*8.11*	*24.32*	*0.48*	*85°C*20h - 22±3°C for 28d*

6. Results of characterization and discussion

All geopolymer binders have been characterized by means of different analytical techniques that are described in paragraph 3. Before these characterizations, all samples were tested for their chemical stability through a so-called Integrity Test (IT). This test consists of a direct observation of the integrity of the sample after immersion of the sample in water with a solid/liquid ratio of 1/10, Fig.26. If the water is clear and the sample compact after 24h, the chemical stability is good, while if the water shows turbidity and there are some residues of the sample in the water, the chemical stability can be considered bad and this is a signal that the alkaline reaction has not been completed (Lancellotti et al. 2013).

Figure 26- Example of Integrity Test

- **Integrity test**

All geopolymers were demoulded undamaged and with no visible cracks at the end of curing procedures. The results for all geopolymer formulations are reported in Table 7. Only clay-based geopolymers cured at room temperature as VC700- 4,6M or NU700-4M did not harden even at 28 days and therefore it was not possible to perform the integrity test. The integrity tests results have been evaluated through direct observations, according to both turbidity of the water, sample disaggregation or cracks formations due to the water penetration into sample pores (Lancellotti I., et al. 2013; Occhipinti et al. 2020). Another parameter to keep in consideration for establish the quality of the geopolymers is the appearance of white efflorescence, generally consisting of Trona ($Na_3(CO_3)(HCO_3)\cdot 2(H_2O)$), after curing at room temperature for 28 days. The mixtures (see also Tab. 7) with the adding of sodium silicate, have shown good results, confirming a higher stability in water. A slightly efflorescence are visible in some samples made only with NaOH.

Table 7- Sample aspect after water attack after integrity test (IT); (* samples cured at 85°C for 20h ; ** samples cured at room temperature 22±).

Samples	IT after 1* day	IT after 28** days	Efflorescence after 28** days
PS700-4M	No crack	No crack	No
PS700-6M	No crack	No crack	No
PS700-8M	No crack	No crack	Slightly
NU700-6M	Crack	No crack	Slightly
NU700-8M	No crack	No crack	Slightly
VC700-8M	No crack	No crack	No
PS700S-4M	No crack	No crack	No
PS700S-6M	No crack	No crack	No
PS700S-8M	No crack	No crack	No
NU700S-4M	No crack	No crack	Slightly
NU700S-6M	No crack	No crack	Slightly
NU700S-8M	No crack	No crack	No
VC700S-4M	No crack	No crack	No
VC700S-6M	No crack	No crack	No
VC700S-8M	No crack	No crack	No

- **Mechanical test**

Compressive strength results of geopolymeric samples cured at 85°C for 20h or at room temperature for 28 days are discussed below. From these data it is possible to demonstrate that the significant increase in compressive strength values depends on several factors such as: the composition of the raw materials, the calcination temperature and the different alkaline solutions (4, 6 and 8 M) and the use of sodium silicate. For what concerns the clay thermally activated at 700°C, two sets of binders product were prepared and cured at 85°C for 20h or at room temperature for 28 days: the first one activated only with NaOH (4, 6 and 8M) solution, the second one activated by adding sodium silicate to the mixture,.

The compressive strength obtained with three different types of clay are described in detail below:

- ***Geopolymers with Plio-Pleistocenic clay (PS):*** The mean values of three test for compressive strength and the comparison with the corresponding samples cured at room temperature for 28d are plotted in Fig. 27 and reported in Tab.8.

Samples activated only with NaOH (4,6 and 8M) and cured at 85 °C for 20 hours, showed a similar trend in compressive strength values with the samples synthesized by using NaOH and cured at room temperature for 28d. Indeed sample PS700-6M showed the highest compressive strength value in respect to the other samples PS700-4M and PS700-8M in both curing conditions.

In detail, concerning samples cured at 85 °C for 20h, the lowest average value of strength, 10.35 MPa, was obtained for the sample prepared mixing the clay with NaOH (4M) solution, while the highest value of about 24.53 MPa was obtained with the sample labelled PS700-6M.Sample PS700-8M shows a value of compressive strength of about 23.31 MPa, as reported in Fig.27a. Samples cured at room temperature for 28d show the following compressive strength values: PS700-4M (14.78 MPa), PS700-6M (29.84 MPa) and PS700-8M (27.95 MPa), as displayed in Fig.27b.

Regarding the samples obtained adding sodium silicate to the mixture, the obtained samples show similar values of mechanical strength to those obtained with NaOH only and cured at 85 °C. Indeed, the highest value is represented by samples labelled PS700S-6M with 25.95 MPa, while the other two sets PS700S-4M and PS700S-8M show respectively 7.80 MPa and 23.33 MPa, Fig.27c. Samples cured at room temperature for 28d show a different trend: sample PS700S-8M shows the highest value at 28.71 MPa, while sample PS700S-4M the lowest one at 9.04 MPa, Fig.27d.

The presence of silica in the sodium silicate solution favors the polymerization process, producing a material with an increased mechanical strength as already reported in literature (Criado, Palomo, and Fernández-Jiménez 2005; Fernández-Jiménez, et al. 1999). It has to be noted that the presence of CaO contributed to improve the compressive strength proprieties likely due to a better hydraulic consolidation.

Tab.8- Compression strength values of Plio-pleistocenic geopolymer binders of samples activated with and without sodium silicate and cured at 85 °C for 20h or at room temperature for 28 days.

Samples cured at 85 °C for 20h	Compressive strength	St. Dev
PS700-4M	10,35	2,29
PS700-6M	24,53	10,48
PS700-8M	23,31	0,34
PS700S-4M	7,80	0,98
PS700S-6M	25,95	11,50
PS700S-8M	23,33	2,10
Samples cured at 22+3°C for 28d	Compressive strength	St. Dev
PS700-4M	14,78	2,80
PS700-6M	29,84	9,02
PS700-8M	27,95	9,34
PS700S-4M	9.02	8,66
PS700S-6M	22,45	2,56
PS700S-8M	28,71	8,04

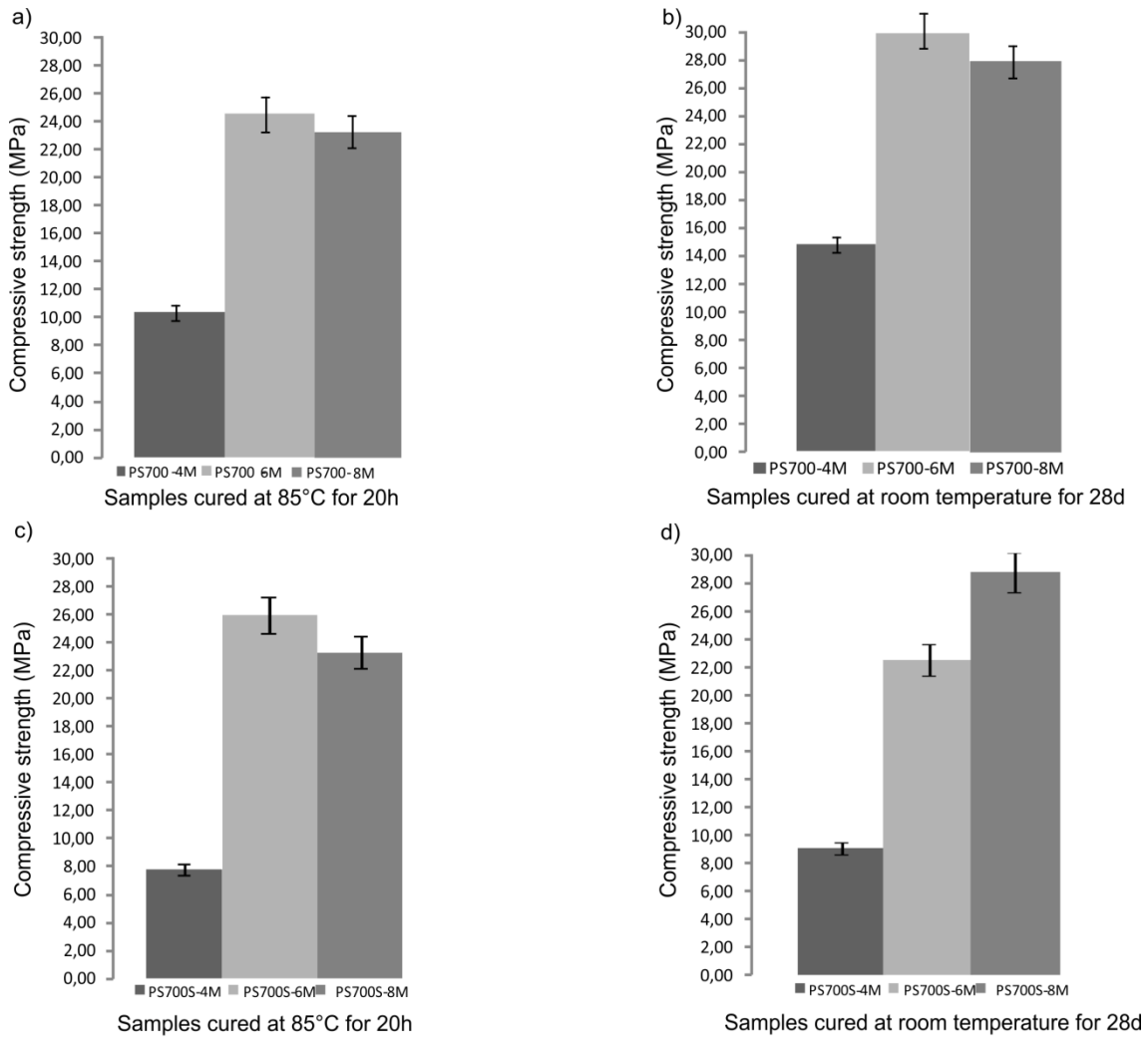

Figure 27- Compression strength values of Plio-pleistocenic geopolymer binders- a) and b) samples cured at 85 °C for 20h while c) and d) samples cured at room temperature for 28 days. The bar indicates the error on the measurement accuracy.

- ***Geopolymers with Numidican clay (NU):*** Results of compressive strength of the samples cured at 85°C for 20h and at room temperature for 28d are displayed in Fig.28a-d and reported in Tab.9. Overall, the measurements on samples cured at 85°C vary from a minimum of 0.61 MPa for sample NU700-4M to a maximum of 6.82 MPa for sample NU700-8M, Fig.28a. Regarding the samples cured at room temperature for 28 days, compressive strength test was not performed on sample NU700-4M because it did not mature at room temperature. Compressive strength values of samples NU700-6M and NU700-8M are worse in comparison to those cured at 85°C for 20h. For these reasons, it is necessary to add sodium silicate to the mixture in order to improve the hardening of the pastes. After the addition of sodium silicate, the specimens had the same thermal treatments as the previous ones and the mechanical properties considerably increased. Indeed, for the first case the minimum value is 2.16 MPa for NU700S-6M while the maximum value is 17.89 MPa for NU700S-8M. In the second case, for a samples matured at room temperature for 28d, the minimum value obtained is 3.91 MPa for NU700S-4M while the maximum is 44.50 MPa for NU700S-8M. Overall, from these results, it is possible to observe that when pastes are activated with only NaOH, notwithstanding the thermal treatment, the values of mechanical strength are low (0.61- 6.82 MPa). After the addition of the sodium silicate, mechanical properties considerably increase as shown in Fig.28d whit sample NU700S-8M 44.50 MPa.

Tab.9- Compression strength values of Numidican clay geopolymer binders of samples activated with and without sodium silicate and cured at 85 °C for 20h or at room temperature for 28 days.

Samples cured at 85 °C for 20h	Compressive strength	St. Dev
NU700-4M	0,61	0,53
NU700-6M	5,35	0,56
NU700-8M	6,82	1,16
NU700S-4M	2,50	0,93
NU700S-6M	2,16	0,48
NU700S-8M	17,89	1,65
Samples cured at 22+3°C for 28d	**Compressive strength**	**St. Dev**
NU700-4M		
NU700-6M	3,09	0,68
NU700-8M	4,57	0,80
NU700S-4M	3,91	0,65
NU700S-6M	6,52	0,81
NU700S-8M	44,50	13,77

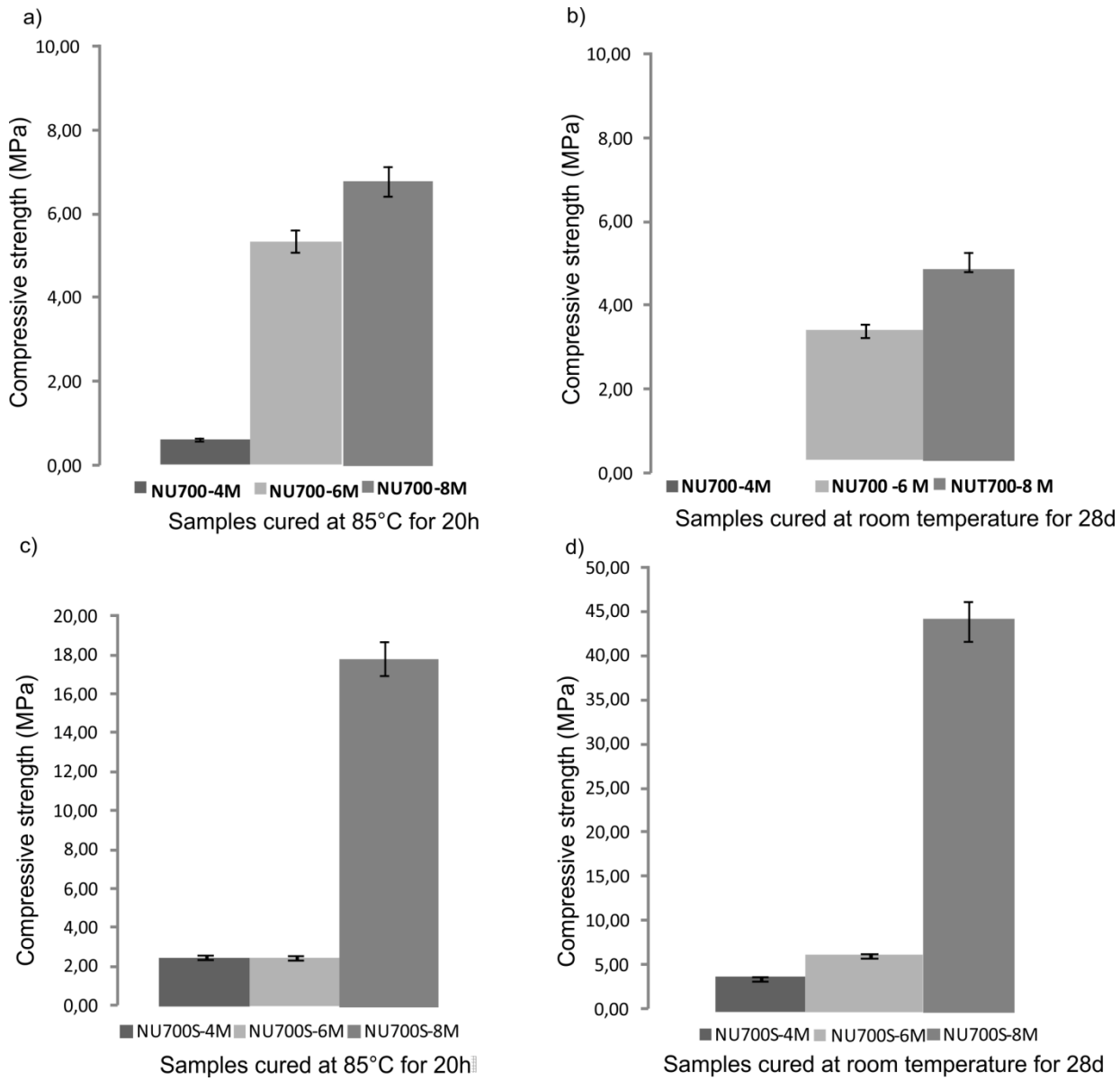

Figure 28 - Compression strength values of Numidican geopolymer binders- a) and b) samples cured at 85 °C for 20h while c) and d) samples cured at room temperature for 28 days. The bar indicates the error on the measurement accuracy.

- ***Geopolymers with Variegated clay (VC):*** Results of compressive strength of the samples cured at 85 °C for 20h and at room temperature for 28d are displayed in Fig.29a-d and reported in Tab.10. VC700-(4, 6, 8M) samples cured at 85 °C show values of compressive strength respectively of 0.89MPa, 1.33 MPa and 2.58 MPa. Samples cured at room temperature were not tested for their compressive strength due to their low hardness, except for sample VC700-8M that yielded a value of 9.49 MPa. After adding sodium silicate, the samples cured at 85 °C show better compressive strength values. In fact VC700S-4M reached about 1.76 MPa, VC700S-6M 7.74 MPa, while VC700S-8M 60.06 MPa. Samples cured at room temperature highlight a decrease for the sample VC700S-8M (12.96 MPa) in respect to the sample cured at 85 °C for 20 hours and an increase for samples VC700S-6,8 M that is 9.55 MPa and 12.96 MPa respectively.

Tab.10- Compression strength values of Numidican clay geopolymer binders of samples activated with and without sodium silicate and cured at 85 °C for 20h or at room temperature for 28 days.

Samples cured at 85 °C for 20h	Compressive strength	St. Dev
VC700-4M	0,89	0,07
VC700-6M	1,33	0,25
VC700-8M	2,58	0,47
VC700S-4M	1,76	0,12
VC700S-6M	7,74	3,15
VC700S-8M	60,06	5,45
Samples cured at 22+3°C for 28d	Compressive strength	St. Dev
VC700-4M		
VC700-6M		
VC700-8M	9,49	0,14
VC700S-4M	4,82	0,97
VC700S-6M	9,55	0,21
VC700S-8M	12,96	2,32

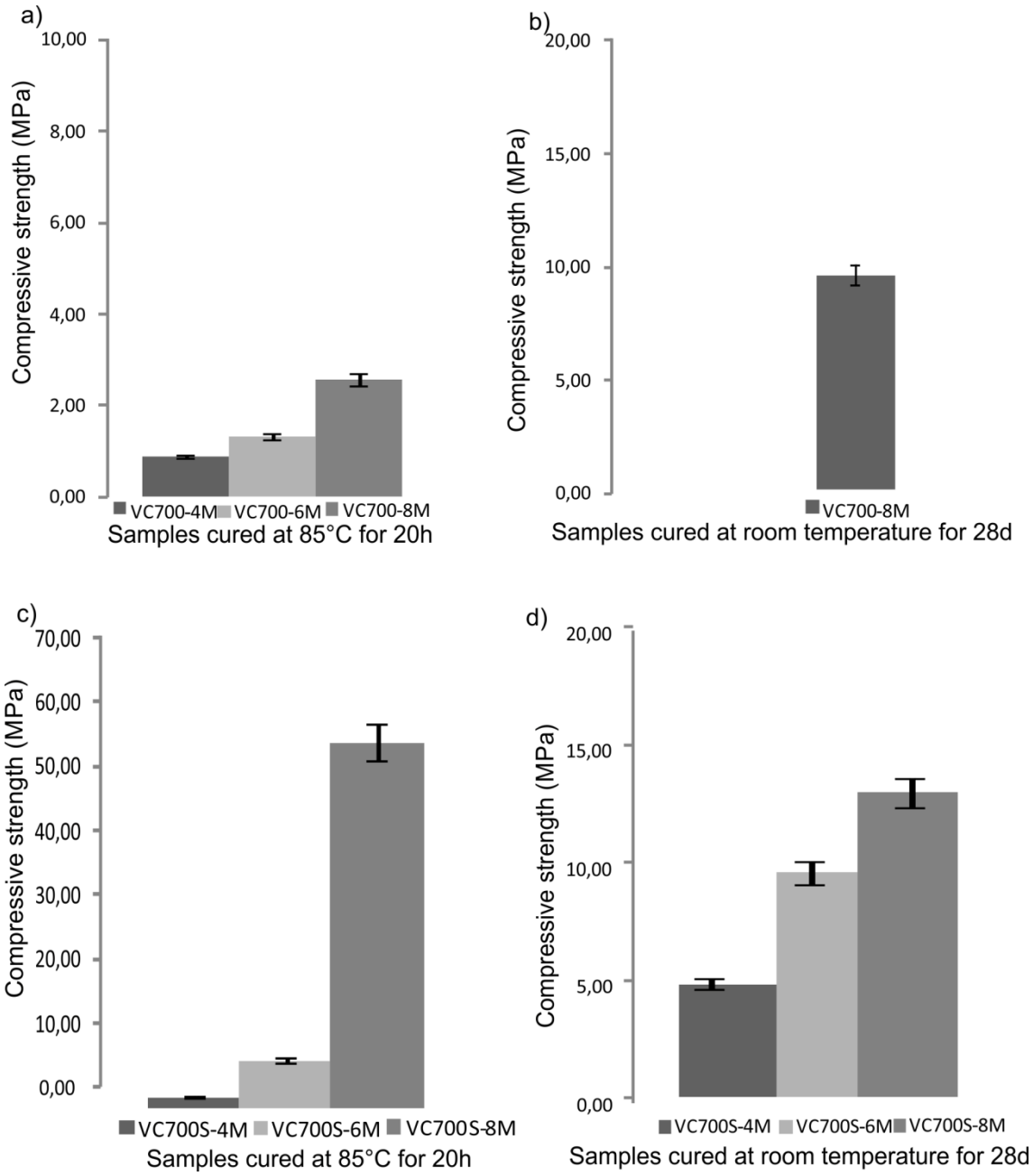

Figure 29- Compression strength values of Variegated geopolymer binders- a) and b) samples cured at 85 °C for 20h while c) and d) samples cured at room temperature for 28 days. The bar indicates the error on the measurement accuracy.

Generally, considering the obtained results, it can be affirm that all geopolymers activated by adding sodium silicate solution at the mixture have the highest values in term of compressive strength in respect to the geopolymer activated only with sodium hydroxide. At the same time, considering the curing condition and the NaOH molarities, geopolymers cured at room temperature and activated by using NaOH (8M) shows good compressive strength values than cured at 85 °C for 20h. Finally, comparing the three sets of geopolymers thermally treated at 22±3 °C for 28d and activated by using sodium

hydroxide (8M) and sodium silicate, sample NU700S-8M showed the highest value of compressive strength (44.50 MPa) compared to sample PS700S-8M (28.71 MPa) and VC700S-8M (12.96 MPa) as displayed in Tab.11.

Tab.11- Compression strength values of samples obtained by using sodium silicate and cured at 22+3°C for 28d.

Samples cured at 22+3°C for 28d	Compressive strength	St. Dev
PS700S-8M	28.71	8.04
NU700S-8M	44.50	13.77
VC700S-8M	12,96	0,14

Finally, comparing geopolymer samples activated only with sodium hydroxide (8M), it can be observe that the highest value of compressive strength is given by the sample PS700-8M (27.95 MPa) in respect to the sample NU700-8M (4.57 MPa) and VC700-8M (9.49 MPa), Tab 12.

Tab.12- Compression strength values of samples obtained by using only sodium hydroxide and cured at 22+3°C for 28d.

Samples cured at 22+3°C for 28d	Compressive strength	St. Dev
PS700-8M	27.95	9,34
NU700-8M	4.57	0,80
VC700-8M	9.49	2,32

- **X-Ray diffraction - Mineralogical analysis (XRPD)**

XRPD results of geopolymeric binders obtained after 20h of curing at 85 °C are described below. From these analyses, it is possible to highlight how during the alkaline reaction different mineralogical phases appear. In detail, geopolymer binders obtained with only sodium hydroxide and those with addition of sodium silicate have been compared. Another important parameter that influences the quantitative ratio of the mineralogical phases present is the different alkaline solution of the sodium hydroxide (4, 6 and 8 M) used for the activation of aluminosilicates.

The obtained XRPD patterns are described below for each clay precursor:

- ***Geopolymers with Plio-pleistocenic clay:*** The used raw material and the produced geopolymers showed, as attested in the literature (J. Davidovits 1991), high amorphous content as evidenced by the broad band in the 20-35 2θ range which is typical of the amorphous gel precipitation (Fernández-Jiménez, A., et al. 1999; Shi, C., Fernandez-Jimenez 2006). The mineralogical phases detected in the raw material (quartz, k-feldspars, calcite and muscovite or illite) are still present in the obtained geopolymer binders activated with sodium hydroxide only at different concentrations (4,6 and 8M) as reported inFig.27 and Tab.8. Only in the sample PS700-8M, several peaks related to new crystalline phases as Tobermorite and Sodalite have been revealed. This phenomenon explains how the pH and the alkaline conditions obtained with 8M NaOH are more advantageous than those linked to NaOH at low molarities, for the alkaline reaction of the geopolymer. In detail, defined peaks at 29° and 34° 2θ reveal the presence of Tobermorite $Ca_4Si_6O_{17}(H_2O)_2 \cdot (Ca \cdot 3H_2O)$ that generally is present in the gel phase of C-A-S-H type cements, due to the presence of calcite, while peaks at 13°, 24° and 36° 2θ are related to Sodalite $Na_4(Si_3Al_3)O_{12}Cl$ that is typical of N-A-S-H gel type cement products, due to the presence in the system of Sodium hydroxide. For this purpose, it seems that the obtained pastes are characterized by a hybrid system, in which the newly formed gel presents parts rich in C-A-S-H and other parts rich in N-A-S-H. Finally, no carbonates phases, generally occurring during crystallization after air exposure, have been detected.

For comparison, the XRPD pattern of the geopolymer binders activated only with sodium hydroxide 8M and that activated by adding sodium silicate are reported in Fig. 30 and labeled PS700S-8M.

The amount of each phase has been quantified by Rietveld refinement method and the results are shown in Tab.13.

Table 13- Mineralogical composition after Rietveld refinement of both geopolymer obtained by using Plio-pleistocenic clay and cured at 85° for 20h - Qtz=Quartz, Ab= Albite, Clc=Calcite, Ms=Muscovite, Sme=Smectiti, To= Tobermorite, So= Sodalite, Hm= Hematite;

		Phase (% Weight)								
	ID	**Qtz**	**Ab**	**Or**	**Clc**	**Ms**	**Sme**	**To**	**So**	**Hm**
Geopolymers	*PS700-4M*	*29.95*	*6.30*	*3.36*	*18.15*	*8.56*	*33.68*	-	-	-
	PS700-6M	*28.31*	*2.34*	*3.81*	*9.44*	*8.32*	*26.66*	*21.12*	-	-
	PS700-8M	*22.43*	*3.51*	-	*6.82*	*7.17*	*48.58*	*10.20*	*1.29*	-
	PS700S-8M	*32.81*	*5.87*	*2.78*	-	*7.17*	*42.02*	*6.50*	-	*2.84*

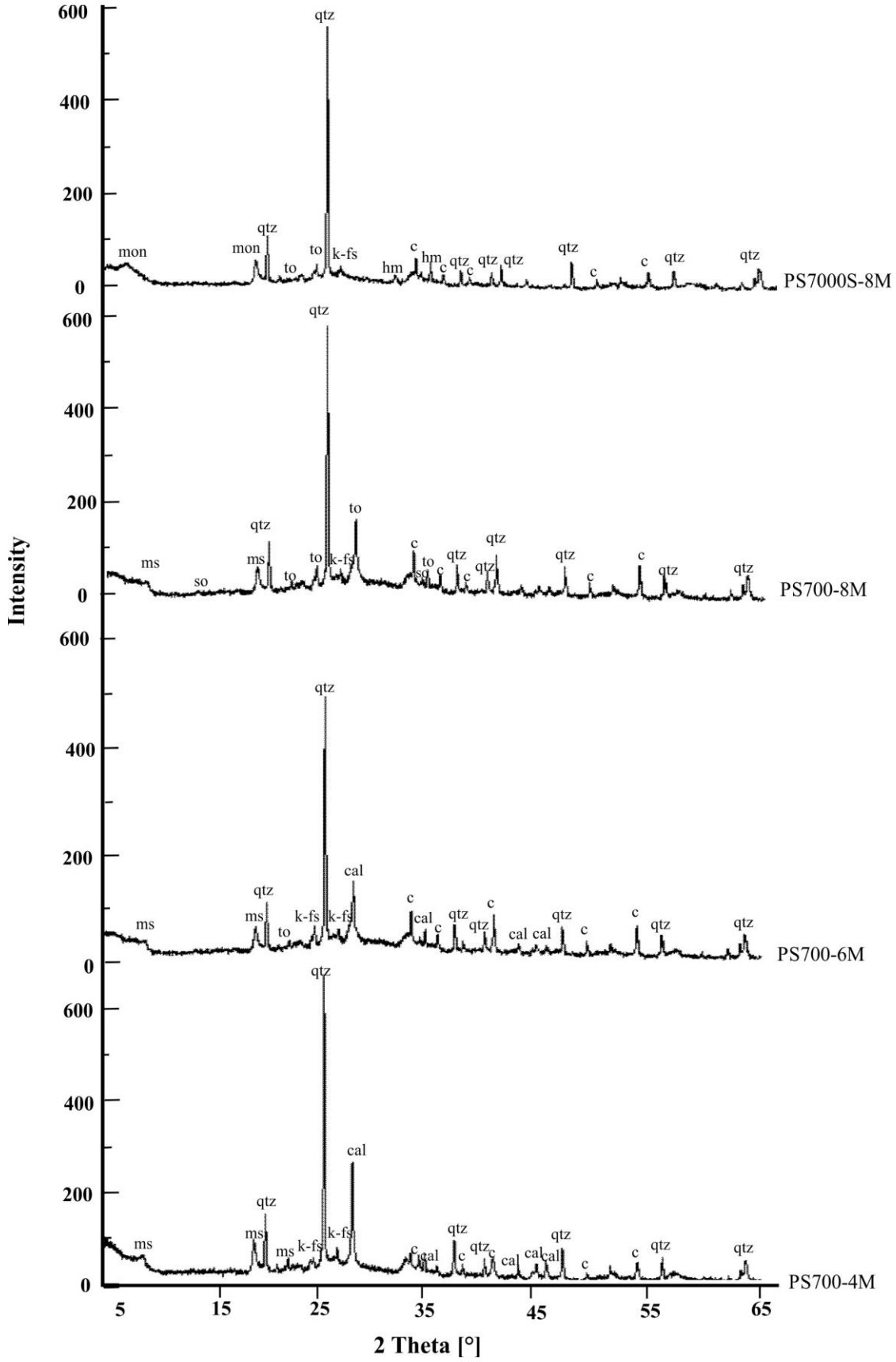

Figure 30- Mineralogical composition of the obtained AAMs by using Plio-pleistocenic clay; ms=muscovite; qtz= quartz; k-fs=k-feldspars; cal=calcite; c= corundum

- ***Geopolymers with Numidican clay:*** The prevalent mineralogical phases typical of Numidian clay (i.e. Quartz, k-feldsprs and Muscovite) are present both in the raw material and in the geopolymers. In these latter, in addition to the high amorphous content as evidenced by the broad band in the 20-35 2θ range, zeolites as Faujasite are present, suggesting the formation of more ordered structure during the polymerization process (Criado et al. 2007). Also smectites have revealed in the samples activated with sodium hydroxide at different concentrations (4,6 and 8M) as reported in Tab.14. Finally, in the sample NU700-8M, Dolomite has been reveled as a new phase.

Table 14- Mineralogical composition after Rietveld refinement of both geopolymer obtained by using Numidican clay cured at 85° for 20h - Qtz=Quartz, Ab= Albite, Or=Orthoclase, Ms=Muscovite, Sme=Smectiti, Do= Dolomite, K=Kaolinite, Fj= Faujasite;

			Phase (% Weight)						
	ID	**Qtz**	**Or**	**Ab**	**Do**	**Ms**	**K**	**Fj**	**Sme**
Geopolymers	*NU700-4M*	*50.77*	*3.55*	*3.96*	*-*	*2.94*	*0.97*	*-*	37.81
	NU700-6M	*46.03*	*6.55*	*4.10*	*-*	*1.58*	*-*	*4.11*	*37.61*
	NU700-8M	*36.12*	*5.07*	*-*	*4.57*	*4.82*	*-*	*16.94*	*32.48*

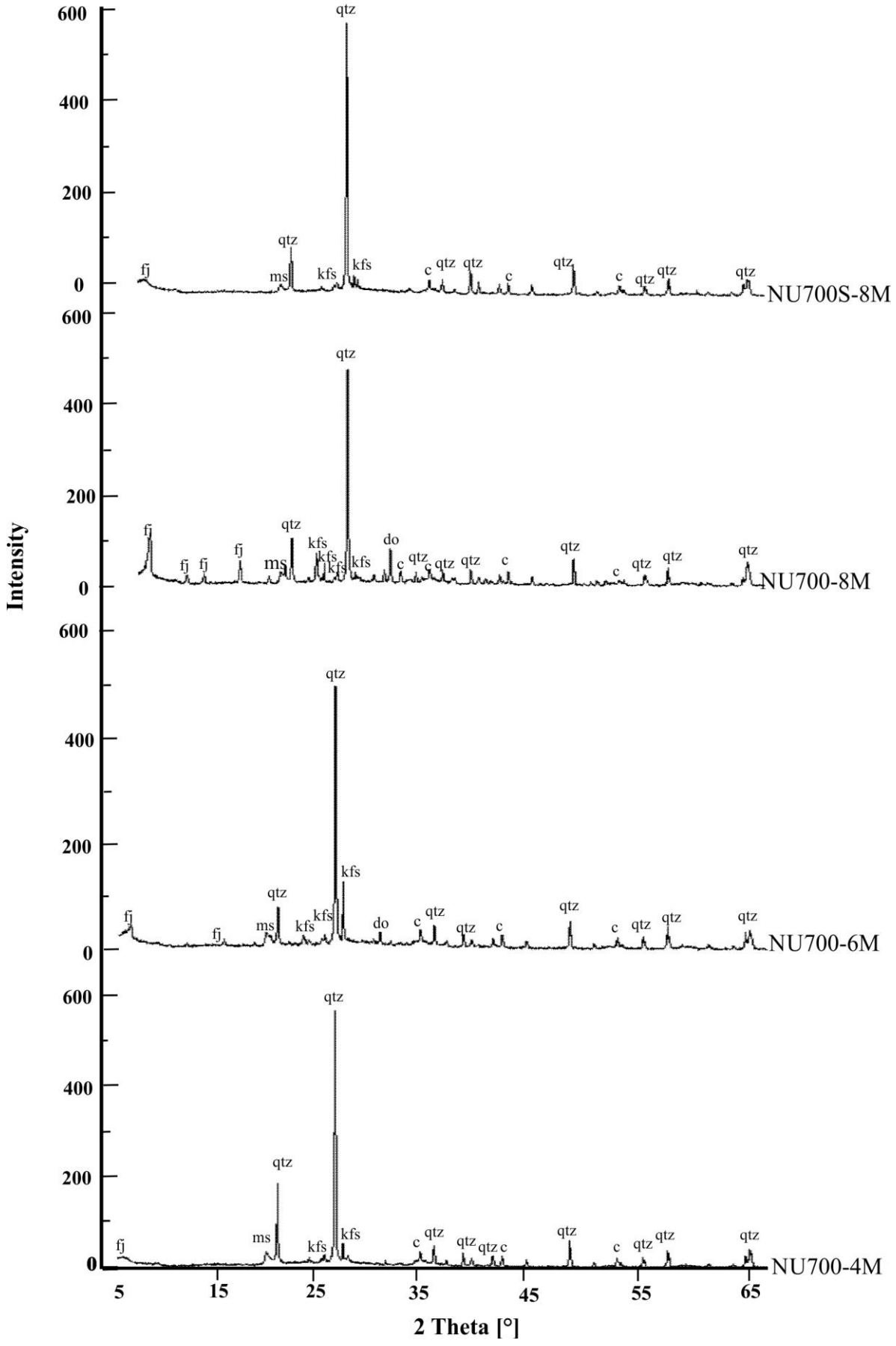

Figure 31- Mineralogical composition of the obtained AAMs by using Numidican clay; ms=muscovite; qtz= quartz; k-fs=k-feldspars; fj=faujasite; c= corundum

- ***Geopolymers with variegated clay:*** Only sample VC700S-8M has been characterized by XRD analysis. Diverse mineralogical phases as quartz, albite, hematite, orthoclase and clay minerals are detected as shown in Fig.32 and reported in Tab.15.

Table 15- Mineralogical composition after Rietveld refinement of both geopolymer obtained by using Variegated clay and cured at 85° for 20h - Qtz=Quartz, Hm= Hematite, Ab= Albite, Or= Ortoclase, Sme= Smectiti;

		Phase (% Weight)				
	ID	**Qtz**	**Hm**	**Ab**	**Or**	**Sme**
Geopolymers	*VC700S-8M*	*32.65*	*1.88*	*6.95*	*3.05*	*55.47*

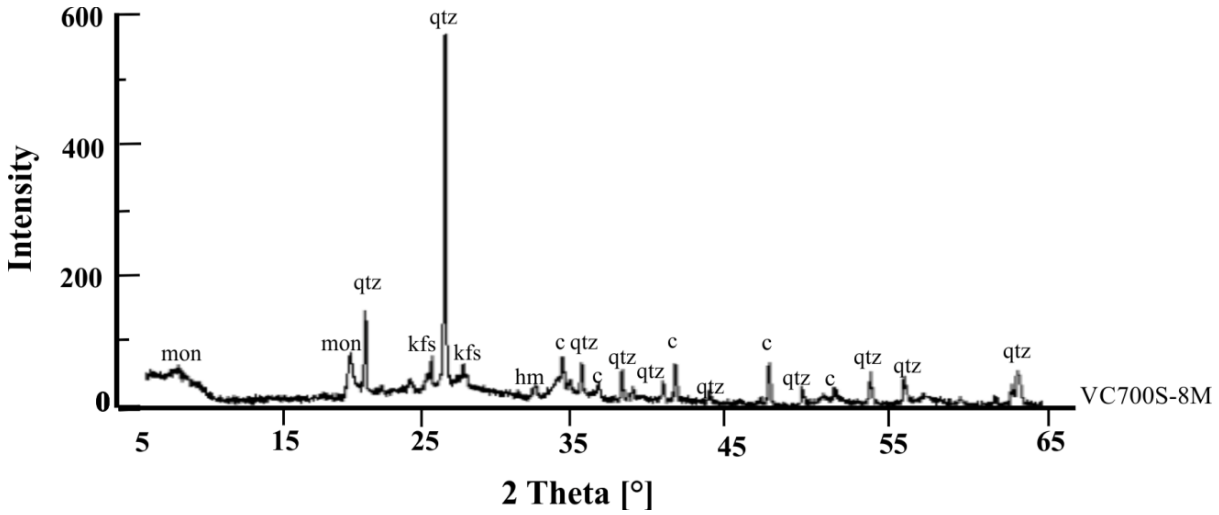

Figure 32- Mineralogical composition of the obtained AAMs by using Variegated clay; mon= montmorillonite; qtz= quartz; k-fs=k-feldspars; hm=hematite; c= corundum

- **Fourier Transform Infrared Spectroscopy (FTIR-ATR)**

FTIR-ATR spectra of the geopolymer binders obtained with curing at 85°C for 20h and at room temperature for 28 days were collected.

Generally, in the obtained geopolymer binders, the maximum of the principal bands of the aluminosilicate phase is centered at lower wavenumber, around 930-960 cm^{-1}, with respect to the raw materials (1023-1000 cm-1). This shift from higher to lower wavenumber is attributed to sodium aluminosilicate gel formation as a consequence of the alkaline activation (Alonso and Palomo 2001; Lee and Van Deventer 2003; Lee, W.K.W., & van Deventer 2004; Khan, M. I., et al. 2015).

All samples show another evident peak in the range between 1080 and 1095 cm^{-1}, that is attributed to the aluminosilicate phase as quartz and k-feldspars. Also, quartz is recognizable in all samples, calcinated raw materials and geopolymer binders, by the presence of peaks at 790-775 cm-1 and 691 cm-1 that are related to the Si-O-Si bending vibration (Farmer 1974b; Lee and Van Deventer 2003).

All geopolymer samples, with respect to the calcinated clay, show bands at 1650 and 3440 cm^{-1}, respectively related to H-O-H bending vibrations of molecular water and O–H asymmetric stretching and bending vibrations respectively (Farmer 1974; Djobo J.N.Y., et al. 2014; Clausi et al. 2016). Both bands, and in particular that ascribed to OH-stretching, are broad and indicate a large disorder of hydroxyl groups and water molecules.

Finally, it can be identified at about 1400 cm^{-1} the presence of carbonates by the bands of CO_3^{2+} asymmetric vibrations characterized by a low intensity in geopolymer samples labelled PS700-4,6,8M. The formation of these bands could be attributed to sodium carbonates (Farmer 1974; John L. Provis and Van Deventer 2009).

Analogous features can be observed in the geopolymer binders cured at room temperature (22±3°C) for 28 days.

The FTIR-ATR results of geopolymers obtained with the three different types of clay are described in detail below:

- ***Geopolymers with Plio-Pleistocenic clay (PS):*** These geopolymer binders, cured at 85°C, present bands in the range 1640-1391 cm^{-1} and 888-869 cm^{-1}, that confirm the presence of $CaCO_3$, mainly in the form of calcite (García-Lodeiro, I., et al. 2010). The effect of the geopolymerization is highlighted by the shift of the band, related to the asymmetric stretch of the Si-O-T bonds where T represent Al or Si in tetrahedral

coordination, passing from 1002 cm^{-1} in the raw material to 948-942 cm^{-1} in the products. In detail, the obtained geopolymer binders PS700 (4,6,8M) showed a gradual displacement of the aluminosilicate band related to increased NaOH molarity (Fig.33a).

Instead, FTIR-ATR spectra of the geopolymer binders PS700S-(4, 6, 8M), showed an aluminosilicate band centered in the range 975-950 cm^{-1} as displayed in (Fig.33b).

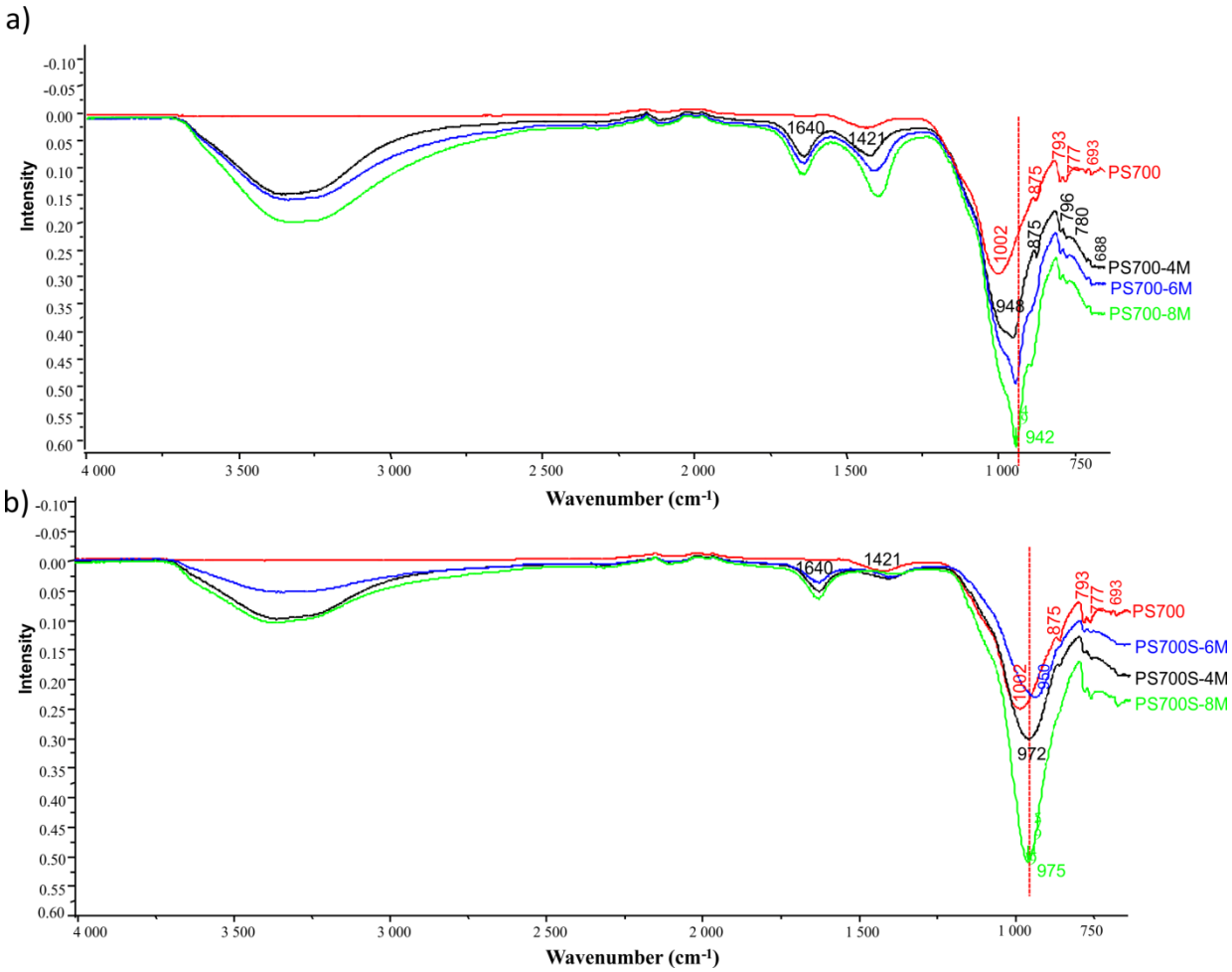

Figure 33- FTIR-ATR spectra of calcined clay raw material PS700 (red line), geopolimyer binder PS700-4M (black line) geopolymers binders (PS700-6M and PS700-8M, blue and green lines respectively) cured at 85 °C for 20h; b) FTIR-ATR spectra of calcinated clay raw m material PS700 (red line), geopolimyer binder PS700S-4M (black line) geopolymers binders (PS700S-6M and PS700S-8M, blue and green lines respectively) cured at 85 °C for 20h. The red line indicates the center of the aluminosilicate band of the obtained geopolymer binders in respect to the raw material.

Concerning geopolymer binders cured at room temperature for 28 days, samples activated with NaOH have similar characteristic to those cured at 85°C. The maximum of the principal band vibration of the aluminosilicate phases are centered at lower wavenumber 948 cm^{-1} and 942 cm^{-1} for samples PS700-(4,6,8M). Regarding the samples obtained adding sodium silicate PS700S-(4,6,8M), the maximum of the principal band vibration of the aluminosilicate phases shows a shift in a range 975-950 cm^{-1}, as displayed in Fig.34a-b.

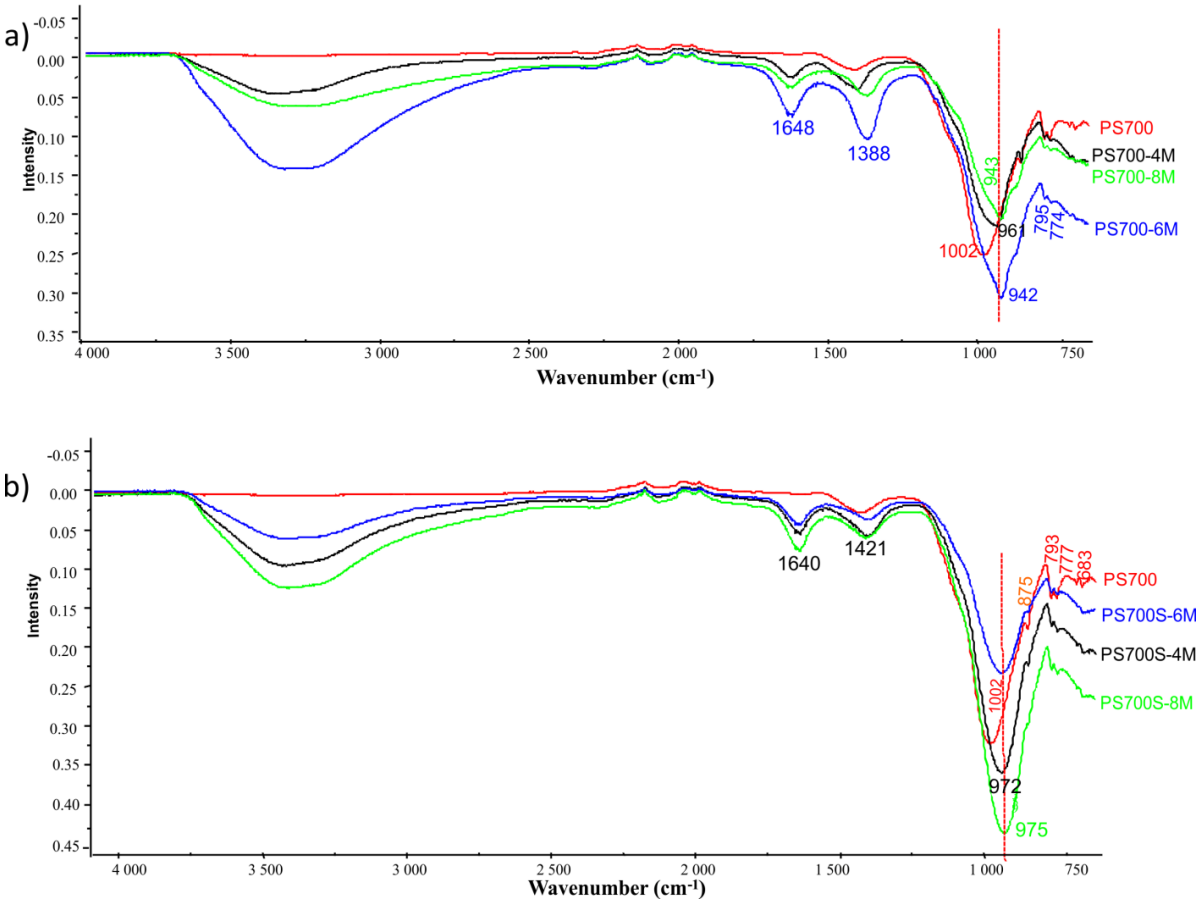

Figure 34- a) FTIR-ATR spectra of calcinated clay raw material PS700 (red line), geopolimyer binder PS700-4M (black line) geopolymers binders (PS700-6M and PS700-8M, blue and green lines respectively) cured at cured at room temperature for 28d; b) FTIR-ATR spectra of calcinated clay raw m material PS700 (red line), geopolimyer binder PS700S-4M (black line) geopolymers binders (PS700S-6M and PS700S-8M, blue and green lines respectively) cured at room temperature. The red line indicates the center of the aluminosilicate band of the obtained geopolymer binders in respect to the raw material.

- ***Geopolymers with Numidican clay (NU):*** The FTIR spectra of the obtained geopolymer binders, prepared only with NaOH (4,6,8 M) and cured at 85°C for 20h and those prepared adding sodium silicate at the mixture are reported for comparison as displayed in Fig.35. In all cases, the main bands related to the stretching of Al-O and Si-O in amorphous aluminosilicate structure are shifted to lower wavenumber. The maximum of the principal band vibration of the aluminosilicate phases are located at (988cm^{-1}, 950 cm^{-1},950 cm^{-1},) with respect to the starting raw material, 1021 cm^{-1}. In detail, as shown in Fig.35a-b, it can be seen that the NU700-6,8M samples show a more pronounced shift than the NU700-4M sample while among the geopolymer binders obtained by adding sodium silicate only the NU700S-8M sample shows a greater shift than the NU700S-4.6M samples.

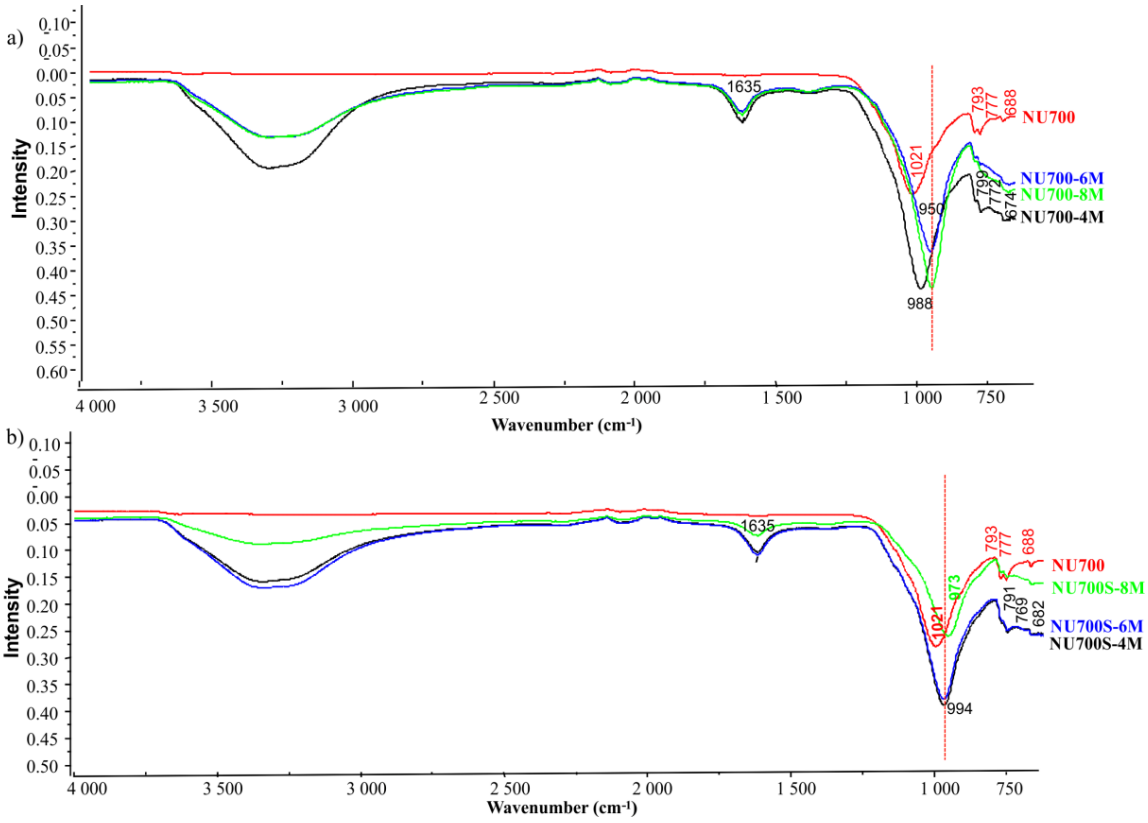

Figure 35- FTIR-ATR spectra of calcinated clay raw material (red line), geopolimyer binder NU700-4M (black line) geopolymers binders (NU700-6M and PS700-8M, blue and green lines respectively) cured at 85 °C for 20h; b) FTIR-ATR spectra of calcinated clay raw m material (red line), geopolimyer binder NU700S-4M (black line) geopolymers binders (NU700S-6M and NU700S-8M, blue and green lines respectively) cured at 85 °C for 20h. The red line indicates the center of the aluminosilicate band of the obtained geopolymer binders in respect to the raw material.

For what concerns the geopolymer binders cured at room temperature for 28 days, samples activated with NaOH have similar characteristic to those cured at 85°C, Fig.36 a-b. The maximum of the principal band vibration of the aluminosilicate phases is centered at 988 cm^{-1} for samples NU700(6,8M). Regarding the samples obtained adding sodium silicate NU700S(4,6,8M), in all curing conditions, samples obtained with NaOH 4,6,8M have the maximum of the principal band vibration of the aluminosilicate phases centered at 991 cm^{-1} while the maximum of the principal band vibration of the raw material is centered at 1021 cm^{-1}.

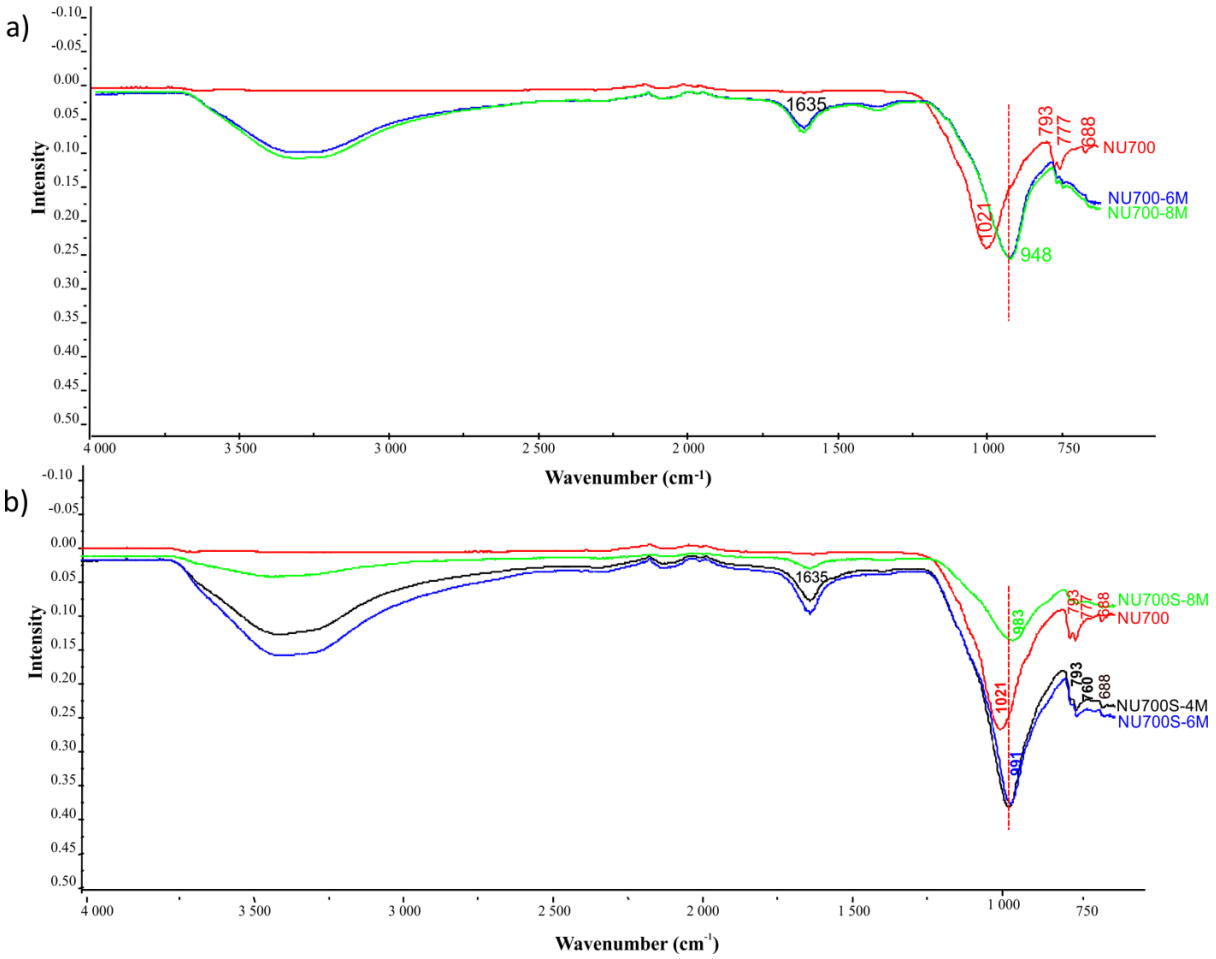

Figure 36- a) FTIR-ATR spectra of calcinated clay raw material (red line), geopolimyer binder NU700-4M (black line) geopolymers binders (NU700-6M and NU700-8M, blue and green lines respectively) cured at room temperature for 28d; b) FTIR-ATR spectra of calcinated clay raw m material (red line), geopolimyer binder NU700S-4M (black line) geopolymers binders (NU700S-6M and NU700S-8M, blue and green lines respectively) cured at room temperature. The red line indicates the center of the aluminosilicate band of the obtained geopolymer binders in respect to the raw material.

- ***Geopolymers with Variegated clay (VC)***: The FTIR spectra of the geopolymer binders obtained with NaOH (4,6,8M) as activator are displayed in Fig.37. Samples obtained with NaOH (4,6,8M) and sodium silicate are also reported for comparison. Indeed, the maximum of the principal bands vibration of the aluminosilicate phases are located in the range 977 cm^{-1}-945 cm^{-1} while samples activated by using NaOH and sodium silicate solution show the maximum band vibration at 985 cm^{-1} for VC700S-4,6M and 948 cm^{-1} for sample VC700S-8M.

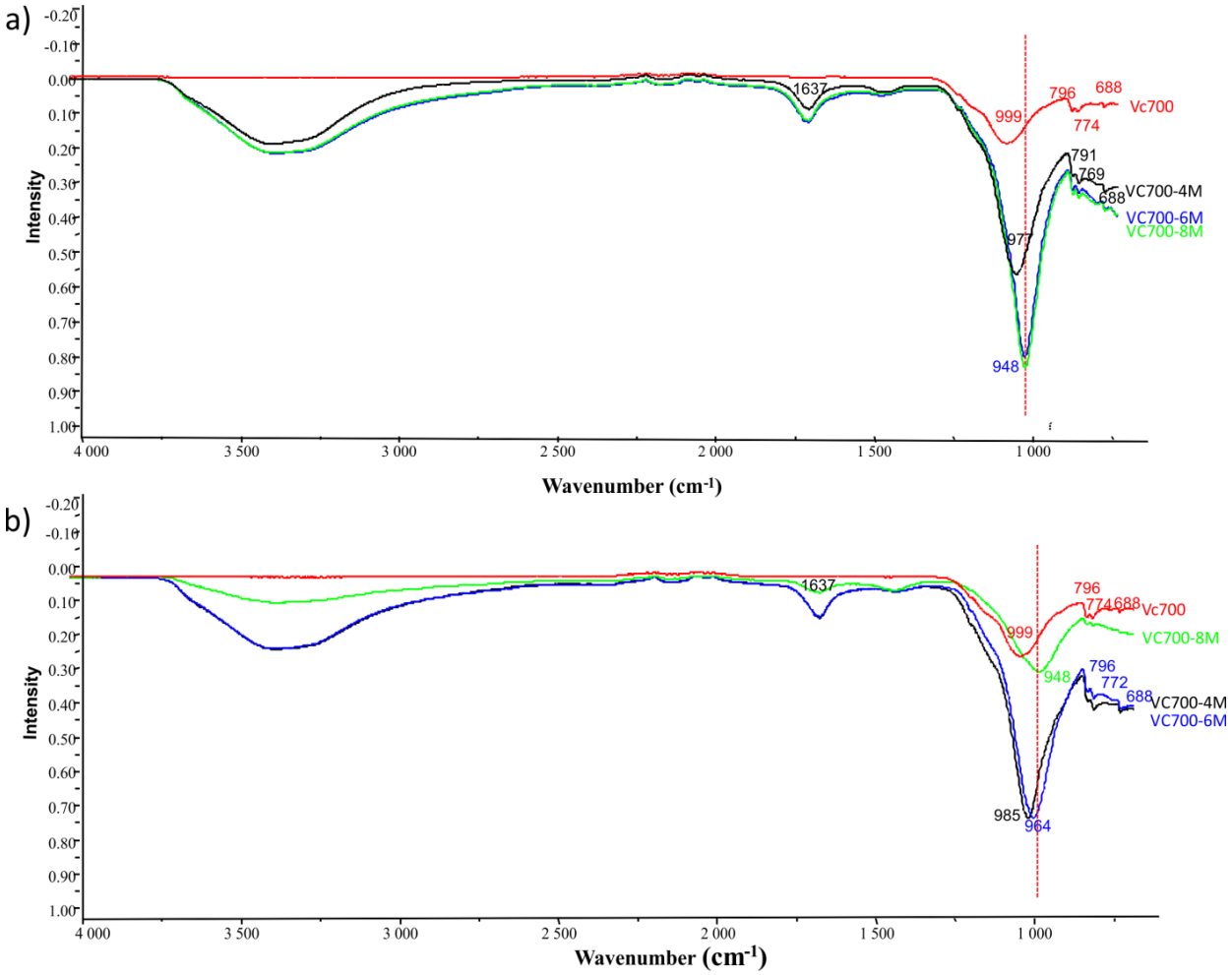

Figure 37- a) FTIR-ATR spectra of calcinated clay raw material (red line), geopolimyer binder VC700-4M (black line) geopolymers binders (VC700-6M and VC700-8M, blue and green lines respectively) cured at 85 °C for 20h; b) FTIR-ATR spectra of calcinated clay raw m material (red line), geopolimyer binder VC700S-4M (black line) geopolymers binders (NU700S-6M and NU700S-8M, blue and green lines respectively) cured at 85 °C for 20h. The red line indicates the center of the aluminosilicate band of the obtained geopolymer binders in respect to the raw material.

Regarding samples cured at room temperature for 28 days, only in the sample VC700-8M FTIR-ATR analysis was carried out whit the maximum of the band vibration at 948 cm^{-1}. Samples obtained adding sodium silicate present a maximum of the principal band vibration at 980 and 969 cm^{-1}, Fig.38.

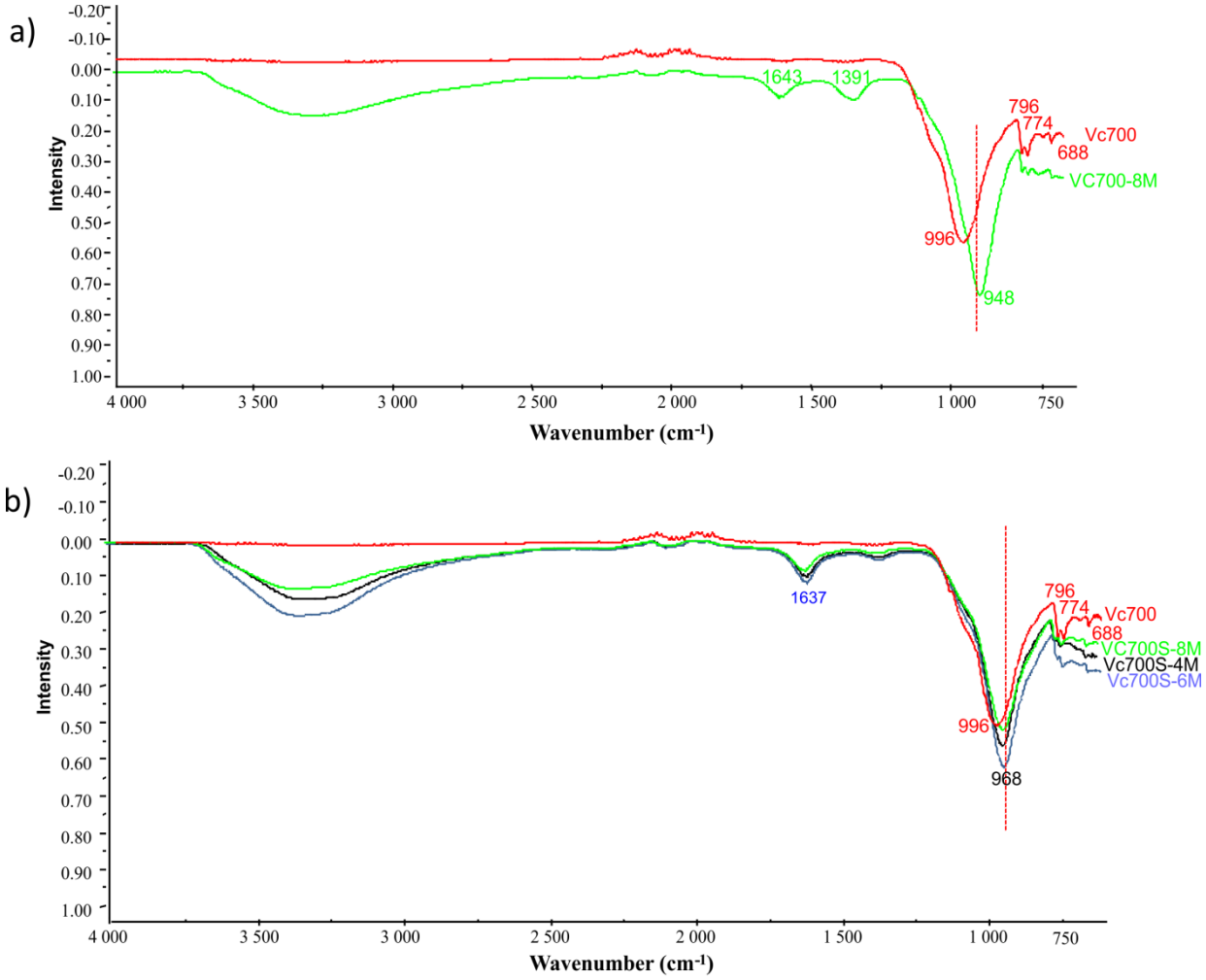

Figure 38- a) FTIR-ATR spectra of calcinated clay raw material (red line), geopolimyer binder VC700-4M (black line) geopolymers binders (VC700-6M and VC700-8M, dashed and dotted lines respectively) cured at room temperature for 28d; b) FTIR-ATR spectra of calcinated clay raw m material (red line), geopolimyer binder VC700S-4M (black line) geopolymers binders (VC700S-6M and VC700S-8M, blue and green lines respectively) cured at room temperature. The red line indicates the center of the aluminosilicate band of the obtained geopolymer binders in respect to the raw material.

- **Diffuse Reflectance Infrared Transform Spectroscopy (DRIFTS)**

In this section, DRIFT spectroscopy results obtained on all the geopolymer pastes cured at 85°C for 20h or at room temperature for 28 days are reported in comparison with the respective raw materials. The complete raw spectra (5500-650 cm^{-1}) are reported in Figs. 39, 40, 41 divided by precursor, check Plio-Pleistocenic (PS), Numidican (NU) and Variegated clays (VC). Four principal high wavenumber bands/groups of bands can be observed, namely:

- 5200 cm^{-1}: combination of stretching (ν) and bending (δ) vibrations of water (Frost and Johanssont 1998; Madejová and Komadel 2001). The intensity of this band seems increased in the geopolymers with respect to the raw materials, this effect is especially evident for Variegated clays;

- ~ 4600 cm^{-1}: ν+δ (OH) (Madejová and Komadel 2001; Miliani et al. 2012): this band either decreases or, more often, disappears in the spectra of the geopolymers;

- ~ 4000 cm^{-1}: probably combinations of ν OH bands (Madejová and Komadel 2001): this appears as a shoulder of variable intensity, on average increasing in the spectra of the geopolymers;

- 3800-2500 cm^{-1}: attributed to ν OH (Belver et al. 2005). This region includes a sharp peak at about 3650 cm^{-1} and a broad band at about 3350 cm^{-1}: the latter is on average strongly decreased passing from the raw materials to the geopolymers, where, instead, a signal around 2900 cm^{-1} appears, whose interpretation is not clear.

The reduction of the contribution of structural OH groups for all the materials and the reduction/elimination of carbonates (bands at 2985, 2875, 2515, 2345, 1867 and 1800 cm^{-1} (Miliani et al. 2012) for PS precursor (Fig.36) is evident, together with the increase of water due to the addition of the activators.

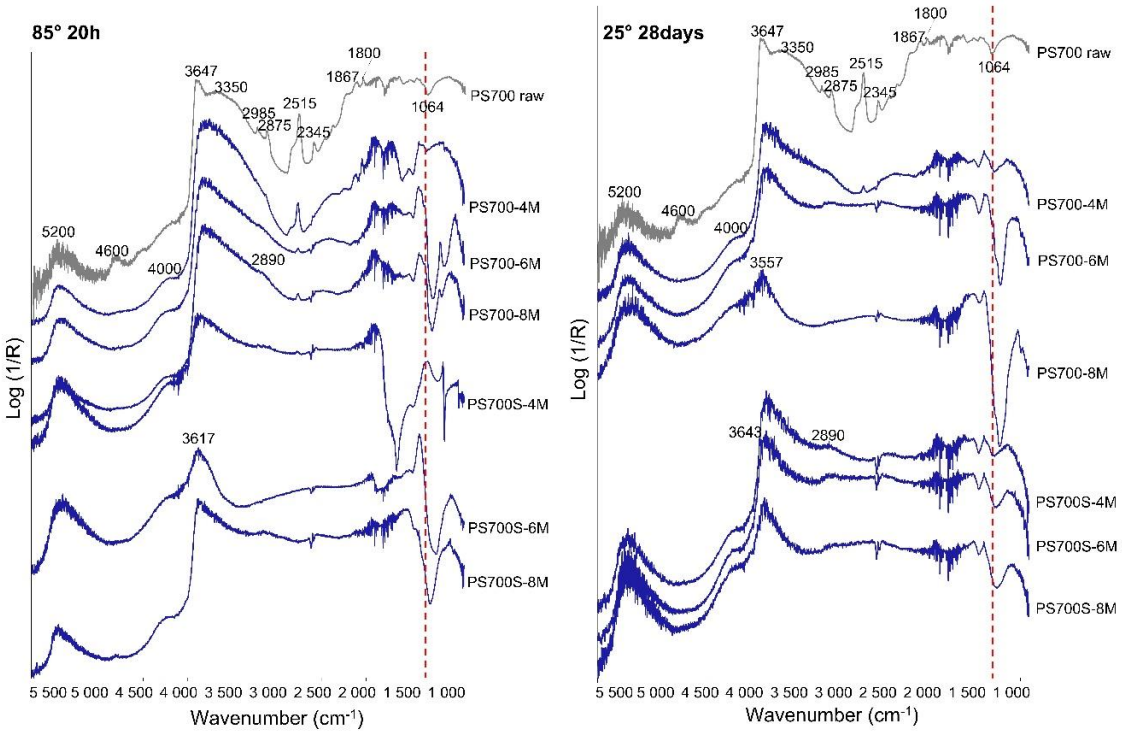

Figure 39- DRIFT spectra in the 5500-650 cm^{-1} range of the Plio-Pleistocene clay and respective geopolymers.

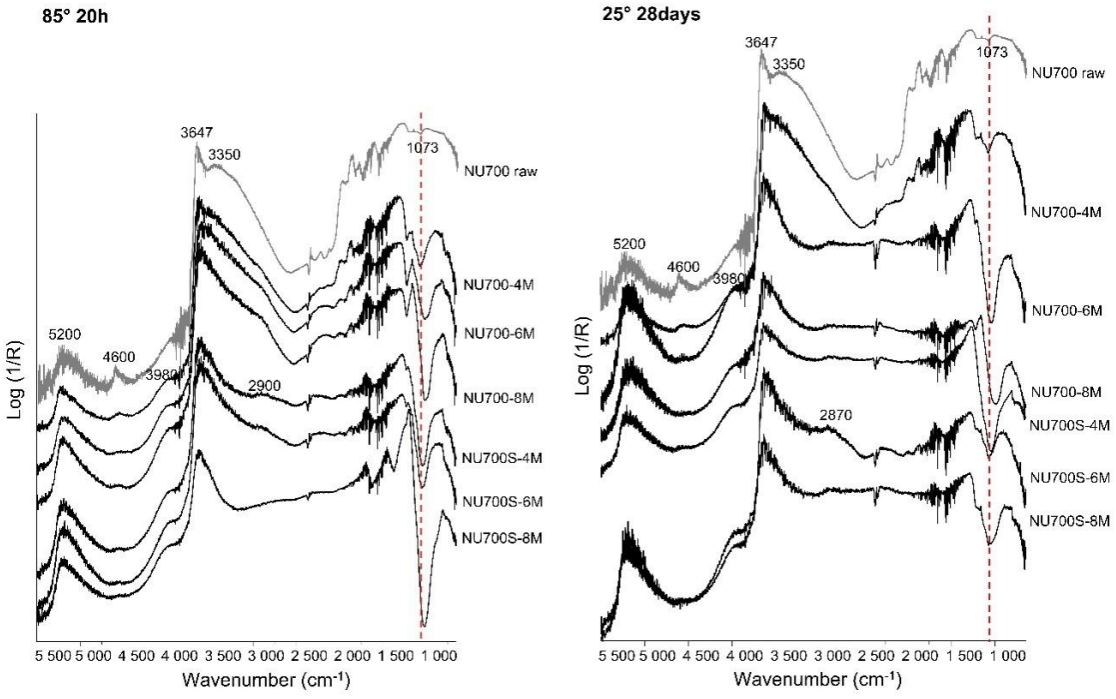

Figure 40- DRIFT spectra in the 5500-650 cm^{-1} range of the Numidican clay and respective geopolymers.

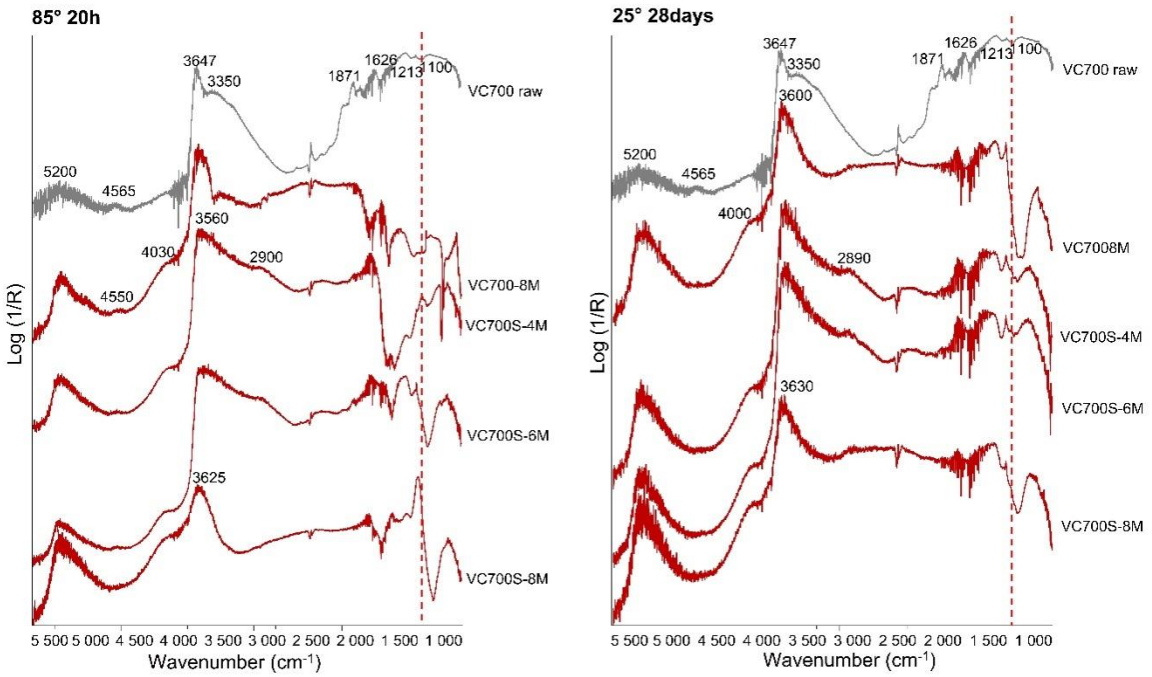

Figure 41- DRIFT spectra in the 5500-650 cm^{-1} range of the Variegated clay and respective geopolymers.

For the aims of this thesis, it is interesting to dwell on the bands connected with the geopolymer aluminosilicate structure. For this reason, the spectra were smoothed, normalized and cut in the region 1320-750 cm^{-1} and are shown in Fig.42. According to (Mladenović et al. 2020), the main aluminosilicate band shift towards lower wavenumbers is indicator of occurred geopolymerization, as much as it is for absorbance infrared spectra, therefore, the position of this signal was evaluated for the precursors and the products synthesized and cured in different conditions.

For the Plio-Pleistocene clay, the raw material aluminosilicate band position is 1070 cm^{-1}, while those of the products range between 1073 and 972 cm^{-1}, the lowest value is reached by sample PS700-6M (both 25°C-28days and 85°C-20h). In general, the bands of the geopolymers activated with NaOH 4M are the highest ones in position. The position of the band of sample PS700-4M (85°C-20h), though, cannot be evaluated because the spectra acquired gave signals of carbonate salts formed on it (~870 cm^{-1}). It is interesting to notice that these spectra display bands structured with different shoulders, especially for samples PS700-6M and 8M (25°C-28days). It might be hypothesized that, being this clayey precursor rich in carbonates, in the respective geopolymers, a complex gel, including both NASH and CASH, is formed.

Concerning Numidican clay-based product, the raw material band position is 1073 cm^{-1}, while those of the geopolymers range between 1075 and 995 cm^{-1}. In detail, except for the geopolymers with addition of sodium silicate and cured at room temperature for 28 days, a clear trend can be noted: the higher the NaOH molarity in the activators' mix, the higher the shift of the band towards lower wavenumbers: the lowest position was reached by sample NU700-8M (25 °C-28days).

The Variegated clay raw material band position is around 1100 cm^{-1}, while those of the geopolymers range between 1032 and 965 cm^{-1}, the latter value is that of sample VC700S-8M (85 °C-20h). The position of the respective geopolymer activated with NaOH only could not be evaluated due to the predominant presence of efflorescences (853 cm^{-1} peak).

In all cases, a band ranging between 1215 and 1225 cm^{-1} is present. A ~1200 cm^{-1} band in infrared spectra is associated in literature to amorphous silica (E.I. Kamitsos and A.P. Patsis 1993).

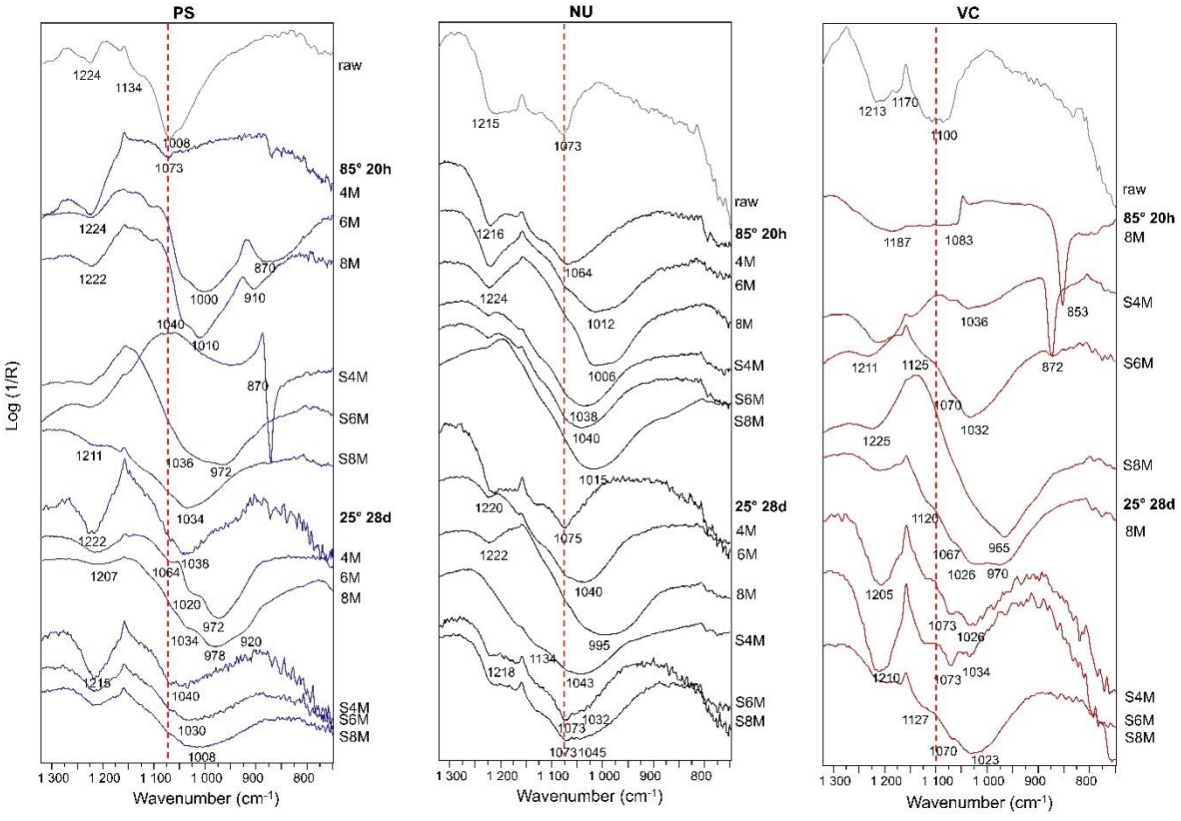

Figure 42- DRIFT spectra in the 1320-750 cm^{-1} range of the Plio-Pleistocene (PS), Numidic (NU), and Variegated (VC) clays and respective geopolymers.

Due to the high number of variables, it was decided to carry out a multivariate statistical analysis in order to help in the distinction of groups of samples and in the definition of those variables that are more influencing for the good production of the geopolymer. Therefore, PCA was performed on the cut (1320-750 cm^{-1}), smoothed, baselined and normalized spectra. Spectra of samples PS700S-4M, VC700-8M and VC700S-4M (85°C-20h) were excluded because in the chosen interval they only showed the peaks of salts. The scores plot of PC1 and PC3 is reported in Fig. 43, while the loadings diagram in Fig.44.

A first distinction between the samples is clear along PC1: samples displaying a positive value of PC1 are all cured at room temperature for 28days, with the exception of PS700-4M. It must also be remarked that no samples activated with NaOH 8M has positive PC1, on the contrary, 5 samples over 8 activated with NaOH 4M fall in this area, the remaining 3 are all associated to Numidican clay. Furthermore, 10 samples over 12 synthesized starting from Numidican clay have negative values of PC1. Observing PC3 too, a cluster of samples seems to form in quadrant 3 (both PC1 and PC2 have negative values): this is formed by 6 geopolymers based on Numidican clay, 1 on Plio-Pleistocene and 1 on Variegated clays, the latter, both activated with a molarity of 8 of NaOH.

Observing the spectra, it is clear that the samples grouped in the first and second quadrants are all characterized by no shift or low shift in the position of the principal aluminosilicate band with respect to the corresponding raw material, leading to hypothesize that the combination of parameters used for their synthesis and curing are less suitable for the achievement of the geopolymer gel.

Observing the loadings, the positive PC1 values are characterized by an almost flat curve, slightly negative values correspond to ca. 1220 cm^{-1}. Considering PC3, the most intensely negative value corresponds to ca. 1255 cm^{-1} position, at the limit of the considered range and with no evident spectral features observable in the spectra.

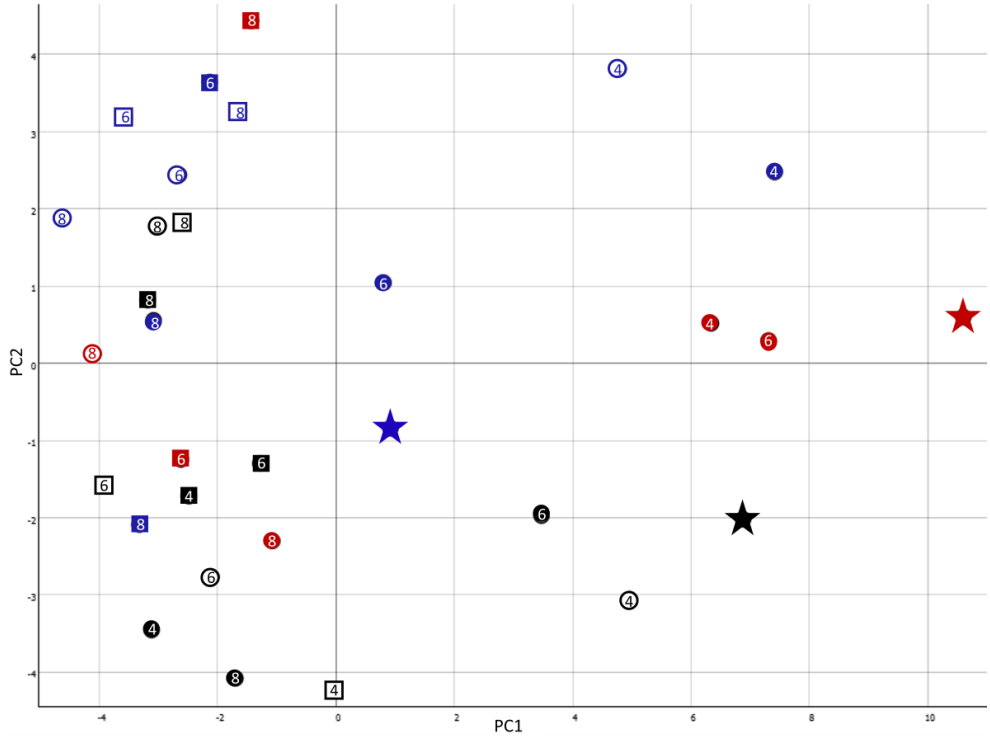

Figure 43- a) Scores plot (PC1 and PC3) of the DRIFT spectra of clay materials. Blue: PS, black: NU, red: VC; square: 85°C 20h, circle: room temperature 28 days, stars: raw materials; empty symbols: only NaOH activator, full symbols: NaOH+Na_2SiO_3 activators' mixture; NaOH molarity (4M, 6M, 8M) is marked in the symbols; explained variance of the first 4 PC= 97,6%;

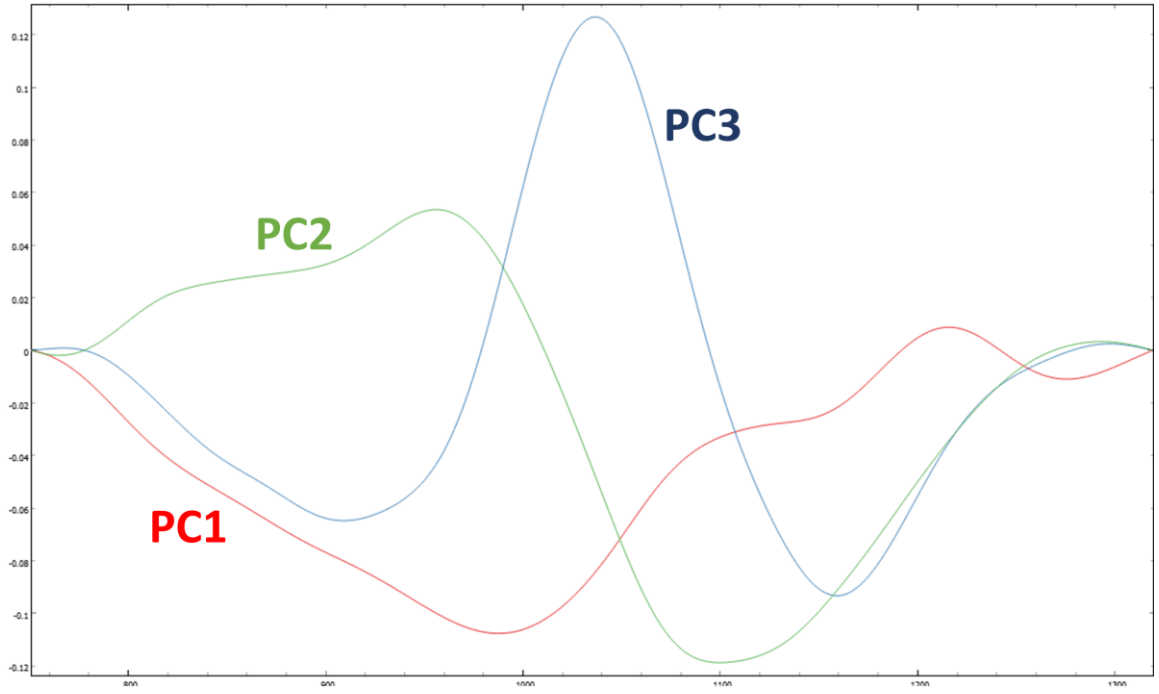

Figure 44- Loadings diagram of the first three principal components.

Sample PS700S-8M was monitored for 8 hours after the mixing, acquiring a DRIFT spectrum each 30 minutes. The results are shown in Fig.45. In detail, the acquired spectra after the first 3 hour, show the appearance, within the main band, of a shoulder around 1150 cm^{-1}, (blue marker in Fig.45), this position is assigned to the presence of amorphous silica. The shoulder positioned at about 1070 cm^{-1} (red marker in Fig.45), indicates the characteristic band of the raw material and the progressive reorganization of the alumino-silicate as geopolymerization proceeds. Immediately after the synthesis, the position of the main peak already results shifted with respect to the raw material (from 1070 to 1004 cm^{-1}). It passes to 1015 cm^{-1} after 8 h, to return to about 1008 cm^{-1} in the mature geopolymer (yellow marker in Fig.45): these shifts could be related to a variation of the Si/Al ratio in the various stages of the process.

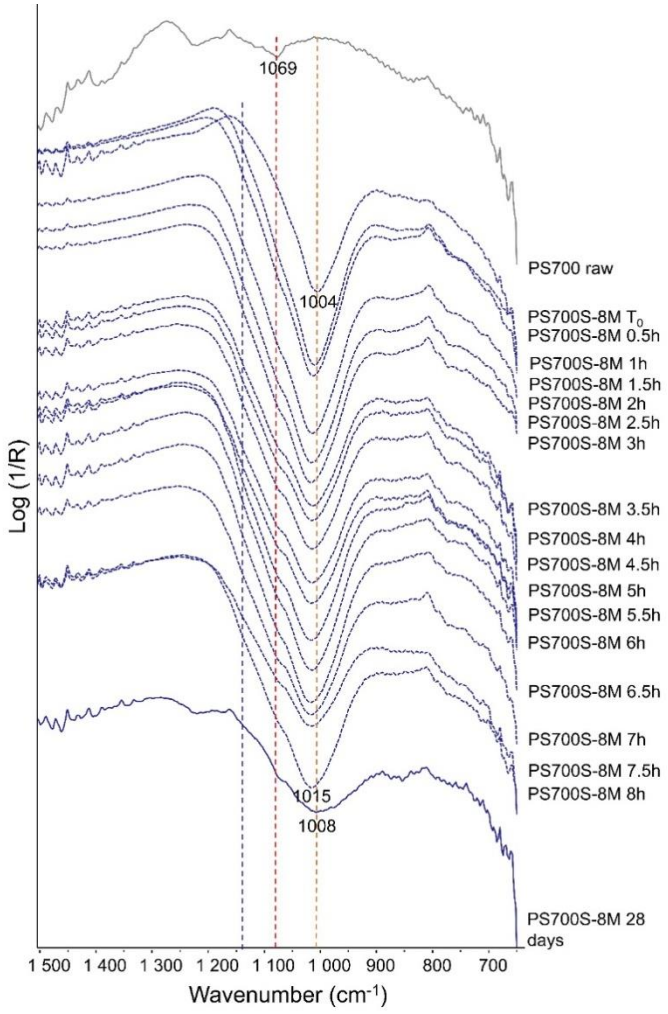

Figure 45- DRIFT spectra in the 1500-750 cm-1 range of the PS clay precursor and PS700S8M sample during the first 8 hours (at a 0.5 hours step) and 28 days after synthesis. The blue dashed line show the appearance, within the main band, of a shoulder around 1150 cm-1, the red one indicates the characteristic alumino-silicate band of the raw material, finally the yellow one indicate the characteristic alumino-silicate band of the mature geopolymer.

- **Raman spectroscopy**

The preliminary results obtained with the portable instrumentation and 785 nm excitation indicated that these conditions were not suitable for the purpose of the work, due both to the wavelength employed and to instrumental features: mainly photoluminescence bands and filter-connected noise were obtained, together with fluorescence. Therefore, the results shown here are those obtained through micro-Raman analysis with a 532 nm excitation. The common, simultaneous presence of crystalline and glassy phases in geopolymer matrices may generate some analytical representativeness issues, especially when using micro-Raman.

Results obtained on the AAMs and published in (M.C. Caggiani, et al. 2021) are reported below and regard only the geopolymer binders obtained by using the plio-pleistocenic clay. Previously, a comparison between clay raw material and geopolymer binder was made in which it was possible to record an increment in the characteristic band of quartz at 464 cm^{-1} and the appearance of two bands at about 960 and 1060 cm^{-1} related to stretching of the Si-O bonds in the SiO_4 tetrahedra as shown in Fig.46. The band at 660 cm^{-1}, as reported in literature, is interpreted both as an indicator of disorder in hematite, but also corresponds to stretching vibrations of SiO_4 tetrahedra in cements (C-A-S-H).

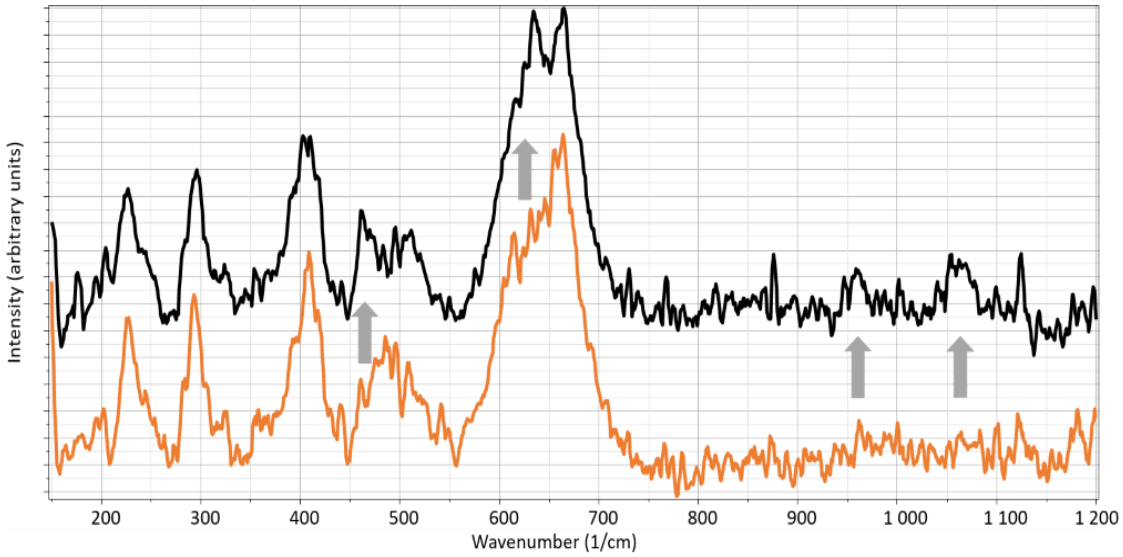

Figure 46- Raman spectra obtained on Plio-pleistocenic clay raw material (line orange), and on geopolymer binder (black line)

In addition, a geopolymer binder was monitored continuously for eight hours, every twenty minutes, starting immediately after alkaline activation of the heat-treated clay. Fig.47 exemplifies the results showing only the spectra where a change could be highlighted. After 100 minutes, quartz main signal (blue line) appears together with those of anatase (red lines). Hematite signature presence is rather constant, while the signals of the other two minerals appear first as weak bands, which in the following spectra increase and decrease, to finally disappear again over the hours. Rather than to a temporal evolution, this seems to be due to micrometric movements of the gel during its polycondensation, also enhanced by the laser excitation. The employ of a 50× LWD objective worsened the representativeness of the results, on the other hand, contact of the objective with the corrosive substance must be avoided. Furthermore, trials with both lower magnification objectives and handheld probes demonstrated that no Raman spectrum at all could be obtained. Starting from 370 minutes after synthesis, the fluorescence background is remarkable and the Raman signals become barely readable. Finally, the Raman analysis performed in the high wavenumber region (3100-3700 cm^{-1}) highlighted a difference between the spectrum of the raw material and that of the respective AAMs. The band at ca. 3440 cm^{-1}, already attested in AAMs analysis with Raman (Steinerová and Schweigstillová 2013) and FT-Raman spectroscopy (Szechyńska-Hebda et al. 2019) and attributed to O-H stretching vibrations, is visible in the reacted product.

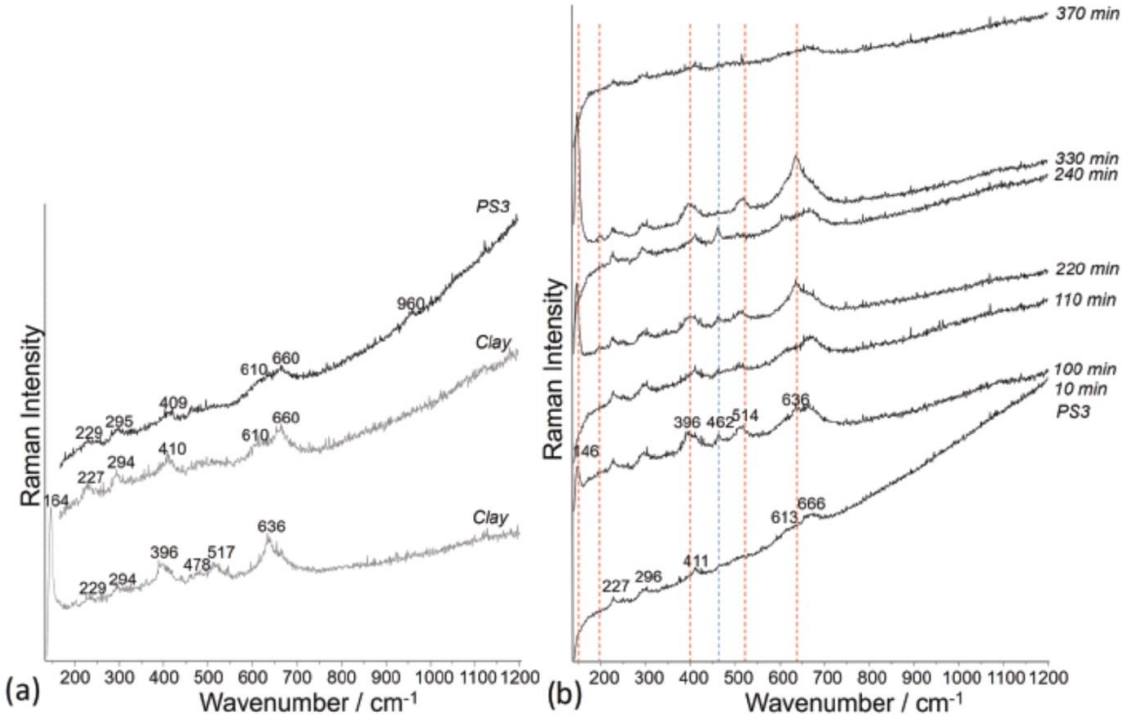

Figure 47- Representative Raman spectra of (a) clay precursor and respective AAM, (b) AAM during geopolymerization; spectra are stacked for clarity by Caggiani et al.2021 The blue line show the presence of quartz, the red one indicates the presence of anatase.

The shown spectra are noisier and most of those acquired are characterized by a stronger fluorescence: the compromise between quality and time of acquisition was more difficult to be achieved, due to the low polarizable character of aluminosilicatic bonds in the clay lattice giving weak Raman scattered signal. The obtained results helped to highlight both advantages and drawbacks of this technique. On one hand, the different kinds of answers that can be provided were pointed out, such as the simultaneous detection of crystalline and amorphous portions, the latter providing information on the reaction degree. On the other hand, the technical and instrumental problems that could hinder its wider usage in the field were clarified, such as check issues and the unsuitability of a red/near-infrared laser for this purpose.

- **Scanning Electron Microscopy and Energy Dispersive X-ray Analysis (SEM-EDX)**

To point out the differences in the microstructure and chemical composition of the obtained AAMs with and without sodium silicate, SEM-EDS analyses were acquired at different magnifications. SEM images depicting the micro-morphological features of the geopolymer binders cured at 85°C for 20h and at room temperature for 28d. Both samples have been described below by distinguishing them according to the raw material used:

- ***Geopolymers with Plio-Pleistocenic clay (PS):*** Overall, PS700-4,6,8M samples cured at 85 °C for 20h showed a quite homogeneous microstructure of the matrix, confirming the amorphous nature of the reaction product, with drying cracks either due to the shrinkage. At 5.00 Kx magnification, unreacted and few rounded grains, bound by geopolymeric gel, can be still recognized as for example on the sample PS700-4,6,8M, as displayed in Fig. 48a-c. At higher magnification (2.74 Kx), spherical voids of 10-30 micron in size are present due to air bubbles trapped in the gel during the synthesis, while fractures are imputable to the shrinkage of the geopolymer paste as you can see in Fig. 48b.

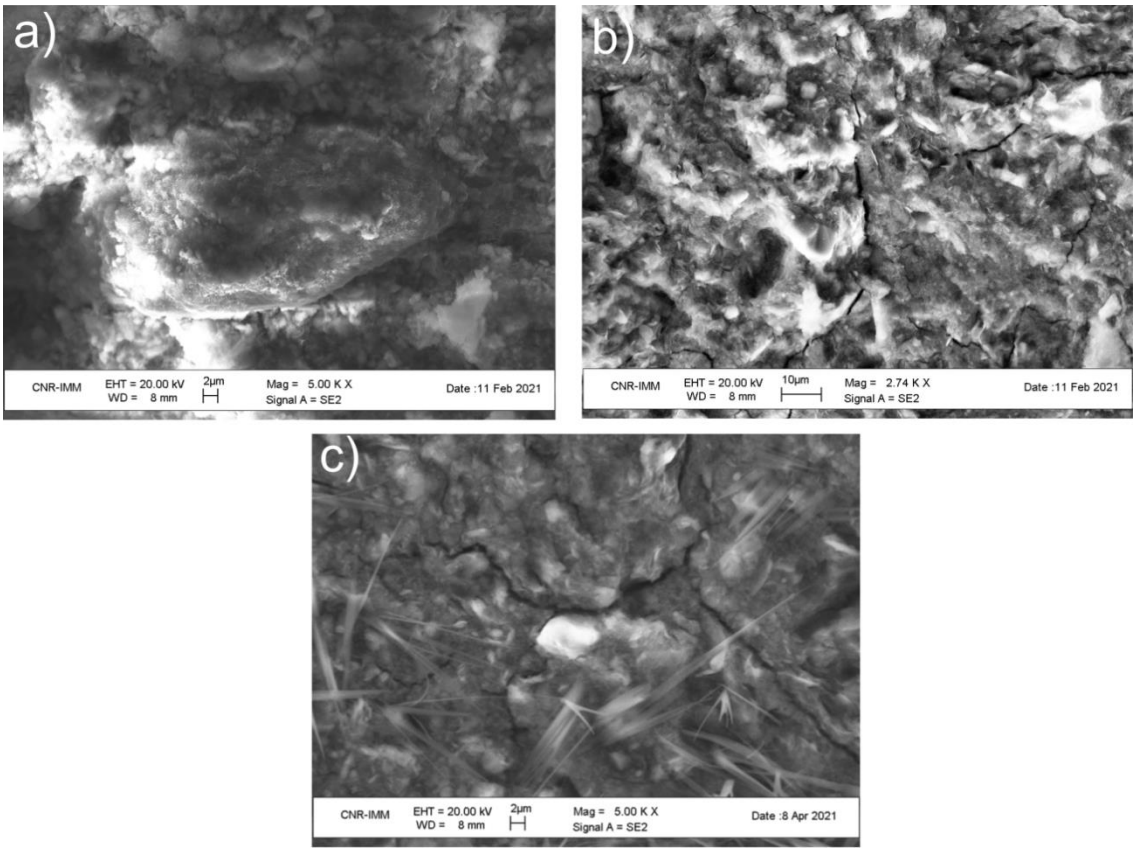

Figure 48- Scanning Electron Microscopy (SE) of PS700-4,6,8 M samples cured at 85 °C for 20h- a) unreacted rounded grain; b-c) details of PS700-6M matrix.

As displayed in Fig.48c, in the sample PS700-8M it is possible to observe, at higher magnification (5.00Kx), how the gel structure formed acicular fibers bounded in divergent clusters that could be distinctive of carbonate salt formation. By EDS analysis, reported in Fig.49, it is possible to observe the chemical composition of the gel matrix in the early crystallization stages of calcium silicate hydrated compounds (N-C-A-S-H) (Hranice, 2002; Taylor, 1986).

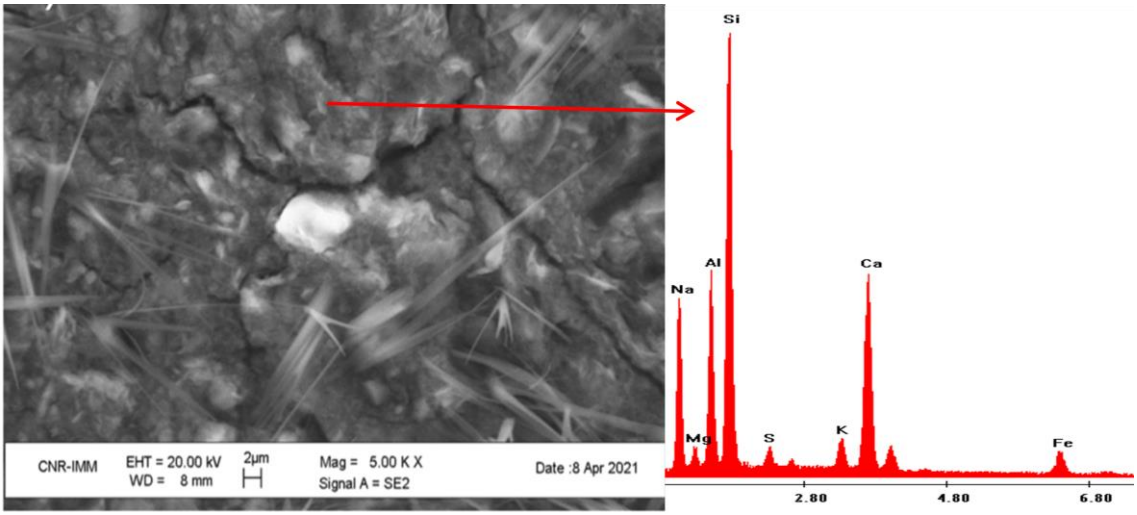

Figure 49-Scanning Electron Microscopy (SE) and EDS analyses on the acicular fibers of PS700-8M sample cured at 85 °C for 20h.

Comparing samples containing sodium silicate (PS700S-4,6,8M) with those without sodium silicate (PS700-4,6,8M), there are no significant differences in their microstructures detectable at lower magnification, as shown in Fig.50.

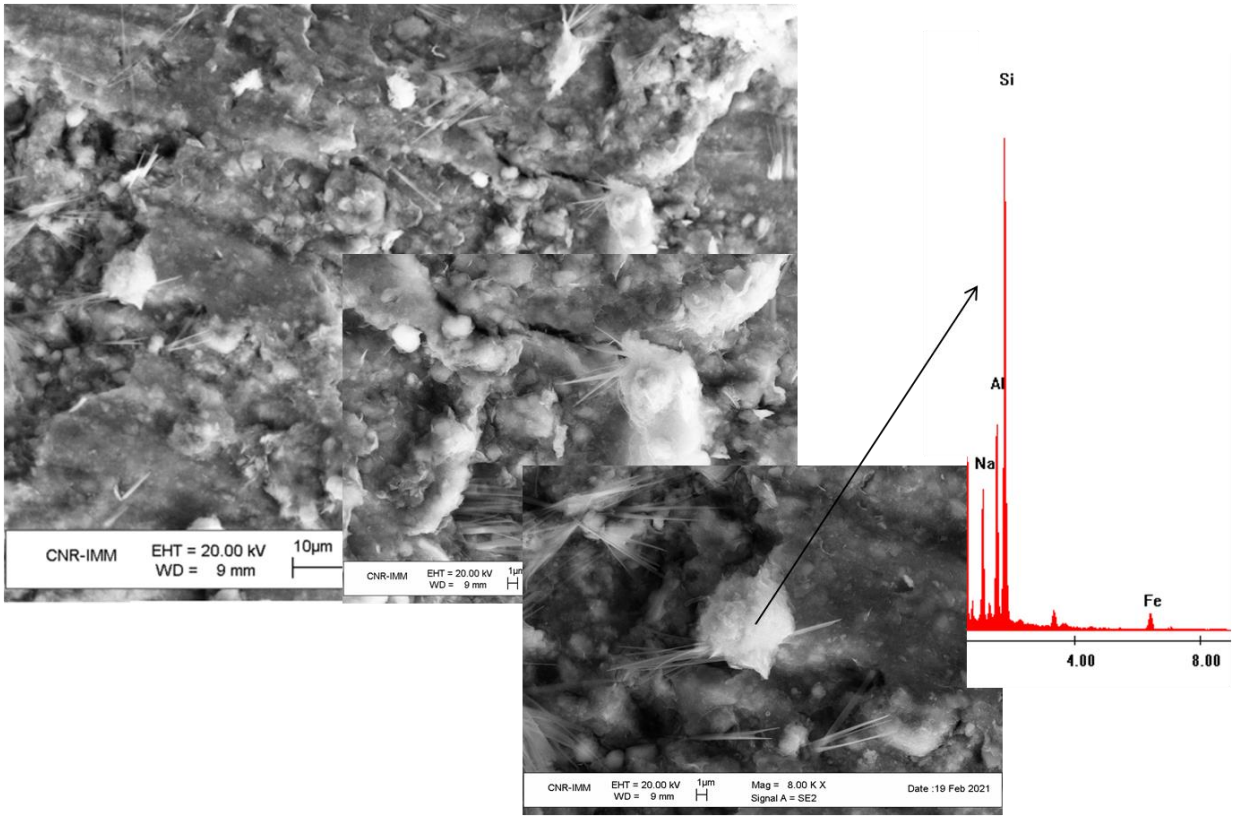

Figure 50- Scanning Electron Microscopy (SE) and EDS analyses of PS700S-8M sample cured at 85 °C for 20h.

Regarding samples cured for 28 days at room temperature and activated with sodium hydroxide and sodium silicate, the geopolymer gel appears to be coating the unreacted particles and binding them together. However, the samples containing sodium silicate appears more interconnected with a denser gel presence than the sample without sodium silicate and the matrix structure appears more compact. Indeed, it can be observed a dense and continuous formation of gel inside and outside voids and a microstructure with regular-shaped particles and variable geometry as displayed in Fig.51.

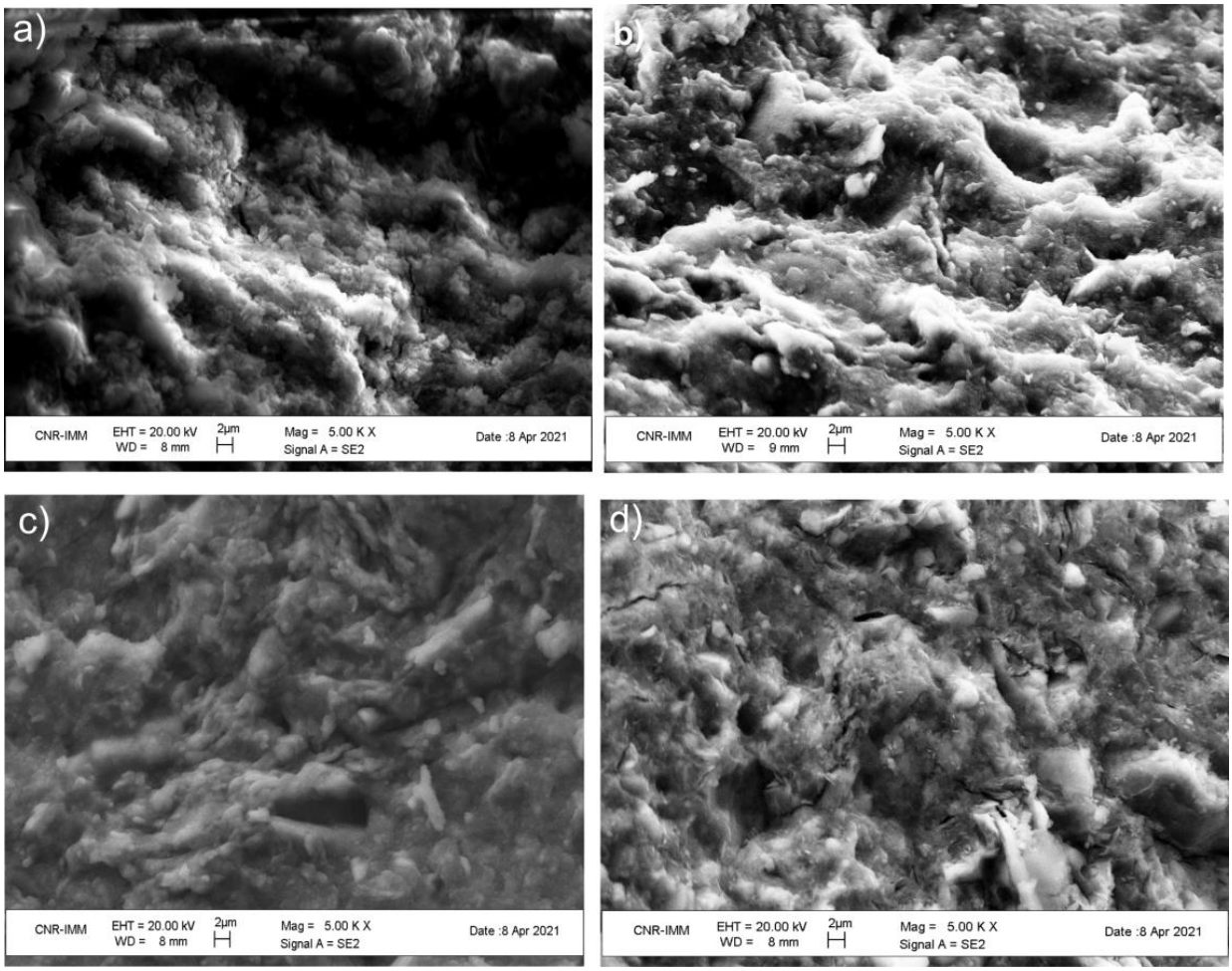

Figure 51- Scanning electron microscopy (SE) of PS700S-4,6,8M samples cured at room temperature for 28d.

SEM-EDS analysis have been conducted in order to investigate the chemical composition of the geopolymer matrix and of the new formed gel phase. The analysis of the microstructure for both samples confirms the development of the alkali activated gel. In Fig.52 and 53, the Al_2O_3/SiO_2 and CaO/SiO_2 ratios of the obtained geopolymer binders, have been plotted in a binary and triplot diagram. Furthermore, the composition ranges which, according to the literature (Garcia-Lodeiro et al 2011; Pardal et al., 2009) characterize the main types of gels, (C-S-H, C-(A)-S- H, C-A-S-H, N-A-S-H and (N,C)-A-S-H), are also marked on the figure. As displayed in the graph, (Fig.49), geopolymer binders obtained only with sodium hydroxide (NaOH) and those obtained adding sodium silicate solution at the mixture, exhibits gel compositions clustered in the N-C-A-S-H field, while only one point plots in the C-A-S-H area. In this multi-component system, the main reaction product was a gel mixture in which sodium silicate plays an important role in the geopolymerization and hardening process. Indeed, C-A-S-H gel derive from the presence

of Ca in the clay raw material while N-C-A-S-H gel derive from the activation of alkaline aluminosilicates, in which during a reaction product much of the original sodium was replaced by calcium as result of well-known ionic exchange mechanisms (García-Lodeiro, I., et al. 2010; Garcia-Lodeiro, I. et al. 2011). The coexistence of N-C-A-S-H and C-A-S-H gels, also shown in the ternary diagram, depends on the initial calcium content and alkalinity of the system.

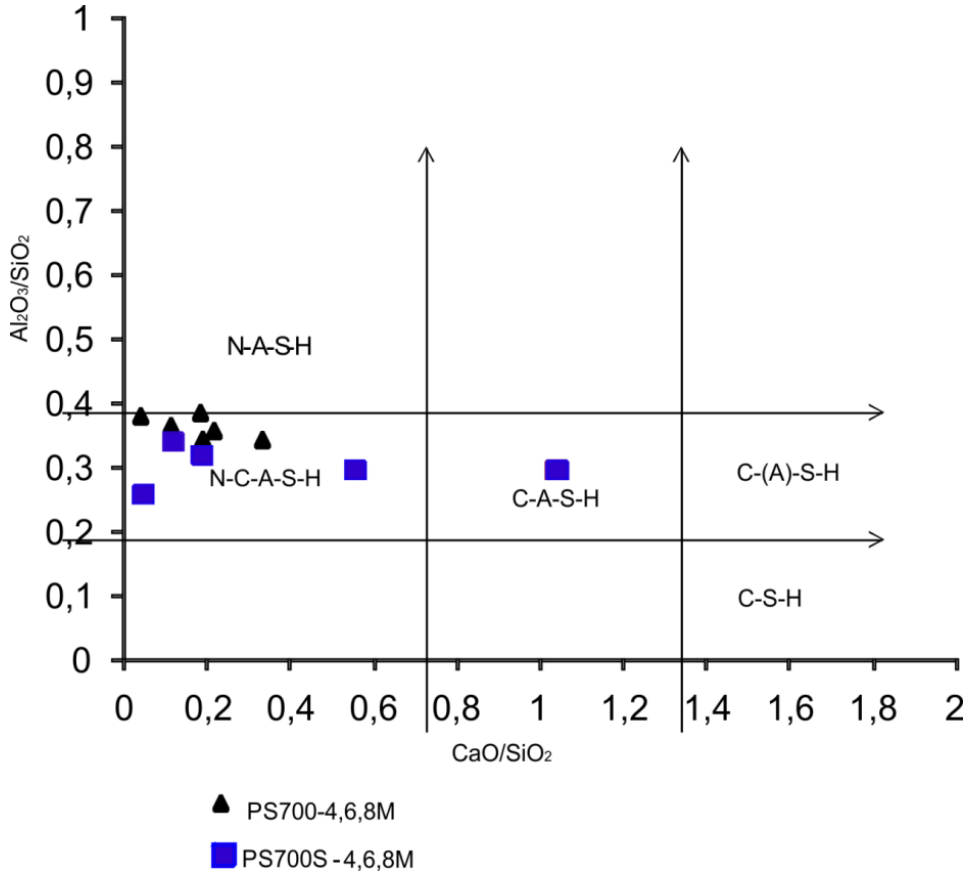

Figure 52- Al_2O_3/SiO_2 vs. CaO/SiO_2 ratios for gels precipitating in hybrid cements (based on EDS findings) on the samples PS700-4,6,8M and PS700S-4,6,8M.

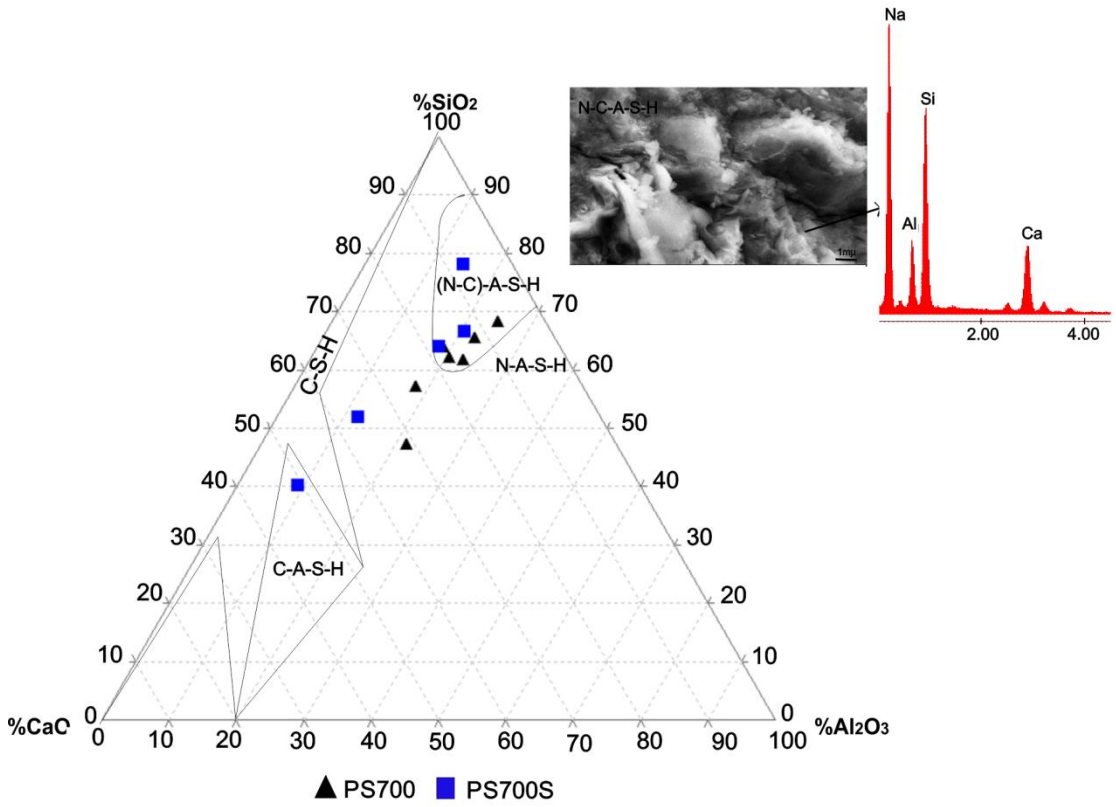

Figure 53- Ternary diagram Al_2O_3-SiO_2-CaO for gels precipitating in hybrid cements (based on EDS findings) on the samples PS700-4,6,8M and PS700S-4,6,8M.

- ***Numidican clay (NU):*** Geopolymer samples (NU700-6,8M) activated with only sodium hydroxide shown a heterogeneous matrix with regular-shaped particles and variable geometry such as angular or sub-spherical morphology. In more detail, NU700-6M sample shows a granular matrix aspect in which the newly formed gel appears to have a lumpy form that seems to attach to the unreacted bodies. While, the NU700-8M sample in respect to the previous one, shows the same granular aspect of the matrix but the morphology of the gel is much more well defined, (Fig.54 a-b).

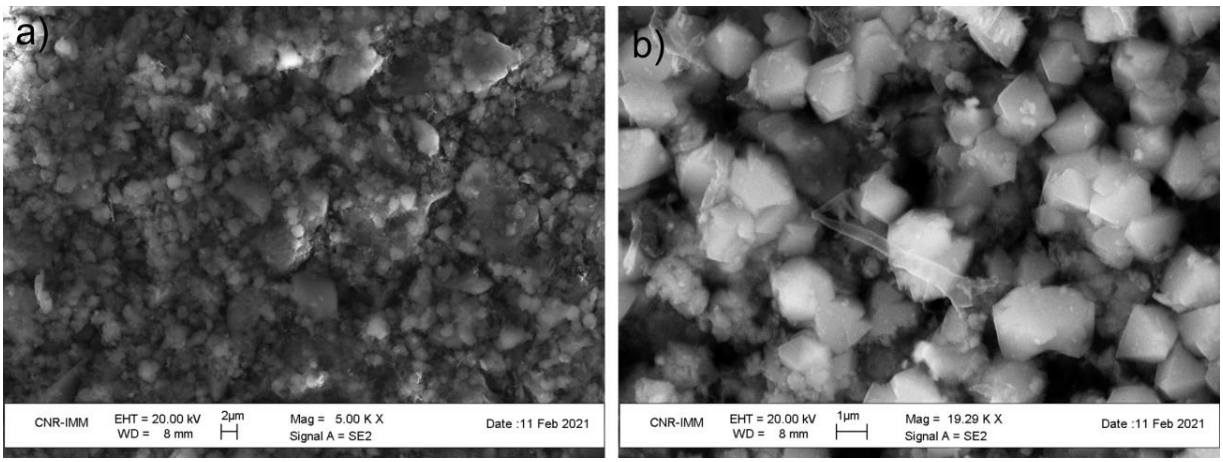

Figure 54- Scanning electron microscopy (SE) on geopolymer samples activated with only sodium hydroxide and cured at 85 °C for 20h: a) NU700-6M; b) NU700-8M

Comparing samples containing sodium silicate (NU700S-4,6,8M) with those without sodium silicate (NU700-4,6,8M), it is possible to observe that there are significant differences in their microstructures detectable at lower magnification, as shown in Fig.55 a-b, in which samples NU700-8M and NU700S-8M are compared.

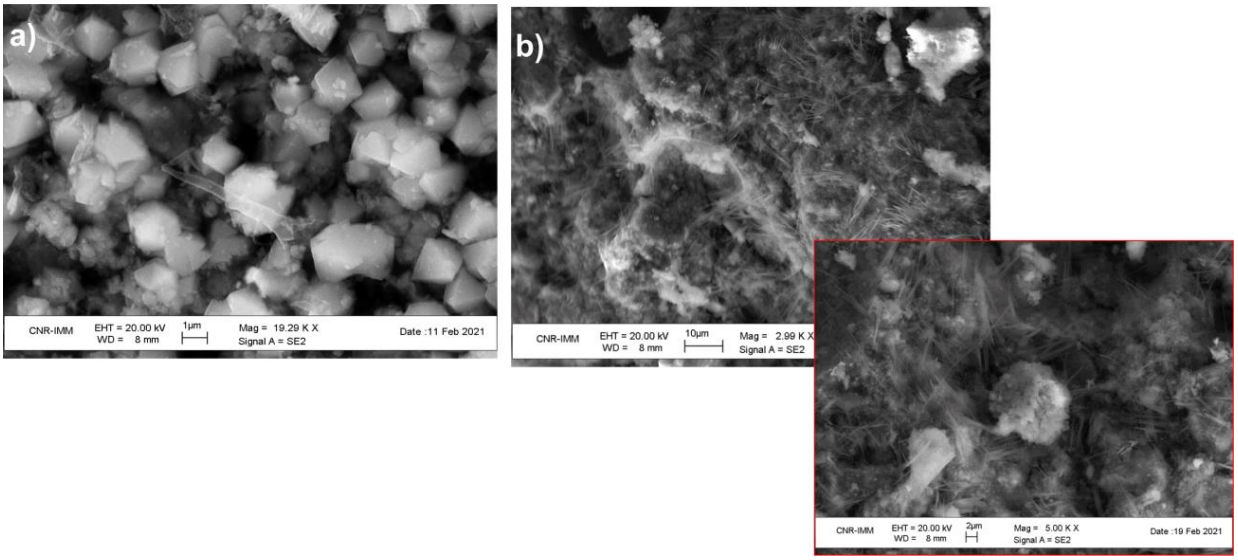

Figure 55- Scanning electron microscopy (SE) on geopolymer samples cured at room temperature for 28d: a) NU700-8M; b) NU700S-8M with a zoom detail.

Indeed, sample NU700S-8M (Fig.55b), present a more dense and homogeneous matrix with spherical object characterized by different acicular fibers.

On the basis of EDS analyses and morphology, the regular-shaped particles, detected in the sample of Fig.55a, could be crystals attributable to zeolites as Faujasite, as reported in Fig.56 and confirmed also by XRD investigation. (Duxon et al., 2007).

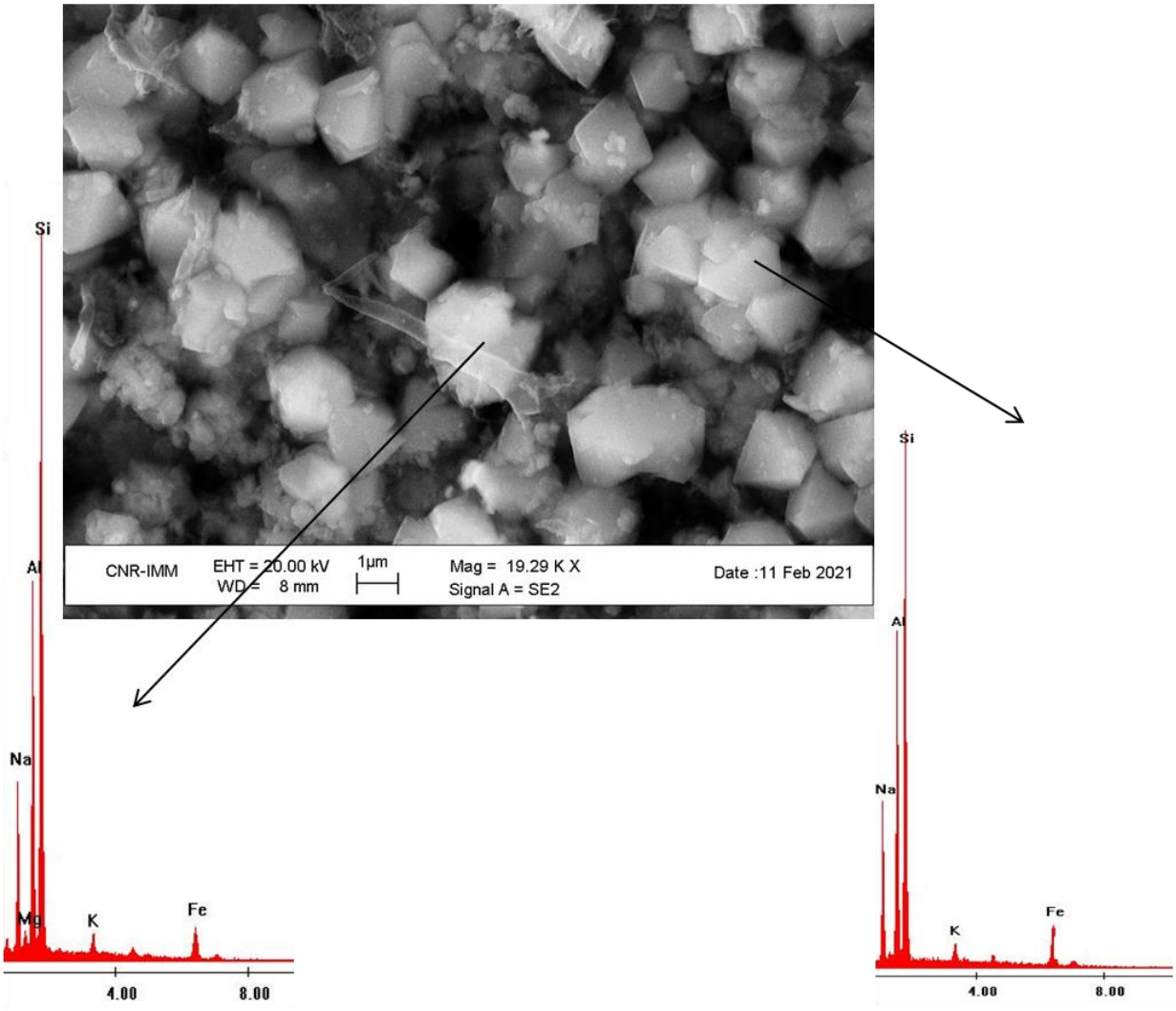

Figure 56- Scanning electron microscopy (SE) and EDS analyses of NU700S-8M sample cured at room temperature for 28d.

Regarding samples cured for 28 days at room temperature and activated with sodium hydroxide and sodium silicate, the geopolymer gel appears to be coating the unreacted particles and binding them together whit a homogeneous network, (Fig.57a). Different cracks probably related to the shrinkage of the geopolymer paste and voids (15-20 micron) due to the formation of air bubble are present, as displayed in Fig.57b .

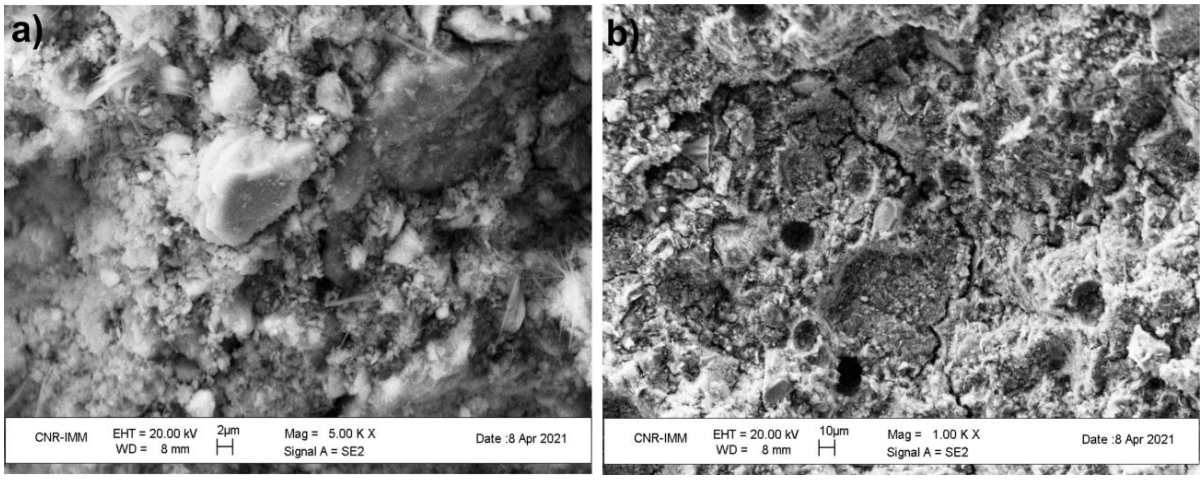

Figure 57- Scanning Electron Microscopy (SE) of NU700S-8M sample cured at room temperature for 28d: a) geopolymer gel appears to be coating the unreacted particle; b) detail of the matrix characterized by the presence of diverse cracks and voids;

In order to better define the chemical composition of the geopolymer matrix, EDS analyses have been carried out in different points of the gel-like material. Trough these analysis it is possible to affirm that the geopolymer binders are composed by Na, Al, Si, and K. In detail, from EDS analyses it is possible to highlight difference in composition between the matrix and the crystals, meaning that these latter are zeolites. These crystals are composed by Na, Al, Si and S, as detected from the EDS spectra, and from their shape and composition, they could be intended as zeolites. In addition, as displayed in Fig.55, the Al_2O_3/SiO_2 and Na_2O/SiO_2 ratios of the obtained geopolymer binders, have been plotted with the diverse main types gels, (C-S-H, C-(A)-S-H, C-A-S-H, N-A-S-H and (N,C)-A-S-H). As displayed in the graph and in the ternary diagram Fig.58-59, geopolymer binders obtained only with sodium hydroxide (NaOH) exhibits a number of compositional clusters that are positioned in the N-A-S-H gel zones, due to the absence of Calcium in the raw material. Samples obtained by adding sodium silicate solution at the mixture maintain the same behaviour of the previous one with diverse points clustered in the N-A-S-H gel zone.

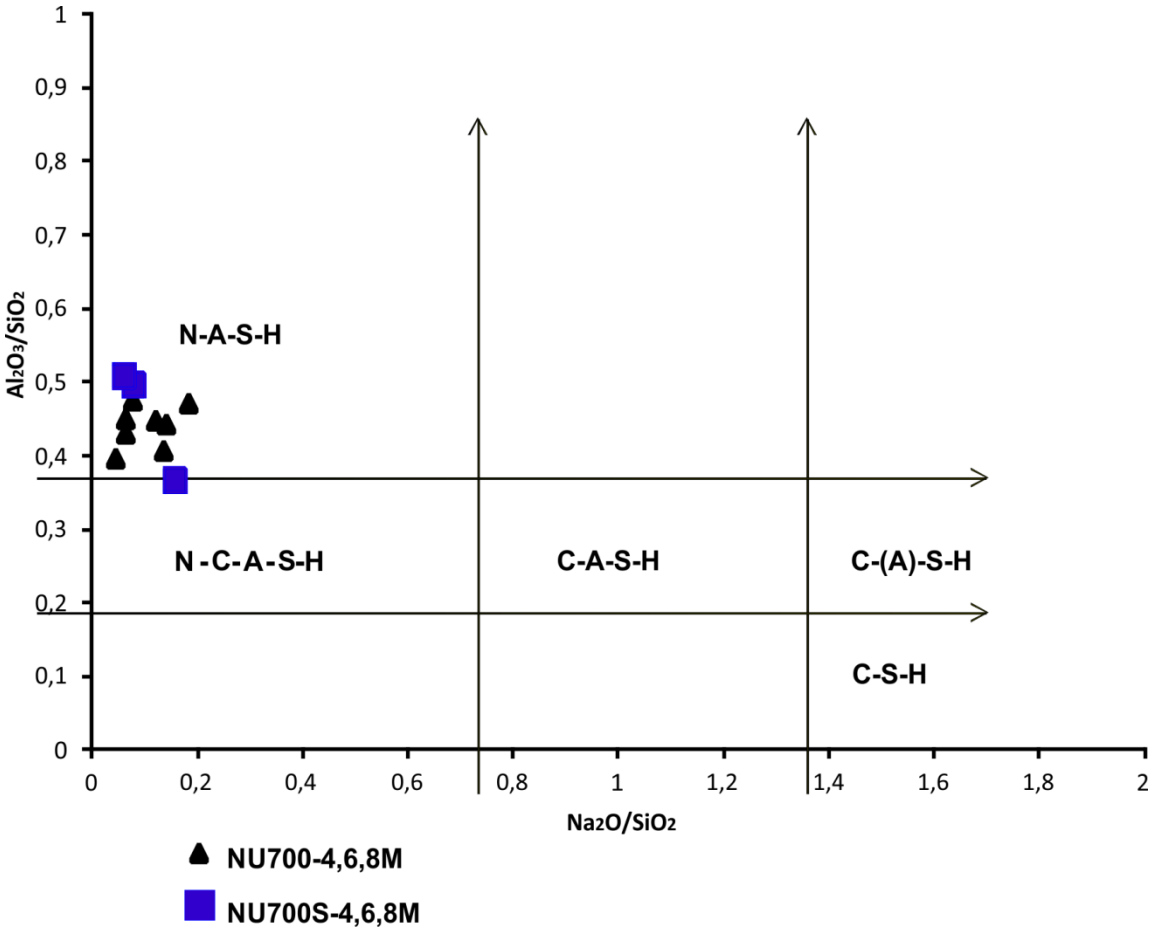

Figure 58 - Al_2O_3/SiO_2 vs. Na_2/SiO_2 ratios for gels precipitating in hybrid cements (based on EDS findings) on the samples NU700-4,6,8M and NU700S-4,6,8M.

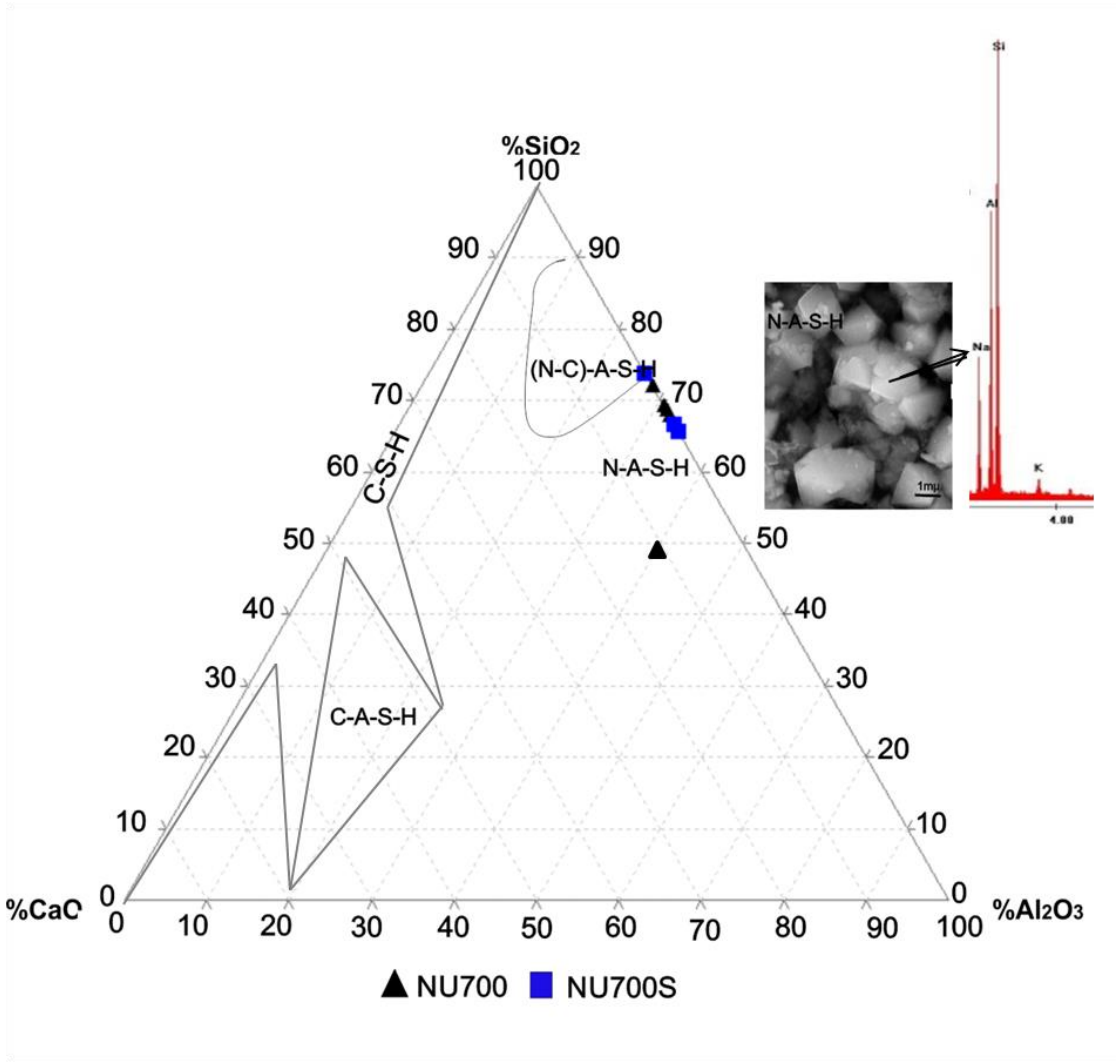

Figure 59- Ternary diagram Al2O3-SiO2-CaO for gels precipitating in hybrid cements (based on EDS findings) on the samples NU700-4,6,8M and NU700S-4,6,8M.

- ***Variegated clay (VC):*** Considering the failure of the geopolymer binders activated with sodium hydroxide 4M and 6M, only the sample labelled VC700-8M cured at 85°C for 20h has been analyzed. This sample shows a homogeneous matrix characterized by unreacted particles and aluminosilicate gel that binds them together. Several fractures are present in the matrix, probably related to the shrinkage of the geopolymer paste. In detail, defects in the gel network are also represented by the presence of small crystals, as shown in Fig.60 a-d.

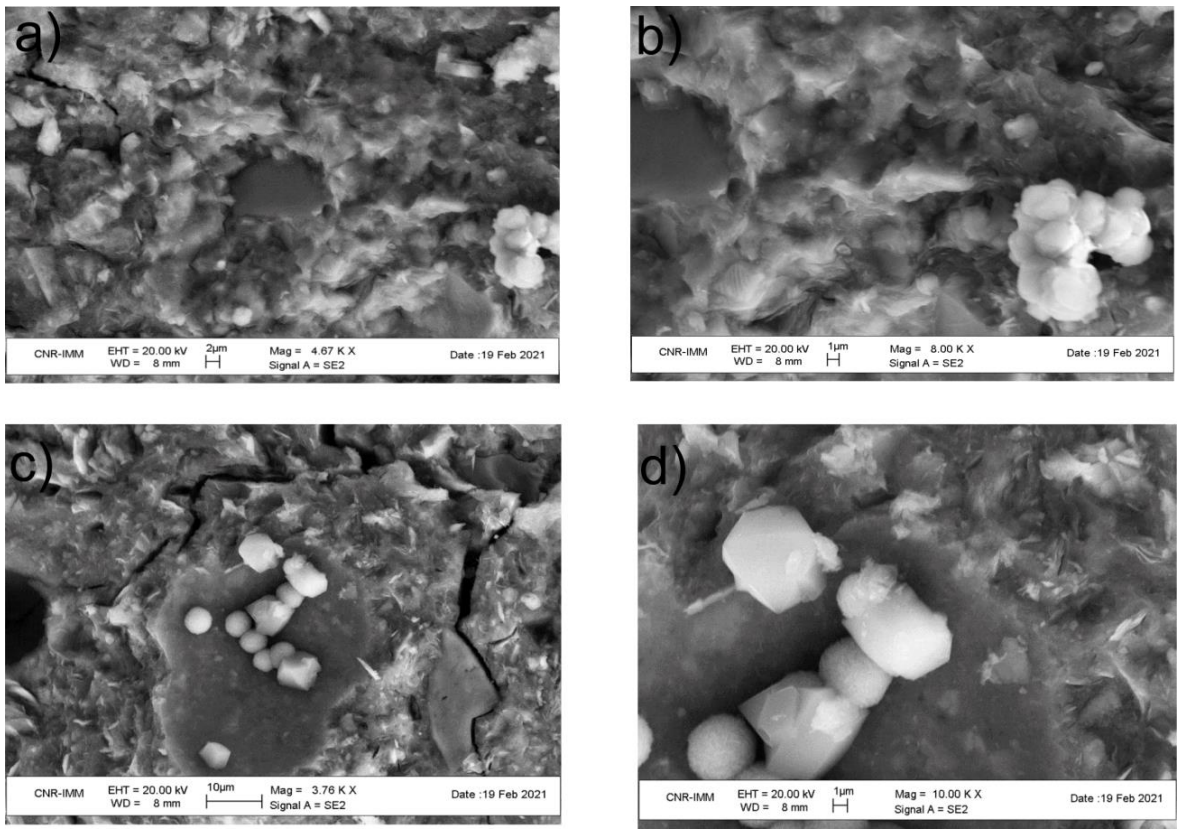

Figure 60 a-d- Scanning Electron Microscopy (SE) at diverse magnification of VC700-8M sample cured at 85 °C for 20h.

These crystals are composed by Na, Al, Si and on these crystal diverse sub-spherical bodies have been identified as shown in Fig.61, and by EDS analysis, the composition allowed to define them as zeolites.

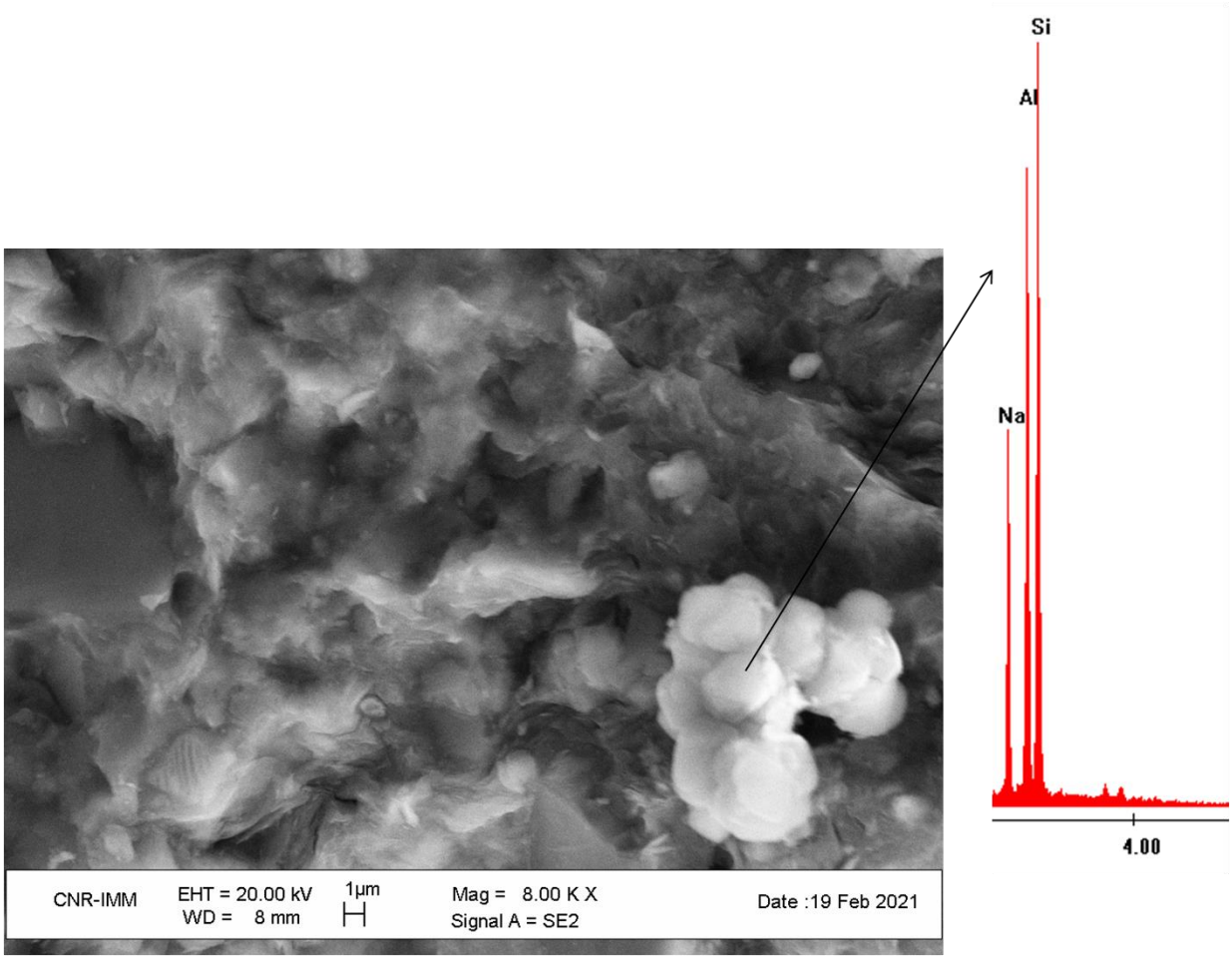

Figure 61- Scanning electron microscopy (SE) and EDS analyses of VC700-8M sample cured at 85 °C for 20h.

Regarding geopolymer binder obtained after 28 days of curing at room temperature, samples VC700-8M, VC700S-6 and 8M have been analyzed.

Sample VC700-8M present the same morphological aspect than the analogues sample cured at 85°C for 20h in which a dense formation of aluminosilicate gel can be detected whit exactly the same unreacted particles Fig.62a. Concerning geopolymer binders activated by adding sodium silicate solution, sample VC700S-6M shows a heterogeneous matrix composed by diverse morphological forms of the new formed aluminosilicate gel and unreacted particles of the raw material (Fig.62b). In detail, at higher magnification, it can also possible to note the chaotic morphological aspect that characterize this sample with a lot of unreacted particles with different geometrical form often enveloped by the aluminosilicate gel.

Sample VC700S-8M shown an homogeneous matrix characterized by the presence of a dense aluminosilicate gel that is predominant in the structure of the geopolymer

binder, (Fig.62c). Finally, few voids and no unreacted particles were detected as displayed in Fig.62d.

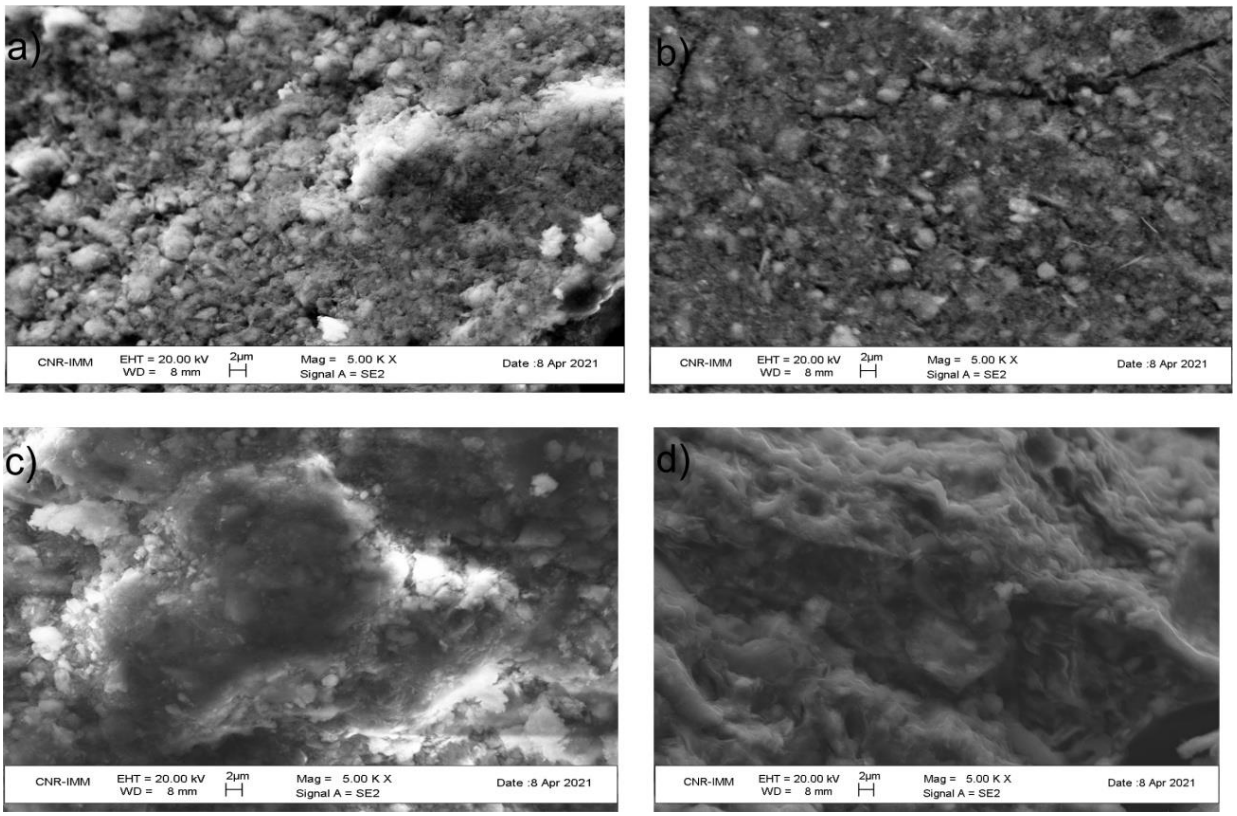

Figure 62- Scanning electron microscopy (SE) on samples cured at 85 °C for 20h: a) sample VC700-8M; b) VC700S-4M; c) VC700-6M; d) VC700S-8M;

EDS analysis of the obtained geopolymer binders, have been conducted in order to determine the chemical composition of the matrix. Also for these binders, the Al_2O_3/SiO_2 and Na_2O/SiO_2 ratios have been reported on the gels type plot, (N-A-S-H- N-C-A-S-H, C-(A)-S-H, C-S-H). As displayed in Fig.63 and in the ternary diagram Fig.64, the matrices are primarily composed by N-A-S-H gel and rarely by N-(C)-A-S-H gel.

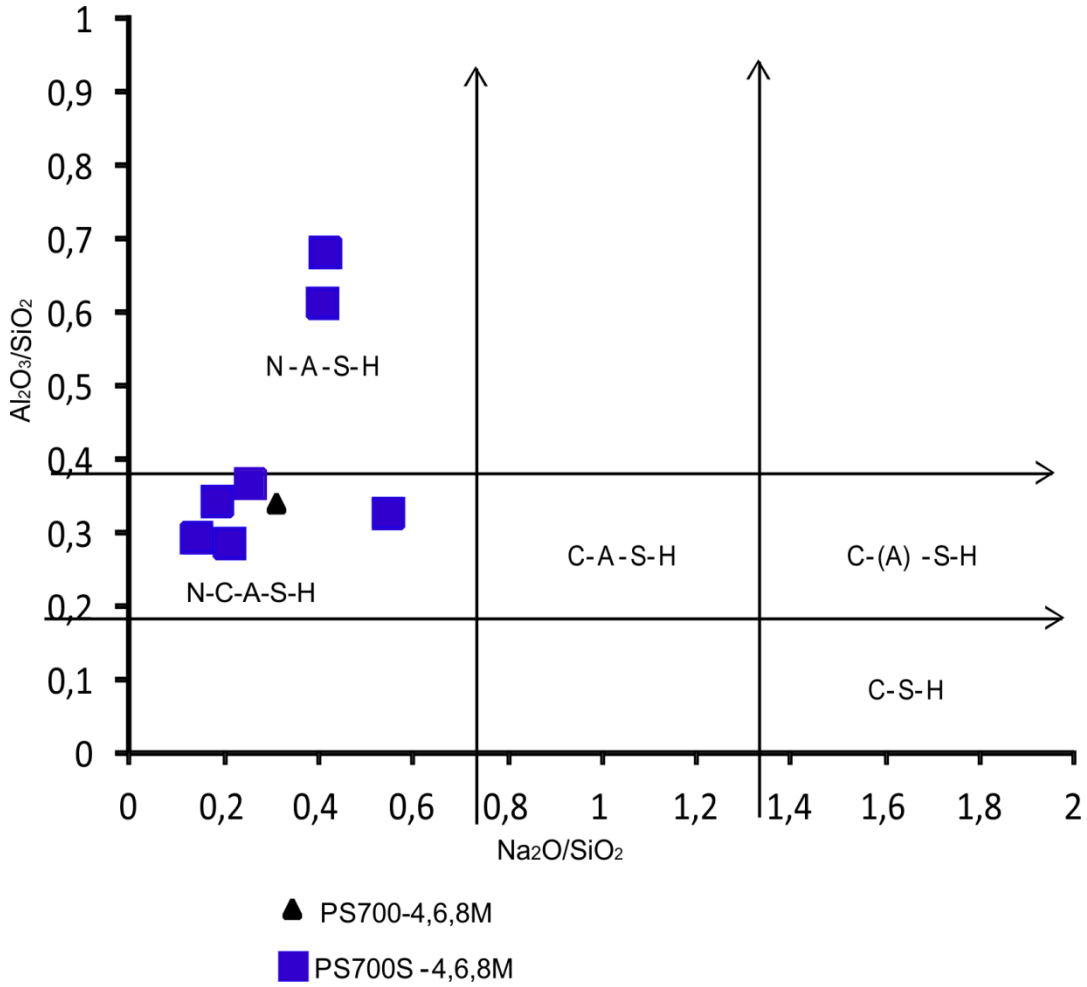

Figure 63- Al_2O_3/SiO_2 vs. Na_2/SiO_2 ratios for gels precipitating in hybrid cements (based on EDS findings) on the samples VC700-4,6,8M and VC700S-4,6,8M.

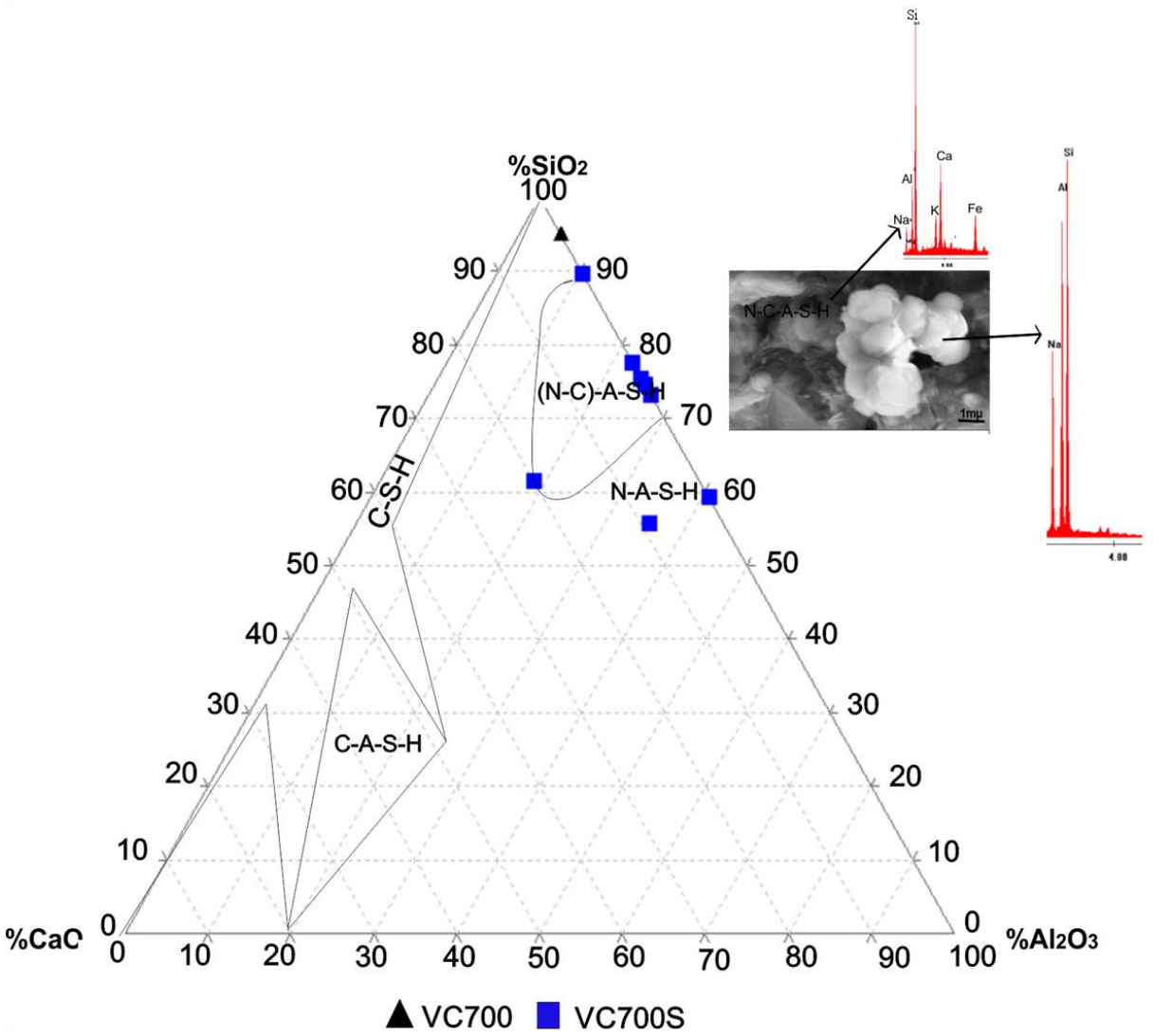

Figure 64- Ternary diagram Al2O3-SiO2-CaO for gels precipitating in hybrid cements (based on EDS findings) on the samples VC700-4,6,8M and VC700S-4,6,8M.

- **Hg intrusion porosimetry test (MIP)**

A few samples of the obtained geopolymer binders, labelled (PS700-4,6,8M and NU700-4,6,8M) have been analyzed by means of Hg intrusion porosimetry (MIP) in order to investigate their porosity at sub-micrometric scale. The comparison of cumulative pore volume trends for each sample, taking into account the influence of the different molarities of sodium hydroxide utilized in the mixture, are shown in Tab.16. Geopolymer binders obtained with plio-pleistocenic clay (*PS700-4,6,8M*) and cured at 85°C for 20h were analyzed. In detail, *PS700-4M* shows a low pore volume of 8.17 cm^3/g in the range 0.1-1 µm and of 8.78 cm^3/g in the range 0.01-0.001 µm with an accessible porosity of 4.13 % and a bulk density 1,42 g/cm^3. Instead, *PS700-6M* and *PS700-8M* recorded an absent pore volume in the range 0.1-0.01 µm and a higher pore volume of about 56.35 cm^3/g in the range 0.01-0.001 whit a quite equivalent accessible porosity (~4.83%) and bulk density of 0.32 g/cm^3 respectively. Regarding geopolymer binders obtained by using Numidican clay, sample labelled *NU700-4,6,8M* and cured at 85°C for 20h were analyzed like the previous one. In this case, *NU700-4M* has a higher pore volume in the range 0.1-0.01 µm of 73.47 cm^3/g and 12.74 cm^3/g in the range 0.1-0.01 µm while *NU700-6M* and *NU700-8M* shows an increase of pore volume in the range 0.1-0.01 µm in respect to the previous one. Regarding the bulk density, *NU700-4M* and *NU700-8M* have similar values, in detail the first one of about 1.84 g/cm^3 and the second one of about 1.62 g/cm^3, while the accessible porosity is of about 4.52% for *NU700-4M* and 3.49% for *NU700-8M*. Sample *NU700-6M* present a bulk density of about 4.18 g/cm^3 and accessible porosity of about 9.34%.

Table 16- Hg intrusion Porosimeter sample (NU and PS) cured at 85°C for 20h

Porosimetric data		NU700-4M	NU700-6M	NU700-8M	PS700-4M	PS700-6M	PS700-8M
Bulk Density (g/cm^3)		1,84	4,18	1,62	1,42	0,32	0,32
Accesible Porosity (%)		4,52	9,34	3,49	4,13	4,83	4,70
Total Pore Volume (g/cm^3)		0,24	0,22	0,21	0,29	0,15	0,14
Average Pore Diameter (µm)		0,04	0,05	0,05	0,02	0,01	0,01
Pore volume (cm^3/g) in the following ranges: (µm)	**100-10 µm**	0,21	0,02	0,07	0,01	5,07	3,74
	10-1 µm	1,03	0,15	0,45	0,05	3.25	2,09
	1-0.1 µm	73,47	49,45	45,16	8,17	0,00	0,000
	0.1-0.01 µm	12,74	52,49	66,09	0,00	0,000	0,000
	0.01-0.001 µm	16,98	14,63	11,19	18,78	56,35	54,28

In general, as noted in Tab.16 and shown in Fig.65, all samples exhibit a total porosity that tends to decrease as the molarity of the soda increases. This trend is very

marked in the samples obtained by using Plio-Pleistocenic clay. Indeed, sample PS700-4M showing a total pore volume of 0.29 (g/cm^3) and sample PS700-8M showing approximately 0.14 (g/cm^3). Regarding to the cumulative pore volume, the highest values are recorded in the range 0.1-0.01 µm (52.49 cm^3/g) for NU700-6M, while 66.09 cm^3/g for NU700-8M, instead in the range 0.01-0.001 µm for PS700-6M and PS700-8, with absent pore volume in the range 0.1-0.01 µm.

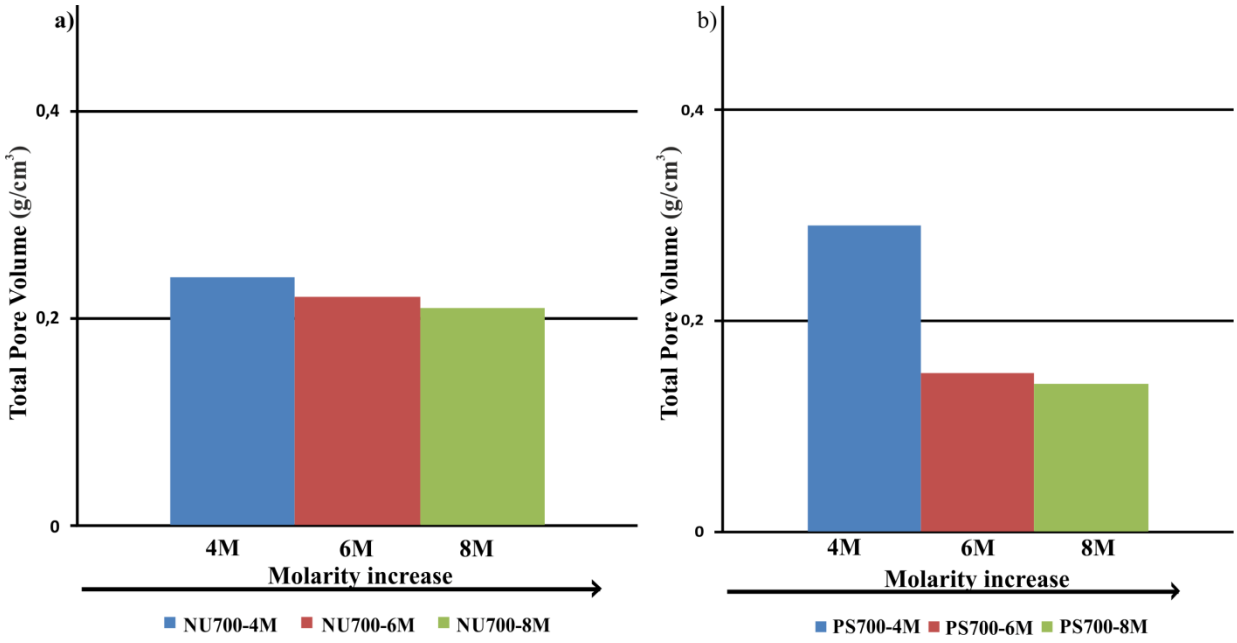

Figure 65a- Total Pore Volume expressed in g/cm^3 of the samples NU700-4,6,8M; b) Total Pore Volume expressed in g/cm^3 of the samples PS700-4,6,8M;

- **Capillary water absorption test**

Capillary water absorption tests were carried out according to the NORMAL 11/82 by using three cubic specimens for each formulation with a dimension of 324 mm^2. In detail, specimens obtained by using sodium hydroxide (8M), with and without sodium silicate, cured at room temperature for 28 days, were analyzed in order to define the amount of water absorbed per unit area as a function of time (t), expressed in g/cm^2.

At each weighing in the various time intervals, the surface of the sample in contact with water was dried with a damp cloth and then the sample was placed on the precision balance to measure its weight, (Tab.11). Overall, the absorption test ended after 4 hours and only VC700-8M failed the test due to numerous cracks that formed during capillary rise. At the end, the amounts of water absorbed were calculated by subtracting the final mass from the initial mass, all divided by the surface area of the sample in contact with the porous surface (cm^2) as reported below:

Mf= mi-mo/s

Mf= Initial mass*

Mr= Final Mass*

S= Surface area of the sample in contact with the porous surface (cm^2)*

From these data, it is possible to observe that sample PS700-8M absorbed 1.21 g of water while no measurements could be made on sample PS700S-8M. Sample NU700-8M shows a different behavior respect to the previous one, having absorbed a lot of water in a short time than 4h, 1.63 g, as shown in (Fig.66), while NU700S-8M has absorbed 1.31 g. Sample VC700S-8M shown the same behavior of sample NU700S-8M with a final absorption of about 1.12 g of water.

Comparing the data obtained from sample NU700-8M and sample PS700-8M with those obtained from porosimetric analysis, it can be possible to find a correlation between accessible porosity and amount of absorbed water.

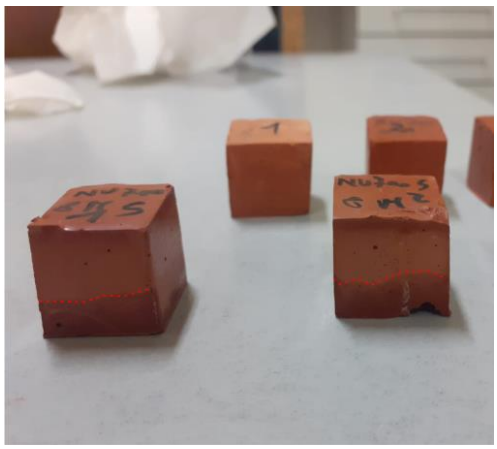

Figure 66- Example of capillary water absorption tests carried out according to UNI EN 10859:2000 on all obtained samples.

Table 17- Amount of water absorbed per unit area as a function of time (t) of the obtained geopolymer binders.

Sample	0 min	1 min	3 min	5 min	10 min	20 min	30 min	40 min	60 min	4h
NU700-8M	12,67	14,34	15,39	15,68	15,68	15,70	15,70	15,70	15,72	15,72
NU700-8M	12,00	14,13	14,79	14,82	14,81	14,83	14,83	14,84	14,85	14,84
NU700-8M	12,08	14,04	14,90	14,94	14,92	14,94	14,95	14,96	14,96	14,95
Media	12,25	14,17	15,03	15,15	15,14	15,15	15,16	15,17	15,18	15,17
St. Dev	0.37	0.15	0.32	0.47	0.47	0.47	0.47	0.47	0.47	0.48
NU700S-8M	12,61	13,11	13,50	13,91	14,34	14,73	14,99	15,00	15,01	15,01
NU700S-8M	12,99	13,51	13,93	14,49	15,05	15,33	15,37	15,37	15,39	15,39
NU700S-8M	12,50	12,98	13,32	13,72	14,36	14,79	14,80	14,81	14,82	14,82
Media	12,70	13,20	13,58	14,04	14,58	14,95	15,06	15,06	15,07	15,07
St. Dev	0.25	0.27	0.31	0.40	0.41	0.33	0.29	0.29	0.29	0.29
PS700-8M	13,19	13,53	14,10	14,48	14,87	15,06	15,14	15,15	15,17	15,15
PS700-8M	13,65	13,99	14,53	15,06	15,38	15,68	15,85	15,87	15,87	15,88
PS700-8M	13,18	13,69	14,61	15,03	15,36	15,51	15,49	15,52	15,52	15,52
Media	13,34	13,74	14,41	14,86	15,21	15,42	15,49	15,51	15,52	15,52
St. Dev	0.27	0.23	0.27	0.32	0.29	0.32	0.36	0.36	0.35	0.36
VC700-8M	11,90									
VC700-8M	12,20									
VC700-8M	11,37									
Media	11,82									
St. Dev	0.42									
VC700S-8M	12,29	13,70	14,04	14,95						
VC700S-8M	12,32	13,97	14,45	14,47	14,57	14,64	14,65	14,77	14,76	14,19
VC700S-8M	11,94	12,96	13,85	13,82	13,97	14,04	14,06	14,13	14,15	14,19
Media	12,15	13,54	14,11	14,48	14,27	14,34	14,36	14,45	14,46	14,19
St. Dev	0.21	0.55	0.31	0.52	0.43	0.42	0.42	0.45	0.42	0.00

- **Vicat Needle test**

Geopolymer binders characterized with this test are: *PS700S-8M*, *NU700S-8M* and *VC700S-8M*.

Thirty minutes after adding the alkaline solution to the precursor, sample *PS700S-8M* has been put under the needle and allowed to settle under its own weight, as displayed in Fig. 67.

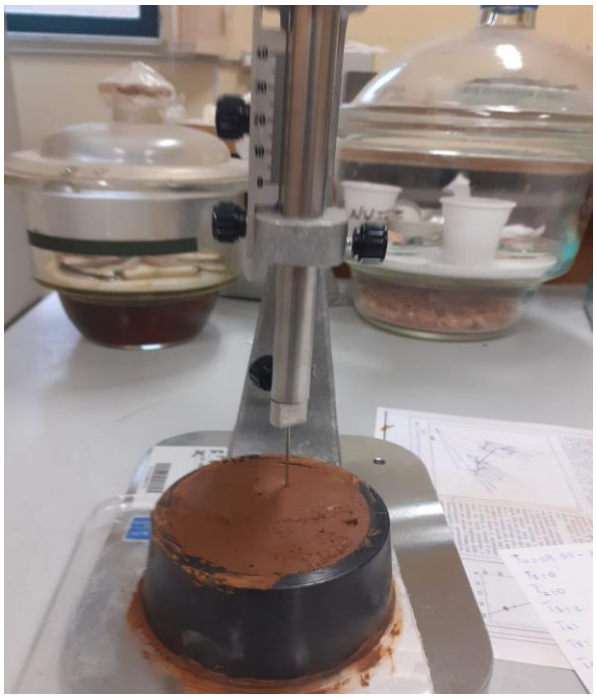

Figure 67 - Vicat Needle test on the samples

After the first thirty minutes, the needle was dropped for the first time measuring the depth reached. The test was repeated every 15 minutes until a depth of less than 25 mm was obtained. In the case of the PS700S-8M sample, only 5 measurements were required to reach a depth of 25 mm as shown in Fig.68.

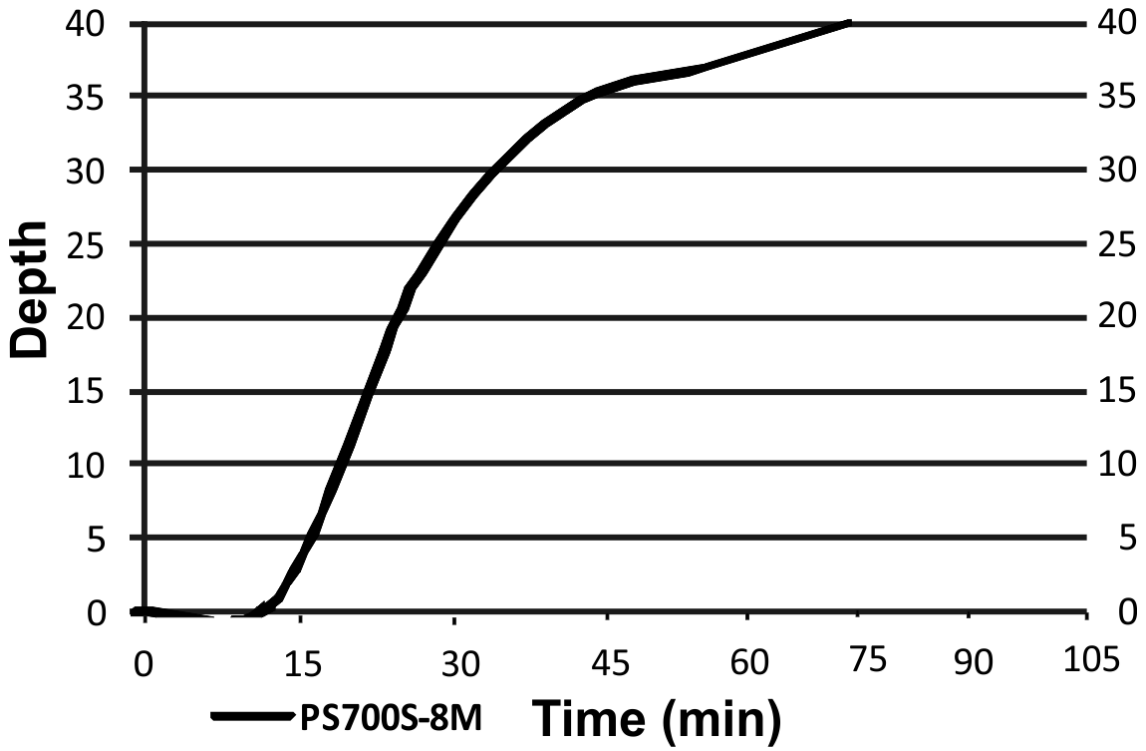

Figure 68- Needle penetration depth on PS700S-8M sample

Regarding samples labelled NU700S-8M and VC700S-8M the geopolymerization process required more time than the previous one. Indeed, after the first thirty minutes, the needle was dropped for the first time measuring the depth reached. The test was repeated every 15 min, but the depth always scored 0 until 22h after obtaining the geopolymer paste. The depth of 25 mm was obtained in both cases after 48 h as shown in Fig. 69.

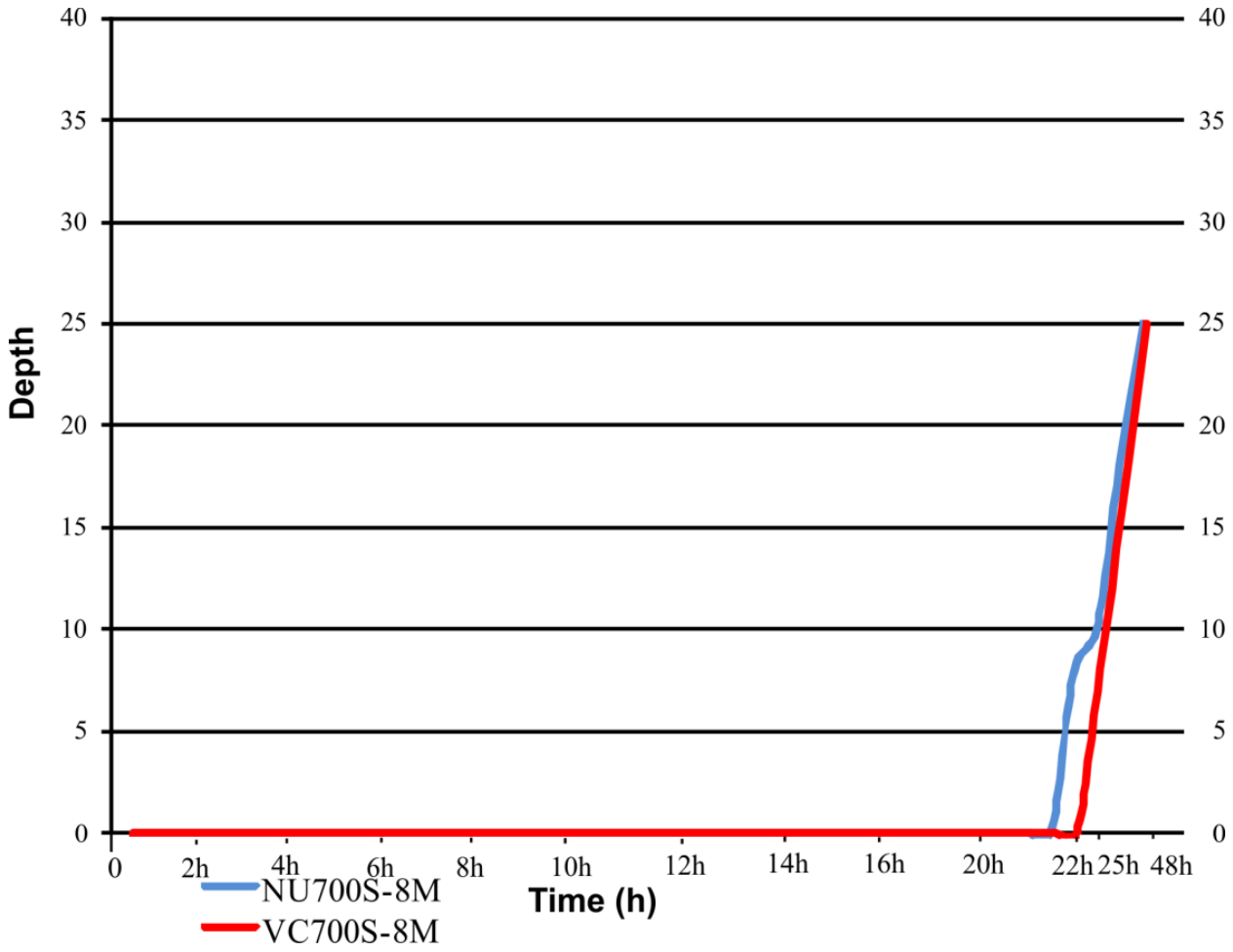

Figure 69- Needle penetration depth on NU700S-8M and VC700S-8M samples

7. Conclusions

This PhD thesis summarizes the results of three years of work focused on exploring the suitability and potentiality of Sicilian clay raw materials for the synthesis of AAMs. The chemical-physical and mechanical properties of AAMs have been studied in order to investigate their compatibility with existing materials. The results are promising, as all the selected clays demonstrated to be reactive in the alkali activation process giving an aluminosilicate gel binder as main product. Through this work, it could be seen that in the design of alkali cement, the raw material and activators must be carefully selected. For this reason, in the first part of the work, a physic-chemical analysis of the starting materials were necessary in order to evaluate the performance of the cement system and to select the most appropriate synthetic parameters and viscosity for the desired application. Parameters as molarity of activating solution and curing temperature have been also evaluated. It can be affirm that clay raw materials selected and analyzed in this study are suitable as precursors for the alkali activation process due to their chemical and mineralogical compositions (SiO_2/Al_2O_3 > 70 %);

In order to investigate the physical and mechanical properties of the obtained geopolymer binders, two set of formulations were obtained: the first one by mixing all selected clay materials thermally treated at 550 °C with sodium hydroxide solutions (NaOH 4M, 6M and 8M) and sodium silicate solution Na_2SiO_3; the second one by using mixtures of clay, only thermally treated at 700 °C, activated with sodium hydroxide solutions (NaOH 4M, 6M and 8M) and sodium silicate solution Na_2SiO_3;

Only samples activated with clay thermally treated at 700 °C have reach maturity after curing at 85 °C for 20h and 28d at room temperature in which the amorphous N-A-S-H and C-A-S-H gel are the main reaction product. Furthermore, the addition of sodium silicate (Na_2SiO_3) in the mixture affects positively the mechanical properties. With increasing temperature, at 85 °C, it has been seen like accelerates setting and strength development with respect to samples cured at room temperature, 22±3 °C, which need 28 days to obtained a good setting and hardening.

New crystalline phases as Tobermorite, Sodalite and zeolites, especially Na-phases zeolites (Faujasite), have been detected in the obtained geopolymer binders, also observed through the SEM analysis. Indeed, a coexistence of two different type of gel (N-A-S-H and C-A-S-H gel) has been detected in sample PS700-8M and find correspondence in the XRD patterns trough the new formed phase Sodalite and Tobermorite.

The co-precipitation of these two gels in hybrid cements is possible as demonstrate in diverse literature studies as (Alonso & Palomo, 2001; Palomo et al., 2007). When sodium silicate solution are added at the mixture, the mechanical strength values increases in all geopolymer binders, an important feature to take into account in the evaluation of structural applications. Overall, the highest mechanical strength values are obtained when pastes are activated with NaOH 8M whit an exception for plio-pleistocenic clay that recorded the highest value when paste is activate with NaOH 6M.

An increase of compaction and reduction of porosity of the matrix with respect to the increase of the molarity of the sodium hydroxide used has also been observed.

Considering the obtained results for each formulation, it can be possible to affirm like using NaOH 8M for the alkali reaction of the geopolymer, the pH and the alkaline condition of the paste is more advantageous than the pastes activated with NaOH at low molarities. Indeed, geopolymer pastes activated only with NaOH 8M reach maturity in terms of setting and hardening in 28 days at room temperature or in 1 days after thermal treatments at 85 °C, while geopolymer binders activated by means NaOH 8M and Na_2SiO_3 shown good properties in terms of mechanical strength values and chemical stability in addition to reach a good setting time and hardening in about 48 hours.

Finally, comparing the obtained results with those reported in literature for the traditional Portland cement, it is possible to assert that geopolymer binders made with clay precursors show good chemical and physical-mechanical properties comparable to traditional cements. These latter will be further characterized to test the durability in acid attack and accelerated aging test following the current normal.

The future goals of this research involve the planning of new formulations, starting from the geopolymer binders obtained in this thesis, in order to:

- Design new geopolymer-based composite materials using two different waste materials as aggregates, i.e., brick and sand waste;
- Implementation of one-parts geopolymer based on clay sediments to simplify the industrial scale up or in situ works.

Another useful study to implement the results obtained in this research could be the use of fine sized zeolite seeds, considering that zeolite synthesis is useful to improve some physicochemical properties of the products. These, in addition to being able to improve the results of geopolymer synthesis, could allow for less use of Na as a hydroxide or silicate and providing significant cost savings on an industrial scale.

Reference

Alonso, Santiago, and Angel Palomo. 2001. “Calorimetric Study of Alkaline Activation of Calcium Hydroxide-Metakaolin Solid Mixtures.” *Cement and Concrete Research* 31 (1): 25–30. https://doi.org/10.1016/S0008-8846(00)00435-X.

Barbera, G., Barone, G., Crupi, V., Longo, F., Maisano, G., Majolino, D., & Venuti, V. 2014. “A Multi-Technique Approach for the Determination of the Porous Structure of Building Stone.” *European Journal of Mineralogy* 26(1): 189–98.

Barbosa, V.F., MacKenzie, K.J. 2003. “Synthesis and Thermal Behaviour of Potassium Sialate Geopolymers.” *Materials Letters* 57: 1477–82.

Barbosa, V.F.F., MacKenzie, K.J.D., Thaumaturgo, C. 2000. “Synthesis and Characterisation of Materials Based on Inorganic Polymers of Alumina and Silica: Sodium Polysialate Polymers.” *International Journal of Inorganic Materials* 2: 309–17.

Barone, Germana, Claudio Finocchiaro, Isabella Lancellotti, Cristina Leonelli, Paolo Mazzoleni, Caterina Sgarlata, and Antonio Stroscio. 2021. “Potentiality of the Use of Pyroclastic Volcanic Residues in the Production of Alkali Activated Material.” *Waste and Biomass Valorization* 12 (2): 1075–94. https://doi.org/10.1007/s12649-020-01004-6.

Belver, Carolina, Christopher Breen, Francis Clegg, Cesar E. Fernandes, and Miguel A. Vicente. 2005. “A Variable-Temperature Diffuse Reflectance Infrared Fourier Transform Spectroscopy Study of the Binding of Water and Pyridine to the Surface of Acid-Activated Metakaolin.” *Langmuir* 21 (6): 2129–36. https://doi.org/10.1021/la048323m.

Bernal, Susan A., and John L. Provis. 2014. “Durability of Alkali-Activated Materials: Progress and Perspectives.” *Journal of the American Ceramic Society* 97 (4): 997–1008. https://doi.org/10.1111/jace.12831.

Buchwald, A., Hohmann, M., Posern, K., Brendler, E. 2009. “The Suitability of Thermally Activated Illite/Smectite Clay as Raw Material for Geopolymer Binders.” *Applied Clay Science* 46: 300–304.

C. Ruiz-Santaquiteria A. Fernández-Jiménez, J. Skibsted, A. Palomo. 2013. “Clay Reactivity: Production of Alkali Activated Cements.” *Apply Clay Science* 73: 11–16.

Caijun Shi, Jueshi Qian. n.d. “High Performance Cementing Materials from Industrial

Slags — a Review." *Resources, Conservation and Recycling* Volume 29 (3): 195–207.

Carbone, S., Grasso, M., & Lentini, F. n.d. "Lineamenti Geologici Del Plateau Ibleo (Sicilia SE). Presentazione Delle Carte Geologiche Della Sicilia Sud-Orientale." *Memorie Della Società Geologica Italiana and Physical–Mechanical Properties. Construction and Building Materials* 33: 122-132.

Catalano, R., Franchino, A., Merlini, S., Sulli, A., Agate, M. and Basilone, L. 1998. "Materiali per La Comprensione Dell'assetto Profondo Della Sicilia Centro-Occidentale. In: La Sicilia: Un Laboratorio Naturale Nel Mediterraneo. Field Guide to the Post-Meeting Trip." *Società Geologica Italiana.*

Clausi, Marina, Serena C. Tarantino, Laura Lorenza Magnani, Maria Pia Riccardi, Cristina Tedeschi, and Michele Zema. 2016. "Metakaolin as a Precursor of Materials for Applications in Cultural Heritage: Geopolymer-Based Mortars with Ornamental Stone Aggregates." *Applied Clay Science* 132–133: 589–99. https://doi.org/10.1016/j.clay.2016.08.009.

Criado, M., A. Palomo, and A. Fernández-Jiménez. 2005. "Alkali Activation of Fly Ashes. Part 1: Effect of Curing Conditions on the Carbonation of the Reaction Products." *Fuel* 84 (16): 2048–54. https://doi.org/10.1016/j.fuel.2005.03.030.

Criado, M, A Fernández-jiménez, A G De Torre, M A G Aranda, and A Palomo. 2007. "An XRD Study of the Effect of the SiO 2 / Na 2 O Ratio on the Alkali Activation of Fly Ash" 37: 671–79. https://doi.org/10.1016/j.cemconres.2007.01.013.

Davidovits, J. 1988. "Geopolymer Chemistry and Properties." *Geopolymer*, 25–48.

Davidovits, J. 1991. "Geopolymers - Inorganic Polymeric New Materials." *Journal of Thermal Analysis*, 1633–56.

Deventer, P. Duxson Æ A. Ferna´ndez-Jime´nez Æ J. L. Provis Æ G. C. Lukey Æ A. Palomo Æ J. S. J. van. 2007. "Geopolymer Technology : The Current State of the Art," no. 4: 2917–33. https://doi.org/10.1007/s10853-006-0637-z.

Djobo, Jean Noël Yankwa, Antoine Elimbi, Hervé Kouamo Tchakouté, and Sanjay Kumar. 2017. "Volcanic Ash-Based Geopolymer Cements/Concretes: The Current State of the Art and Perspectives." *Environmental Science and Pollution Research* 24 (5): 4433–46. https://doi.org/10.1007/s11356-016-8230-8.

Djobo JNY, Tchadjié LN, Tchakoute HK, et al. 2014. "Synthesis of Geopolymer

Composites from a Mixture of Volcanic Scoria and Metakaolin." *J Asian Ceram Soc*.

Duxson, P., Lukey, G.C., van Deventer, J.S. 2007. "Thermal Evolution of Metakaolin Geopolymers: Part 1-Physical Evolution." *Journal of Non-Crystalline Solids* 352: 5541-5555.

Duxson, P., Provis, J.L., Lukey, G.C., van Deventer, J.S.J. 2007. "The Role of Inorganic Polymer Technology in the Development of 'Green Concrete'." *Cement and Concrete Research* 37: 1590–97.

Duxson, P., Provis, J.L. 2008. "Designing Precursors for Geopolymer Cements." *Journal of the American Ceramic Society* 91: 3864–69.

E.I. Kamitsos and A.P. Patsis. 1993. "Infrared-Reflectance Spectra of Heat-Treated, Sol-Gel-Derived Silica." *Physical Review B - Condensed Matter and Materials Physics* 48. https://doi.org/10.1103/PhysRevB.53.14656.

Elert, K., Pardo, E.S., Rodriguez-Navarro, C. 2015. "Alkaline Activation as an Alternative Method for the Consolidation of Earthen Architecture." *Journal of Cultural Heritage* 16: 461–69.

Elimbi, A., Tchakoute, H., Njopwouo, D. 2011. "Effects of Calcination Temperature of Kaolinite Clays on the Properties of Geopolymer Cements." *Construction and Building Materials* 25: 2805–12.

Farmer, V. C., ed. 1974a. *The Infrared Spectra of Minerals*. Londan: Mineralogical Society of Great Britain and Ireland. https://doi.org/10.1180/mono-4.

Fernández-Jiménez, A., Monzó, M., Vicent, M., Barba, A., Palomo, A. 2008. "Alkaline Activation of Metakaolin-Fly Ash Mixtures: Obtain of Zeoceramics and Zeocements. Microporous and Mesoporous Materials."

Fernández-Jiménez, A., Palomo, J.G., Puertas, F. 1999. "Alkali-Activated Slag Mortars: Mechanical Strength Behaviour." *Cement and Concrete Research* 29: 1313–21.

Fernández-Jiménez, A., Palomo, A. 2005. "Mid-Infrared Spectroscopic Studies of Alkali-Activated Fly Ash Structure." *Mid-Infrared Spectroscopic Studies of Alkali-Activated Fly Ash Structure*. 86: 207–14.

Fernández-Jiménez, A., and A. Palomo. 2003. "Characterisation of Fly Ashes. Potential Reactivity as Alkaline Cements." *Fuel* 82 (18): 2259–65. https://doi.org/10.1016/S0016-2361(03)00194-7.

Fernández-Jiménez, A., Pastor, J.Y., Martín, A., Palomo, A. 2010. “High-Temperature Resistance In Alkali-Activated Cement.” *Journal Of The American Ceramic Society* 93: 3411–17.

Ferone, C., B. Liguori, I. Capasso, F. Colangelo, R. Cioffi, E. Cappelletto, and R. Di Maggio. 2015. “Thermally Treated Clay Sediments as Geopolymer Source Material.” *Applied Clay Science* 107: 195–204. https://doi.org/10.1016/j.clay.2015.01.027.

Ferraris, Chiara F. 1999. “Measurement of the Rheological Properties of High Performance Concrete: State of the Art Report.” *Journal of Research of the National Institute of Standards and Technology* 104 (5): 461–78. https://doi.org/10.6028/jres.104.028.

Flatt, R.J., Roussel, N., Cheeseman, C.R. 2012. “Concrete: An Eco Material That Needs To Be Improved.” *Journal Of The European Ceramic Society* 32: 2787–98.

Frost, Rayl and Ursula Johanssont. 1998. " Combination bands in the infrared spetroscopy of kaolins- a Drift Spetroscopy Study". *Industrial Research* 46 (4): 466–77.

García-Lodeiro, I., Fernández-Jiménez, A., Palomo, A., Macphee, D.E. 2010. “Effect of Calcium Additions on N-A-S-H Cementitious Gels.” *Journal of the American Ceramic Society* 93(7): 1934–40.

Garcia-Lodeiro, I., Palomo, A., Fernández-Jiménez, A., & Macphee, D.E. 2011. “Compatibility Studies between NASH and CASH Gels. Study in the Ternary Diagram Na_2O-CaO-Al_2O_3-SiO_2-H_2O.” *Cement and Concrete Research* 41(9): 923–31.

Gasparini, E., Tarantino, S.C., Conti, M., Biesuz, R., Ghigna, P., Auricchio, F., Zema, M. 2015. “Geopolymers from Low-T Activated Kaolin: Implications for the Use of Alunite-Bearing Raw Materials.” *Applied Clay Science* 114: 530–39.

Gasparini, E., Tarantino, S.C., Ghigna, P., Riccardi, M.P., Cedillo-González, E.I., Siligardi, C., Zema, M. 2013. “Thermal Dehydroxylation of Kaolinite under Isothermal Conditions.” *Applied Clay Science* 80–81: 417–25.

Geraldes, C.F.M., Lima, A.M., Delgado-Rodrigues, J., Mimoso, J.M., Pereira, S.R.M. 2016. “Geopolymers as Potential Repair Material in Tiles Conservation.” *Applied Physics A: Materials Science and Processing* 122: 1–10.

Glukhovsky,V.D. 1959. "Gruntosilicaty (Soil Silicates).

Gualtieri, AF, M Zanni - Materials Science Forum, and undefined 1998. n.d. “Quantitative

Determination of Crystalline and Amorphous Phase in Traditional Ceramics by Combined Rietveld-RIR Method." *Trans Tech Publ*.

Habert, G., De Lacaillerie, J.D.E., Roussel, N. 2011. "An Environmental Evaluation of Geopolymer Based Concrete Production: Reviewing Current Research Trends." *Journal of Cleaner Production* 19: 1229–38.

Hanzlíček, Tomas, Michaela Steinerová, Pavel Straka, Ivana Perná, Petr Siegl, and Tereza Švarcová. 2009. "Reinforcement of the Terracotta Sculpture by Geopolymer Composite." *Materials and Design* 30 (8): 3229–34. https://doi.org/10.1016/j.matdes.2008.12.015.

Heller-Kallai, L. 2006. "Thermally Modified Clay Minerals." *Handbook of Clay Science. Development in Clay Science*, 289–308.

Hughes, T.L., Methven, C.M., Jones, T.G., Pelham, S.E., Fletcher, P., Hall, C. 1995. "Determining Cement Composition by Fourier Transform Infrared Spectroscopy." *Advanced Cement Based Materials* 2(3): 91–104.

J. Davidovits. 1991. "Geopolymers: Inorganic Polymeric New Matrials." *Journal of Thermal Analysis and Calorimetry*.

Kamseu, E., Leonelli, C., Perera, D.S., Melo, U.C., Lemougna, P.N. 2009. "Investigation of Volcanic Ash Based Geopolymers as Potential Building Materials." *Int. Ceram. Rev.* 58: 136–140.

Kani, E.N., Allahverdi, A. 2009. "Effect of Chemical Composition on Basic Engineering Properties of Inorganic Polymeric Binder Based on Natural Pozzolan." *Ceram. - Silikaty.* 53: 195–204.

Khalifa, Ahmed Z., Özlem Cizer, Yiannis Pontikes, Andrew Heath, Pascaline Patureau, Susan A. Bernal, and Alastair T.M. Marsh. 2020. "Advances in Alkali-Activation of Clay Minerals." *Cement and Concrete Research* 132 (February): 106050. https://doi.org/10.1016/j.cemconres.2020.106050.

Khan, M. I., Azizli, K., Sufian, S., Man, Z. 2015. "Sodium Silicate-Free Geopolymers as Coating Materials: Effects of Na/Al and Water/Solid Ratios on Adhesion Strength." *Ceramics International* 41(2): 2794–2805.

Kloprogge, J.T. 2017. "Infrared and Raman Spectroscopies of Clay Minerals." *Develoomment in Clay Science* 8: 150.

Košařová, D. Hradil, I. Němec, P. Bezdička, V. Kanický. 2013. “Microanalysis of Clay-Based Pigments in Painted Artworks by the Means of Raman Spectroscopy.” *Journal Raman Spectroscopy* 44: 1570.

Krivenko, P., Kovalchuk, G., Palomo, A., FernÁndez-JimÉnez, A. 2007. “Fly Ash Based Geocements: Genesis of Microstructure and Properties at Hydration-Dehydration Process.” *Brittle Matrix Composites* 8: 55–64.

Krivenko, P. 1997. “Alkaline Cements: Terminology, Classification, Aspects of Durability.” *Proceedings of the 10th International Congress on the Chemistry of Cement, Gothenburg, Sweden, Amarkai and Congrex Göteborg, Gothenburg, Sweden*.

Kühl, H. 1908. “Slag Cement and Process of Making the Same.”

Lancellotti I., Catauro M., Ponzoni C., Bollino F. 2013. “Inorganic Polymers from Alkali Activation of Metakaolin: Effect of Setting and Curing on Structure.” *Journal of Solid State Chemestry* 200: 341–48.

Lancellotti, I., Ponzoni, C., Barbieri, L., Leonelli, C.: Alkali activation processes for incinerator residues management. Waste Manag. 33, 1740–1749 (2013). doi:10.1016/j.wasman.2013.04.013

Lee, W.K.W., & van Deventer, J.S.J. 2004. “The Interface between Natural Siliceous Aggregates and Geopolymers.” *Cement and Concrete Research* 34: 195–206.

Lee, W.K.W., van Deventer, J.S.J. 2007. “Chemical Interactions between Siliceous Aggregates and Low-Ca Alkali-Activated Cements.” *Cement and Concrete Research* 37: 844–55.

Lee, W. K.W., and J. S.J. Van Deventer. 2003. “Use of Infrared Spectroscopy to Study Geopolymerization of Heterogeneous Amorphous Aluminosilicates.” *Langmuir* 19 (21): 8726–34. https://doi.org/10.1021/la026127e.

Lentini F., Carbone S., Catalano S., Grasso M. 1996. “Elementi per La Ricostruzione Del Quadro Strutturale Della Sicilia Orientale.” *Mem. Soc. Geol. It.* 51: 145–56.

LentiniF., Carbone S., Catalano S., and Monaco 1990. "Tettonica a thrust neogenica nella Catena Appennino-Magrebide: esempi della Lucania e della Sicilia. Autore: Lentini F."

Leonelli C., Romagnoli M.,2013. Geopolimeri:polimeri inorganici attivati alcalinamente, 2nd ed. ICers, Bologna.

Liu, Yiwei, Caijun Shi, Zuhua Zhang, and Ning Li. 2019. “An Overview on the Reuse of Waste Glasses in Alkali-Activated Materials.” *Resources, Conservation and Recycling* 144 (December 2018): 297–309. https://doi.org/10.1016/j.resconrec.2019.02.007.

M.C. Caggiani, A.Coccato, G.Barone, C.Finocchiaro, M.Fugazzotto, G. Lanzafame, R. Occhipinti, A. Stroscio, P. Mazzoleni; 2021. “Raman Spectroscopy Potentiality in the Study of Geopolymers Reaction Degree.” *Journal of Raman Spectroscopy*.

M.L. Granizo, M.T. Blanco-Varela. 1998. “Alkaline Activation of Metakaolin:Isothermal Conduction Calorimetry Study.” *J. Therm. Anal. 52*.

Madejová, Jana, and Peter Komadel. 2001. “Baseline Studies of the Clay Minerals Society Source Clays: Infrared Methods.” *Clays and Clay Minerals* 49 (5): 410–32. https://doi.org/10.1346/CCMN.2001.0490508.

Mendes, Marta T, Teresa A Ferreira, José Delgado Rodrigues, João Manuel Mimoso, and Sílvia R M Pereira. n.d. “Laboratório Nacional De Engenharia Civil Volumetric and Chromatic Reintegration in Conservation of in Situ Glazed Tiles.”

Miliani, C., F. Rosi, A. Daveri, and B. G. Brunetti. 2012. “Reflection Infrared Spectroscopy for the Non-Invasive in Situ Study of Artists’ Pigments.” *Applied Physics A: Materials Science and Processing* 106 (2): 295–307. https://doi.org/10.1007/s00339-011-6708-2.

Mladenović, Nataša, Ljiljana Kljajević, Snežana Nenadović, Marija Ivanović, Bojan Čalija, Jelena Gulicovski, and Katarina Trivunac. 2020. “The Applications of New Inorganic Polymer for Adsorption Cadmium from Waste Water.” *Journal of Inorganic and Organometallic Polymers and Materials* 30 (2): 554–63. https://doi.org/10.1007/s10904-019-01215-y.

MOORE, D. M. & REYNOLDS, R. C., Jr. 1997. “X-Ray Diffraction and the Identification and Analysis of Clay Minerals, 2nd Ed.”

Occhipinti R., Palomo Angel Zema Michele , Fernández-Jiménez Ana, Tarantino Serena Chiara. 2021. “Sulfate-Bearing Clay and Pietra Serena Sludge: Raw Materials for the Development of Alkali Activated Binders.” *Construction and Building Materials*.

Occhipinti, Roberta, Antonio Stroscio, Claudio Finocchiaro, Maura Fugazzotto, Cristina Leonelli, Maria José Lo Faro, Bartolomeo Megna, Germana Barone, and Paolo Mazzoleni. 2020. “Alkali Activated Materials Using Pumice from the Aeolian Islands

(Sicily, Italy) and Their Potentiality for Cultural Heritage Applications: Preliminary Study." *Construction and Building Materials* 259: 120391. https://doi.org/10.1016/j.conbuildmat.2020.120391.

Palomo, A., Glasser, F. 1992. "Chemically-Bonded Cementitious Materials Based on Metakaolin." *British Ceramic Transactions and Journal* 91: 107–12.

Polettini, R. Pomi, G. Carcani. 2005. "The Effect of Na and Ca Salts on MSWI Bottom Ash Activation for Reuse as a Pozzolanic Admixture." *Resources, Conservation and Recycling* 43 (4): 403–18.

Provis, J.L., Bernal, S.A. 2014. "Geopolymers and Related Alkali-Activated Materials." *Annual Review of Materials Research,* 299–327.

Provis, J. L., P. Duxson, Jannie S.J. van Deventer, and G. C. Lukey. 2005. "The Role of Mathematical Modelling and Gel Chemistry in Advancing Geopolymer Technology." *Chemical Engineering Research and Design* 83 (7 A): 853–60. https://doi.org/10.1205/cherd.04329.

Provis, John L., and Jan Stephanus Jakob Van Deventer. 2009. *Geopolymers : Structure, Processing, Properties and Industrial Applications*. Woodhead.

Provis, John L., and Jannie S.J. van Deventer. 2014. *Alkali Avtivated Materials: State of Art Report. Rilem Tc 224*.

Puertas, F., Martínez-Ramírez, S., Alonso, S., Vázquez, T. 2000. "Alkali-Activated Fly Ash/Slag Cements: Strength Behaviour and Hydration Products." *Cement and Concrete Research* 30: 1625–32.

Purdon, A.O. 1940. "Action of Alkalis on Blast-Furnace Slag." *J Soc Chem Ind* 59: 191–202.

Rahier, H., Simons, W., Van Mele, B., Biesemans, M. 1997. "Low-Temperature Synthesized Aluminosilicate Glasses: Part III Influence of the Composition of the Silicate Solution on Production, Structure and Properties." *Journal of Materials Science* 32: 2237–47.

Rashad, A.M. 2013. "Alkali-Activated Metakaolin: A Short Guide for Civil Engineer – An Overview." *Construction and Building Materials* 41: 751–65.

Rees, C. A., Provis, J. L., Lukey, G. C. and Van Deventer, J. S. J. 2007. "Attenuated Total Reflectance Fourier Transform Infrared Analysis of Fly Ash Geopolymer Gel

Ageing.” *Langmuir*.

Ricciotti, Laura, Antonio Molino, Valentina Roviello, Elena Chianese, Paola Cennamo, and Giuseppina Roviello. 2017. “Geopolymer Composites for Potential Applications in Cultural Heritage.” *Environments* 4 (4): 91. https://doi.org/10.3390/environments4040091.

Shi, C., Fernandez-Jimenez, A. 2006. “Stabilization/Solidification of Hazardous and Radioactive Wastes with Alkali-Activated Cements.” *Journal of Hazardous Materials* 137: 1656–63.

Shi, C., Jiménez, A.F., Palomo, A. 2011. “New Cements for the 21st Century: The Pursuit of an Alternative to Portland Cement.” *Cement and Concrete Research* 41: 750-763.

Siemer, D.D. 2002. “Hydroceramics, a ‘New’ Cementitious Waste Form Material for U.S. Defense- Type Reprocessing Waste.” *Materials Research Innovations* 6: 96–104.

Steinerová, Michaela, and Jana Schweigstillová. 2013. “Porous Microstructure of the Interfacial Transition Zone in Geopolymer Composites.” *Ceramics - Silikaty* 57 (4): 328–35.

Szechyńska-Hebda, M., J. Marczyk, C. Ziejewska, N. Hordyńska, J. Mikuła, and M. Hebda. 2019. “Neutral Geopolymer Foams Reinforced with Cellulose Studied with the FT-Raman Spectroscopy.” *IOP Conference Series: Materials Science and Engineering* 706 (1). https://doi.org/10.1088/1757-899X/706/1/012017.

Thomas Poinot, Michael E. Laracy, Cecilio Aponte, Hamlin M. Jennings, Elsa A. Olivetti. 2018. “Beneficial Use of Boiler Ash in Alkali-Activated Bricks.” *Resources, Conservation and Recycling*, 128: 1–10.

Toby, Brian H., and Robert B. Von Dreele. 2013. “GSAS-II: The Genesis of a Modern Open-Source All Purpose Crystallography Software Package.” *Journal of Applied Crystallography* 46 (2): 544–49. https://doi.org/10.1107/S0021889813003531.

Wastiels, J., Wu, X., Faignet, S., Patfoort, G. 1994. “Mineral Polymer Based on Fly Ash.” *J RESOUR MANAGE TECHNOL* 22: 135–41.

Xu, Hua, and Jannie S.J. Van Deventer. 2002. “Geopolymerisation of Multiple Minerals.” *Minerals Engineering* 15 (12): 1131–39. https://doi.org/10.1016/S0892-6875(02)00255-8.

Yadollahi, Mehrzad Mohabbi, Ahmet Benli, and Ramazan Demirbog. 2015. “The Effects

of Silica Modulus and Aging on Compressive Strength of Pumice-Based Geopolymer Composites" 94: 767–74. https://doi.org/10.1016/j.conbuildmat.2015.07.052.

Zuhua, Z., Y. Xiao, Z. Huajun, and C. Yue. 2009. "Role of Water in the Synthesis of Calcined Kaolin-Based Geopolymer." *Applied Clay Science* 43 (2): 218–23. https://doi.org/10.1016/j.clay.2008.09.003.

NORMAL UNI EN 1926:20073

NORMAL 11/82